論文 / 著書情報
Article / Book Information

題目(和文)	
Title(English)	Discovery of Inhibitors Targeting p300/Transcription Factors Protein-Protein Interactions
著者(和文)	FITRIASTUTI DHINA
Author(English)	Dhina Fitriastuti
出典(和文)	学位:博士(理学), 学位授与機関:東京科学大学, 報告番号:甲第250号, 授与年月日:2025年3月26日, 学位の種別:課程博士, 審査員:中村 浩之,岡田 智,西山 伸宏,田中 克典,神谷 真子,柘植 丈治
Citation(English)	Degree:Doctor (Science), Conferring organization: Institute of Science Tokyo, Report number:甲第250号, Conferred date:2025/3/26, Degree Type:Course doctor, Examiner:,,,,,
学位種別(和文)	博士論文
Type(English)	Doctoral Thesis

Doctoral Thesis

Discovery of Inhibitors Targeting p300/Transcription Factors Protein-Protein Interactions

Dhina Fitriastuti

Academic Supervisors: Prof. Hiroyuki Nakamura and
Assoc. Prof. Satoshi Okada

Department of Life Science and Technology

Institute of Science Tokyo

2025

TABLE OF CONTENTS

LIST OF ABBREVIATIONS

AML	acute myeloid leukemia
Alpha screen	amplified luminescent proximity homogeneous assay screen
Asp	aspartic acid
ATP	adenosine triphosphate
B2M	β2-microglobulin
BAX	Bcl-2 associated X
BCA	bicinchoninic acid
Bcl-2	B-cell lymphoma
BSA	bovine serum albumin
CAIX	carbonic anhydrase IX
CBB	Coomassie brilliant blue
CBP	CREB-binding protein
cDNA	complementary DNA
CH1	cysteine/histidine-rich region 1
CIAP	calf-intestinal alkaline phosphatase
CO_2	carbon dioxide
CREB	cAMP response element-binding protein
CTAD	C-terminal activation domain
CTSL	cathepsin L
DBU	1,8-diazabicyclo[5.4.0]undec-7-ene
DCM	dichloromethane
DIAD	diisopropyl azodicarboxylate
DIC	diisopropylcarbodiimide
DMEM	dulbecco's modified Eagle's medium
DMF	*N*,*N*-dimethylformamide
DMSO	dimethyl sulfoxide
DNA	deoxyribonucleic acid
DTT	dithiothreitol
ECL	enhanced chemiluminescence
EDTA	ethylenediaminetetraacetic acid
ELISA	enzyme-linked immunosorbent assay
ESI	electrospray ionization
Et_3N	triethylamine
EtBr	ethidium bromide
FA	fluorescence anisotropy
FDA	Food and Drug Administration
FITC	fluorescein isothiocyanate
FP	fluorescence polarization
FRET	Förster resonance energy transfer
Gln	glutamine
GST	glutathione-S-transferase
HIF-1α	hypoxia-inducible factor 1-α

His	histidine
HOAt	1-hydroxy-7-aza-*1H*-benzotriazole
$HOBt \cdot H_2O$	1-hydroxybenzotriazole monohydrate
HPLC	High-Performance Liquid Chromatography
HREs	hypoxia-responsive elements
HRMS	high-resolution mass spectra
HRP	horseradish peroxidase
HTS	high-throughput screening
IC_{50}	half-maximal inhibitory concentration
IgG	immunoglobulin G
Ile	isoleucine
IPTG	isopropyl β-D-1-thiogalactopyranoside
Leu	leucine
Lys	lysine
MALDI-TOF	matrix-assisted laser desorption ionization-time of flight
MeCN	methyl cyanide or acetonitrile
MeOH	methanol
MMPs	matrix metalloproteinases
mRNA	messenger RNA
MS	mass spectrometry
MTT	3-[4,5-dimethylthiazol-2-yl]-2,5 diphenyl tetrazolium bromide
NRID	nuclear receptor interaction domain
NMM	*N*-methyl morpholine
NMR	Nuclear Magnetic Resonance
NPDepo	Natural Products Depository
NTAD	N-terminal activation domain
OD_{600}	optical density at 600 nm
OHM 1	oxopiperazine helix mimetic 1
o-Ns-Cl	*o*-nitrobenzenesulfonyl chloride
PAL	photoaffinity labeling
PBS	phosphate buffered saline
PCAF	p300/CBP-associated factor
PCR	polymerase chain reaction
PDB	Protein Data Base
PPh_3	triphenylphosphine
PPIs	protein-protein interactions
Pro	proline
PTLC	preparative thin-layer chromatography
PVDF	polyvinylidene fluoride
PyBOP	*1H*-benzotriazole-1-yloxytris(pyrrolidine-1-yl)phosphonium hexafluorophosphate
RIPA buffer	radioimmunoprecipitation assay buffer
RNA	ribonucleic acid

RT-qPCR	reverse transcription-quantitative polymerase chain reaction
SARS-CoV-2	severe acute respiratory syndrome coronavirus 2
SDS	sodium dodecyl sulfate
SDS-PAGE	sodium dodecyl-sulfate polyacrylamide gel electrophoresis
STAT 3	signal transducer and activator of transcription-3
TAZ	transcriptional adaptor zinc-binding domain
TFA	trifluoroacetic acid
THF	tetrahydrofuran
TIPS	triisopropylsilane
TLC	thin-layer chromatography
TNBS	2,4,6-trinitrobenzene sulfonic acid
TOF	time of flight
TR-FRET	time-resolved fluorescence resonance energy transfer
Tris-HCl	tris (hydroxymethyl) aminomethane (THAM) hydrochloride
tRNA	transfer RNA
Trp	tryptophan
TTBS	tween-tris-buffered saline
UV	ultraviolet
Val	valine
VHL	von Hippel-Lindau

LIST OF PUBLICATION

Paper

1. **Fitriastuti, D**.; Miura, K.; Okada, S.; Hirano, H.; Osada, H.; Nakamura, H. (accepted in *Bioorg. Med. Chem.*)

Conferences

1. Development of HIF-1α/p300 Protein-Protein Interaction Evaluation System for Screening Novel Inhibitors
   Fitriastuti, D.; Miura, K.; Okada, S.; Hirano, H.; Osada, H.; Nakamura, H.;
   The 17th Annual Meeting of Japanese Society for Chemical Biology, June 2023.
2. Identification of Niclosamide as a p300/Transcription Factors Protein-Protein Interaction Inhibitor
   Fitriastuti, D.; Miura, K.; Okada, S.; Hirano, H.; Osada, H.; Nakamura, H.;
   The 18th Annual Meeting of Japanese Society for Chemical Biology, May 2024.

Chapter 1

Introduction

1.1 Protein-protein interactions (PPIs)

The central dogma is the fundamental flow of genetic information from DNA to protein involving three key stages: replication, transcription, and translation. Initially, DNA replication occurs, where the DNA molecule makes an identical copy of itself, ensuring that each daughter cell receives a complete set of genetic information. Following replication, transcription occurs in the nucleus, where a specific segment of DNA is used as a template to synthesize messenger RNA (mRNA). The mRNA carries the genetic code from the DNA to the cytoplasm. In the final stage, translation, the mRNA binds to a ribosome, which decodes the mRNA sequence into a specific sequence of amino acids, facilitated by transfer RNA (tRNA). These amino acids are linked to form a polypeptide chain that folds into a functional protein. Based on the central dogma of molecular biology, stated by Francis Crick[1] and presented in Figure 1-1, whole-genome sequencing of DNA yield information similarly obtained from RNA and/or proteins. Once proteins are synthesized, they will interact with other proteins in a highly specific and regulated manner, making several networks known as protein-protein interactions (PPIs).[2,3]

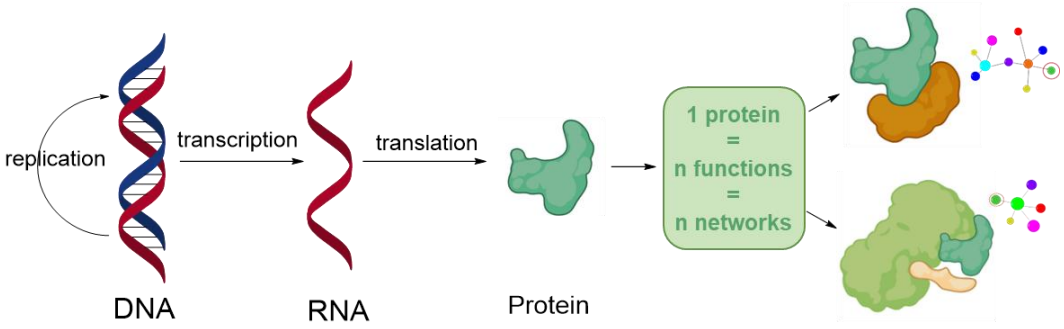

Figure 1-1. The process of protein-protein interaction formation of proteins produced from DNA through transcription and translation

PPIs play an important role in all biological processes and cellular functions, regulating many biochemical reactions such as signalling transmission and metabolism.[4] For example, the interaction of receptor tyrosine kinases (RTKs) with protein ligands (growth factors, cytokines etc.) in tumor cells activates the downstream PI3K/Akt signaling pathway, which plays an important role in promoting angiogenesis and recruiting inflammatory factors.[5,6] Therefore, PPI is a potential target for the regulation of various biological processes, and the regulation of PPI is an attractive approach to achieve therapy of many diseases in which PPI is deeply involved.

1.2 Drug development targeting PPIs

Targeting PPIs in drug discovery aims to modulate protein interactions to achieve therapeutic effects. PPIs can be inhibited or stabilized through directly bind to a few key residues at the PPI interface by orthosteric modulators or indirectly bind to active regions outside the PPI interface that can induce conformational changes by allosteric modulators (Figure 1-2).[7–10]

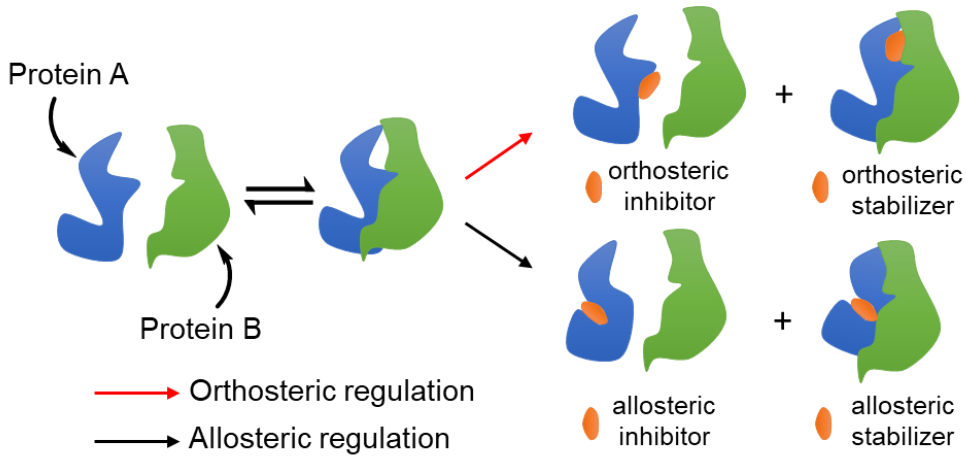

Figure 1-2. Mechanisms for PPI modulators: allosteric and orthosteric

PPI modulators can be classified into antibodies, peptides, and small molecules (Table 1-1). The first category is antibodies. When targeting a large PPI interface, antibodies are advantageous as they can cover the extensive interaction surface. However, due to their large molecular weight, monoclonal antibodies are primarily limited to extracellular targets. Despite this limitation, monoclonal antibodies have been successfully applied in clinical treatments for various diseases. Nevertheless, their use may trigger adverse reactions, such as immunogenicity and infusion-related immune responses.[11,12]

The second category of PPI modulators is peptides. These peptides are designed based on structural information of PPI hotspots. Designed peptides mimic key residues at the interface of PPIs, enabling them to bind proteins with high specificity and affinity. Compared to monoclonal antibodies, peptides have a lower molecular weight, providing better tissue penetration. Peptides also exhibit high target specificity and affinity, making them promising PPI modulators. However, they are prone to hydrolysis by various proteases in the body, leading to a short half-life and requiring modifications to improve their stability and pharmacokinetics.[13,14]

The third category of PPI modulators is small molecules. Unlike classic drug targets such as enzymes or ion channels, PPI interfaces are generally large, flat, and hydrophobic, often lacking well-defined pockets suitable for small molecule binding. Effective small-molecule modulators must cover significant surface areas and establish numerous hydrophobic interactions. While this poses pharmacokinetic challenges, such as poor solubility and large molecular weight[15], small molecules remain more suitable for targeting tight and narrow PPI interfaces.[16]

Table 1-1. The advantages and disadvantages of the three types of PPI modulators

Modulators	Advantages	Disadvantages
Antibodies	High affinity	Side effect (immunogenicity)
	Strong target specificity	High production cost
Peptides	High affinity	Short half-life
	Strong target specificity	Poor oral administration
		Poor solubility
		Unstable physicochemical properties
Small molecules	Oral administration	Low selectivity
	Penetration cell membrane	
	Cost-effective and scalable	

The PPIs modulation through small molecules is generally considered difficult and PPIs were regarded as "undruggable" targets. Several well-described factors contribute to this issue. Firstly, proteins that interact with other proteins typically use relatively large contact surfaces (1500–3000 $Å^2$)[17] which is larger than that of receptor-ligand contact area (300–1000 $Å^2$) and the interface is highly hydrophobic.[18] Second, the PPIs interface tends to be flat and contains few grooves or pockets, thus making it difficult for the designed small molecule compounds to bind. The Arora group reported an interesting study in which they analysed PPI structures from the Protein Data Base (PDB), focusing on those PPIs involving α-helical interactions. They categorize these PPIs into examples with well-defined clefts and those with extended, flat interfaces and use this information to suggest that PPIs with shallow surfaces are less likely to be readily inhibited.[19] Third, the presence of noncontiguous binding sites thus results in high-affinity binding between the proteins, making it difficult for the small molecular compounds to inhibit such high-affinity

interaction.[20] Fourth, there is a general lack of natural ligands. Compared with traditional drug target enzymes or receptors, PPIs lack endogenous small molecular ligands for reference.[20]

Despite challenges, small molecules offer significant advantages for PPI-targeted drug discovery. Their cell-permeability allows access to intracellular PPIs, crucial in diseases like cancer and neurodegenerative disorders. They are cost-effective, chemically modifiable for improved potency, and often suitable for oral administration, enhancing patient convenience.[21,22] By addressing PPI challenges, small molecules offer a versatile, accessible approach to drug discovery.

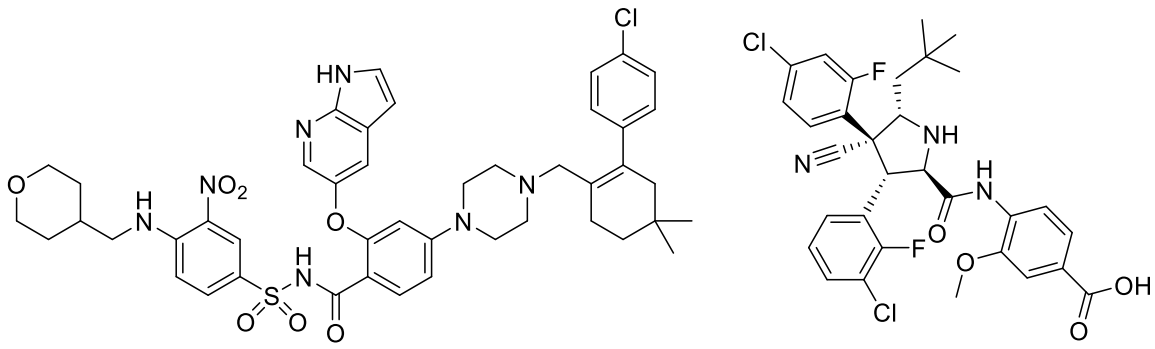

1 (ABT-199, Bcl-2/BAX inhibitor)

2 (RG7388, MDM2-p53 inhibitor)

Figure 1-3. Small molecule PPI inhibitors

In recent years, some PPIs inhibitors have entered clinical studies, some of which have been approved as novel drugs, indicating that the inhibitors targeting PPIs have broad prospects (Figure 1-3).[10,23] Other PPI inhibitor, such as the B-cell lymphoma (Bcl-2)/ Bcl-2 associated X (BAX) PPI inhibitor venetoclax (ABT-199, **1**), have been clinically tested and exhibit efficacy in chronic leukemia treatment.[10] Idasanutlin (RG7388, **2**) is MDM2-p53 inhibitor that has been investigated in clinical trials. It has shown activity in several cancers, particularly in acute myeloid leukemia (AML) and other hematologic malignancies. Idasanutlin has shown promise in phase 1 and phase 2 clinical trials, but it has not been Food and Drug Administration (FDA)-approved.[24] Hence, the development of small molecules targeting PPIs has emerged as one of the most significant obstacles in drug discovery.

1.3 HIF-1α/p300 interaction

Hypoxia inducible factor (HIF)-1α is an essential transcription factor that facilitates the adaptation of cancer cells to hypoxic conditions. In normoxic environments, HIF-1α undergoes degradation through the von Hippel-Lindau (VHL)-mediated ubiquitin-proteasome pathway.[25,26] During hypoxia, HIF-1α becomes stabilized and translocates to the nucleus, where it dimerizes with HIF-1β and binds to hypoxia-responsive elements (HREs) on the promoters of target genes.[27–29] This enhances the transcription of genes associated with angiogenesis, glycolysis, and erythropoiesis, facilitating cellular adaptation to oxygen deficiency (Figure 1-4).[30–33]

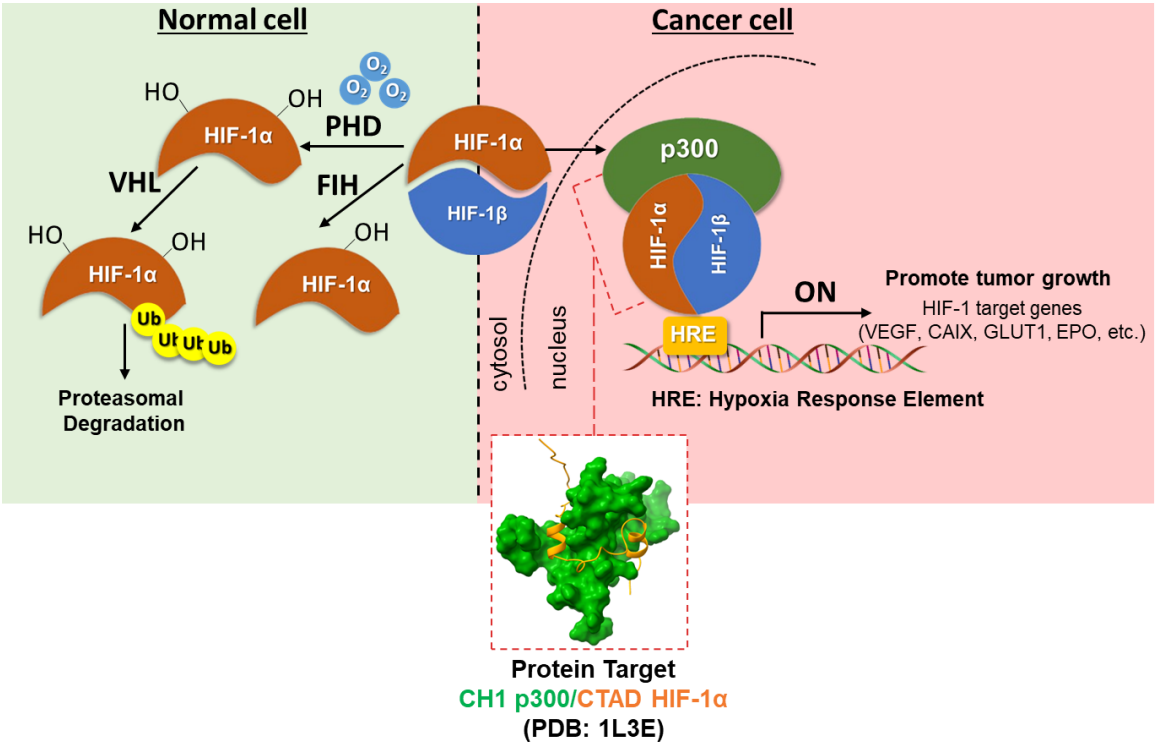

Figure 1-4. Regulation of HIF-1α signal pathway in cells

The transcriptional activity of HIF-1α depends on its interaction with coactivators, such as p300/CBP (CREB-binding protein). HIF-1α possesses two transactivation domains, namely the N-terminal activation domain (NTAD) and the C-terminal activation domain (CTAD), facilitating transcriptional activation in hypoxic conditions.[34–37] Only the HIF-$1\alpha^{782\text{-}826}$ (CTAD) has been shown to interact directly with coactivator proteins, such as CBP, via the cysteine/histidine-rich region 1 (CH1).[38,39] CH1 is triangular, consisting of four α-helices and three Zn^{2+}-coordinating centers. CH1 serves as a scaffold for folding the CTAD, which forms a vice-like clamp on the CH1 domain that is stabilized by extensive

hydrophobic and polar interactions. Structural studies provide a molecular basis for this interaction and identify two short α-helical domains, α_A and α_B, from HIF-1α as key determinants for its recognition by p300 (Figure 1-5).[39] High-resolution structures and computational alanine scan of the HIF-1α/p300 complex reveal that four helical residues from the HIF-1α $\alpha_B^{816–824}$ (Leu^{818}, Leu^{822}, Asp^{823}, and Gln^{824}) contribute to the binding energy as opposed to Leu^{819}.[40,41]

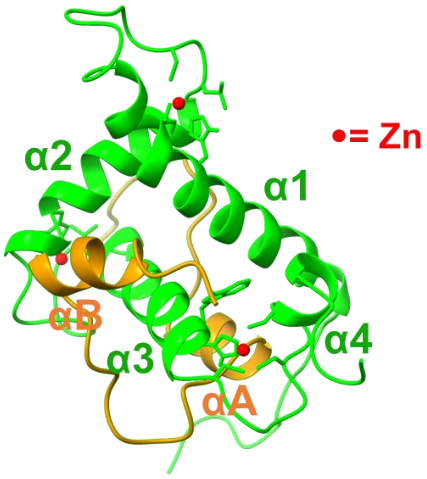

Figure 1-5. Ribbon model of CH1 p300/CTAD HIF-1α structure (PDB: 1L3E)

The p300 CH1 domain consists of four alpha helices and three zinc(II) coordination sites created by HCCC sequence motifs. The three elongated helices (labeled α1, α2, and α3) interlace to create an approximately triangular configuration. The three Zn^{2+} sites are positioned at the triangle's vertices, while the coordinating histidine and cysteine residues constituting the HCCC motif are located near the ends of the helices and between loops. The short C-terminal helix, α4, finalizes the third Zn^{2+} coordination site and aligns parallel to α1. The binding of Zn^{2+} contributes to the stabilization of the CH1 domain conformation. The CH1 fold is similarly stabilized by a singular hydrophobic core formed by all four helices. The unique open-packing arrangement of helices α1, α2, and α3 exposes substantial areas of the hydrophobic core. The exposed hydrophobic regions are situated on both sides of the domain and function as the principal recognition surface for the associated HIF-1α-CTAD. Thus, CTAD envelops the CH1 domain in a clamping manner. The CH1 and CTAD residue possess a common hydrophobic core, forming a unified structural domain.[39]

1.4 Drug development targeting HIF-1α/p300 interaction

Drug development targeting the HIF-1α/p300 interaction holds significant potential for regulating HIF target gene expression, especially tumor growth.[40–43] Disrupting the HIF-1α/p300 interaction using small molecules, peptides, or allosteric inhibitors could inhibit the pathological activation of hypoxia-driven genes, potentially limiting tumor progression.[44] However, targeting this pathway comes with challenges, such as ensuring specificity to avoid broad disruptions in other vital processes regulated by p300.[45]

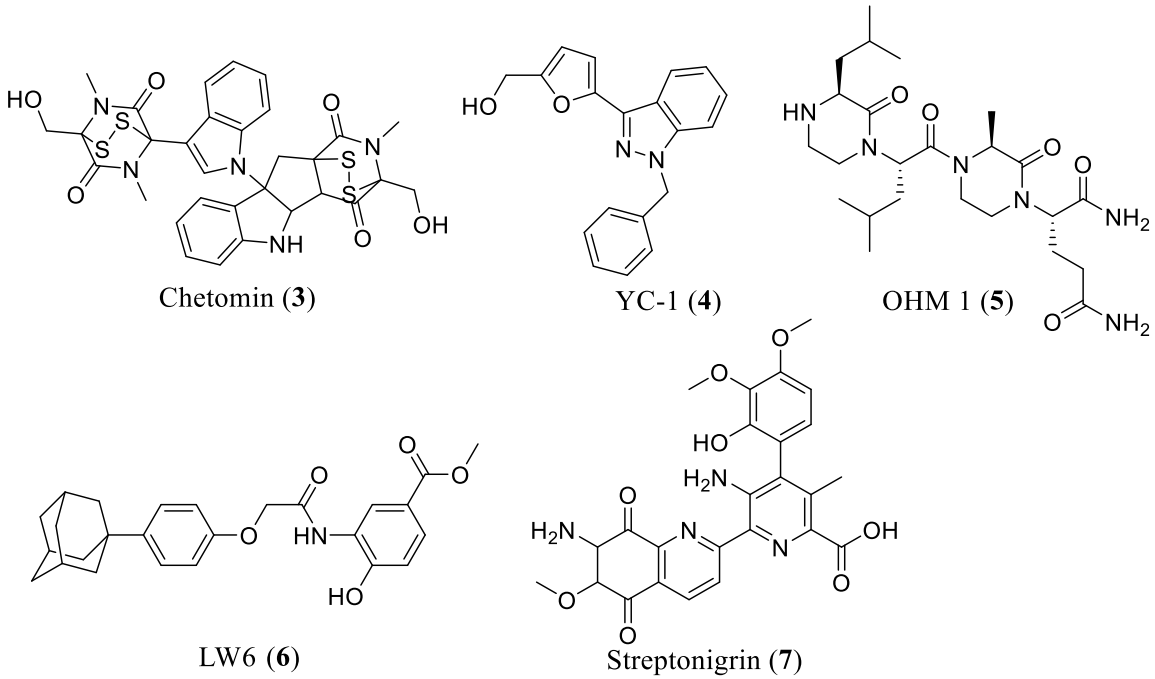

Figure 1-6. Small molecule HIF-1α/p300 PPI inhibitors

Currently, several small compounds have been identified as HIF-1α/p300 inhibitors (Figure 1-6), including chetomin (**3**) and lificiguat (YC-1, **4**).[46,47] Nonetheless, chetomin has local toxicity, and the specificity of YC-1 for HIF-1α is insufficient, constraining its therapeutic utility.[47,48] Oxopiperazine helix mimetic 1 (OHM 1, **5**), an analogue of HIF-1α CTAD, is reported to inhibit its interaction with p300/CBP. *In vivo* studies indicate that the compound can diminish the median tumor volume by around 50% relative to the untreated group.[40]

LW6 (**6**), an (aryloxyacetylamino)benzoic acid derivative, has activity to inhibit HIF-1α/p300 PPI with IC_{50} of 4.4 μM but has an issue in low oral bioavailability.[49] Streptonigrin (**7**) is a quinone-based antibiotic that has also been reported to inhibit HIF-1α/p300 PPI with IC_{50} of 3 μM by using an enzyme-linked immunosorbent assay (ELISA) competition assay.[50] Despite the HIF-1α/p300 interaction being a promising pharmacological target, there are currently no approved inhibitors for HIF-1α/p300.

1.5 Screening assay system for PPIs detection

The substrate binding pocket of proteins, which is the target of many drugs, is a distinct area where small molecules interact with the protein. A well-defined ligand-binding spot on these proteins lets small molecules attach and interact with them. The traditional approach to studying protein-ligand complex structures focuses on the structural or physico-chemical properties that are assumed to be unique to that particular pocket. Conversely, the PPI interface is often planar, and traditional medicinal chemistry techniques are less efficacious for designing and identifying PPI inhibitors.[10,21] Hence, developing more efficient methodologies for screening PPI inhibitors is essential.

Regarding HIF-1α/p300 PPI, several attempts have been made to develop screening assay systems for the discovery of HIF-1α inhibitors, such as cell-based luciferase reporter assay[51–53], ELISA[54], amplified luminescent proximity homogeneous assay screen (Alpha screen) assay[55], time-resolved fluorescence resonance energy transfer (TR-FRET) assay[56], Förster resonance energy transfer (FRET) assay[57], and fluorescence polarization (FP)/anisotropy(FA)-based assay[43,58]. Among these systems, FP/FA assays offer significant advantages in sensitivity, real-time monitoring, and direct measurement of HIF-1α PPIs, particularly compared to traditional screening methods like luciferase reporter assays or ELISA. These attributes make FP/FA suitable for drug screening and quantitative analysis of HIF-1α inhibitors, especially when targeting the HIF-1α/p300.

1.6 Fluorescence anisotropy (FA) assay system

In the 1950s, Weber developed the first instrument to measure FP and applied it to studying proteins.[59–61] To measure FP in the laboratory, a fluorescent sample is excited by polarized light and emission intensities are collected from channels that are parallel ($I_{\parallel}$) and perpendicular ($I_{\perp}$) to the electric vector of the excitation light (Figure 1-7).

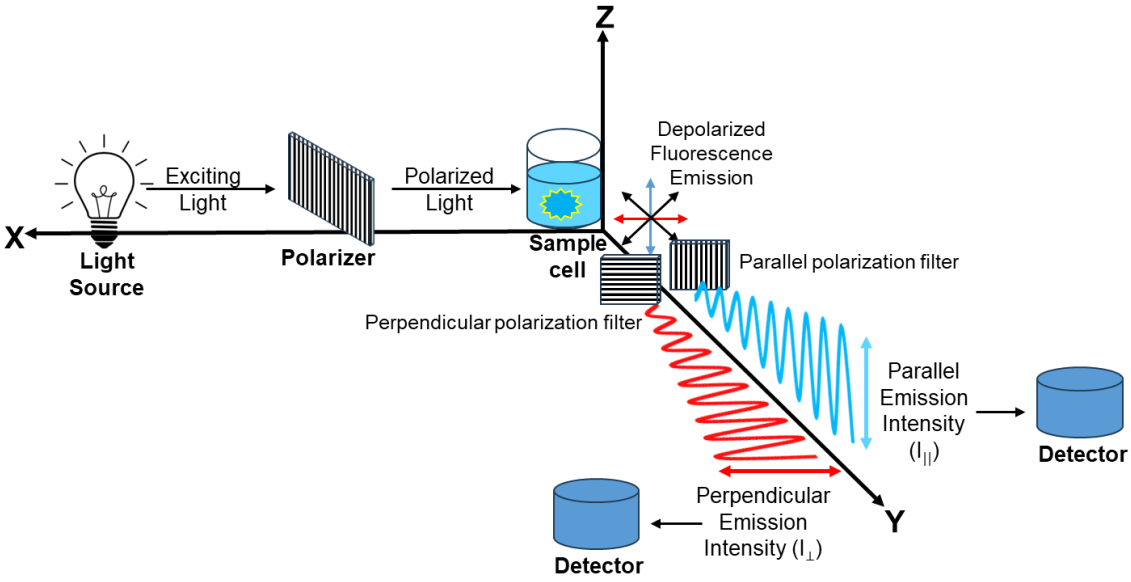

Figure 1-7. Schematic diagram of a fluorescence polarization instrument

These measurements can be used to calculate either FP or FA, which are both widely used. Equation (1) shows the calculation of FP or *P*, which is quantified as the difference between the parallel ($I_{\parallel}$) and perpendicular ($I_{\perp}$) emission intensities normalized by the total fluorescence intensity of the emission beam.

$$P = \frac{I_{\parallel} - I_{\perp}}{I_{\parallel} + I_{\perp}} \qquad (1)$$

Equation (2) defined FA or *r* as the difference between the parallel ($I_{\parallel}$) and perpendicular ($I_{\perp}$) emission intensities normalized by the total fluorescence intensity from the sample.

$$r = \frac{I_{\parallel} - I_{\perp}}{I_{\parallel} + 2I_{\perp}} \qquad (2)$$

FA does not provide any additional information over polarization, and both functions are commonly utilized. Although FP is referenced more frequently in the PubChem BioAssay database compared to FA, anisotropy is preferred because the deconvolution of anisotropy into its component values appears simpler than that of polarization, although the differences are minor.[62,63]

FP or FA is frequently employed in biological research to investigate interactions between proteins and peptides or proteins and nucleic acids. The fluorophore labeled on

the substrate is excited by the linearly polarized light through a polarization filter. When the substrate binds with a protein, the rotation of the fluorophore becomes slow, leading to polarized light emission. When a compound competes with the fluorophore-labeled substrate in binding to the protein, the fluorophore is released from the binding site, leading to depolarized light emission. FP is then measured as the difference of the emission light intensity parallel ($I_{\parallel}$) and perpendicular ($I_{\perp}$) to the excitation light plane normalized by the total fluorescence emission intensity (Figure 1-8).[64]

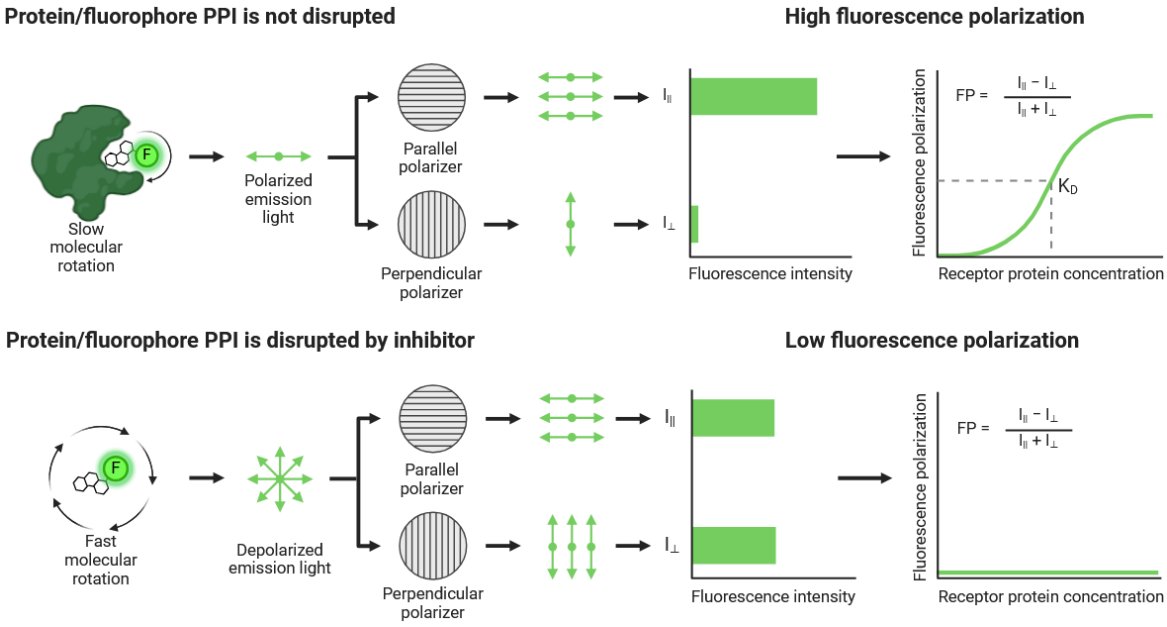

Figure 1-8. Principle of fluorescence polarization assay for PPI detection. The figure was created by Biorender.com.

FP/FA assay application in drug discovery targeting PPIs has been widely developed.[65–68] Due to its versatility to low volumes and simple procedure without separation or washing steps, FP/FA is particularly suitable for screening assay systems.[64] Recently, Zhou et al. developed a FP assay to screen cathepsin L (CTSL) inhibitor, which plays a role in the processing of the severe acute respiratory syndrome coronavirus 2 (SARS-CoV-2) spike protein, providing a potential avenue to block coronavirus host cell entry and thereby inhibit SARS-CoV-2 infection in humans. The optimized assay demonstrated its appropriateness for high-throughput screening (HTS) with a Z'-factor of 0.9 in a 96-well format. Upon screening over 2000 small molecules, they identified the anti-CTSL properties of a benzothiazole derivative named IMB 8015.[69]

Previous reports of FA assays for detecting HIF-1α/p300 inhibitors have focused on the interaction between the p300 CH1 domain (~12 kDa) and a CTAD peptide labeled with the fluorescein isothiocyanate (FITC).[41,43] However, these FA assays have not yet been applied for screening compound libraries targeting HIF-1α/p300 interactions.

1.7 Compound library for drug discovery

A compound library in drug discovery refers to a curated collection of diverse chemical compounds utilized for screening in the early stages of drug development. Compound libraries can be classified into several types, including targeted libraries[70], fragment-based libraries[71], natural product-derived libraries[72], and virtual libraries[73], each catering to specific chemical or pharmacological considerations. These libraries are often sourced from commercial providers, academic institutions, or custom synthesis efforts, emphasizing favorable drug-like properties, such as appropriate lipophilicity, solubility, and minimal toxicity.

The compound library used in this research is an in-house collection that includes carborane (dicarba-*closo*-dodecaborane) and a peptidomimetic compound with a (di)azatricyclododecene scaffold, both of which possess three-dimensional (3D) hydrophobic properties. Compound libraries based on 3D natural product scaffolds have demonstrated a wide range of biological activities.[78] Due to its unique 3D hydrophobic characteristics, carborane has attracted significant attention over the past two decades as a hydrophobic pharmacophore for drug discovery.[74–77] Additionally, the (di)azatricyclododecene scaffold, a sp^3 carbon-rich tricyclic 3D peptidomimetic structure, has been reported to inhibit HIF transcription activity, where α-helix peptide-mediated interactions play a pivotal role.[78,79]

In addition to the in-house compound library, an authentic curated collection of 80 compounds from the Natural Products Depository (NPDepo) at RIKEN, featuring extensively documented biological activities, was also used. This library included antibiotics, anticancer and anti-inflammatory drugs, as well as compounds with protein synthesis inhibitory and corticosteroid-like activities. The highly active compound library was utilized for efficient compound screening.

1.8 Purpose of study

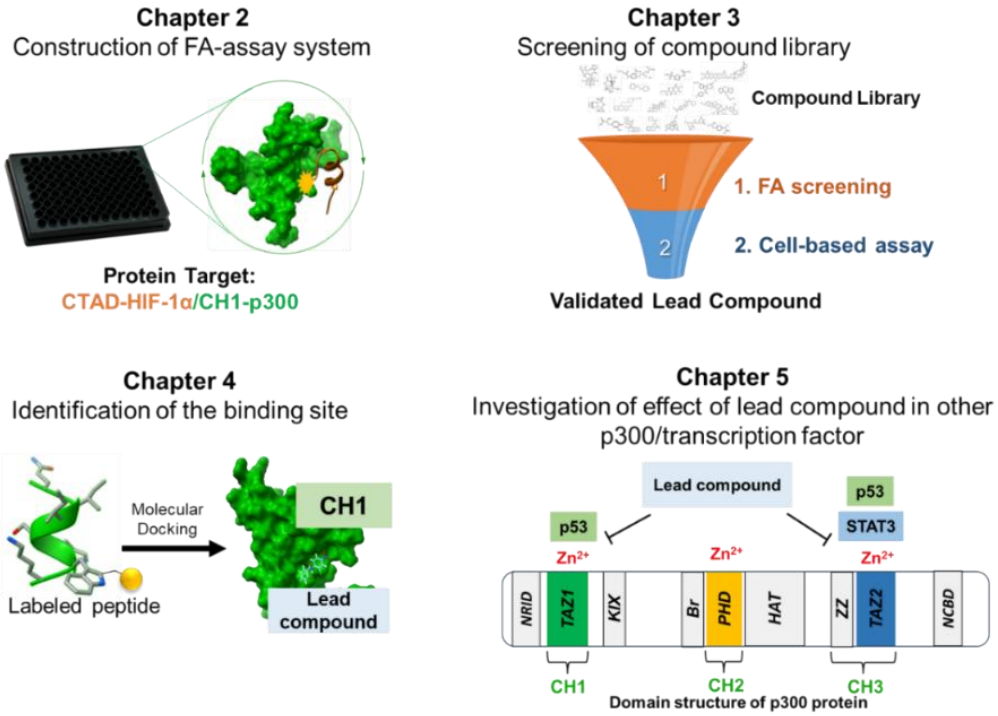

Figure 1-9. Overview of this study

This thesis is titled “Discovery of inhibitors targeting p300/transcription factors protein-protein interactions” and consists of the following six chapters.

In chapter 1, the significance of HIF-1α/p300 PPI as a cancer drug target is highlighted, along with drug development efforts targeting this interaction. It covers the HIF-1α/p300 PPI detection screening assay, the FA assay system, and the role of compound libraries in drug discovery. The chapter also discusses modifying the FA-based screening system and screening compound libraries to identify HIF-1α/p300 PPI inhibitors.

In chapter 2, “Construction of FA screening assay system for the discovery of HIF-1α/p300 PPI inhibitors,” this study aimed to construct and validate the FA screening assay system using several parameters such as binding affinity measurements, competition assay using unlabeled peptide and positive control and determination of Z′-factor value.

In chapter 3, “Screening of compound library using constructed assay system and validation of lead compounds as HIF-1α/p300 PPI inhibitors,” this study aimed to screen the compound library using the established FA assay and validate the lead compound using cell-based assay system.

In chapter 4, “Identification of the binding site of niclosamide using photoaffinity labeling,” this study aimed to identify binding site of the lead compound using photoaffinity labeling and molecular docking.

In chapter 5, “Investigation of the effect of niclosamide in other p300/transcription factor protein-protein interaction,” this study aimed to further investigate lead compound as inhibitor targeting p300/transcription factors PPIs.

Chapter 6 summarizes the thesis.

1.9 References

(1) Crick, F. Central Dogma of Molecular Biology, *Nature* **1970**, *227*, 561-563.

(2) Venkatesan, K.; Rual, J. F.; Vazquez, A.; Stelzl, U.; Lemmens, I.; Hirozane-Kishikawa, T.; Hao, T.; Zenkner, M.; Xin, X.; Goh, K. Il; Yildirim, M. A.; Simonis, N.; Heinzmann, K.; Gebreab, F.; Sahalie, J. M.; Cevik, S.; Simon, C.; de Smet, A. S.; Dann, E.; Smolyar, A.; Vinayagam, A.; Yu, H.; Szeto, D.; Borick, H.; Dricot, A.; Klitgord, N.; Murray, R. R.; Lin, C.; Lalowski, M.; Timm, J.; Rau, K.; Boone, C.; Braun, P.; Cusick, M. E.; Roth, F. P.; Hill, D. E.; Tavernier, J.; Wanker, E. E.; Barabási, A. L.; Vidal, M. An Empirical Framework for Binary Interactome Mapping. *Nat. Methods.* **2009**, *6* (1), 83-90.

(3) Koh, G. C. K. W.; Porras, P.; Aranda, B.; Hermjakob, H.; Orchard, S. E. Analyzing Protein-Protein Interaction Networks. *J. Proteome Res.* **2012**, *11* (4), 2014-2031.

(4) Westermarck, J.; Ivaska, J.; Corthals, G. L. Identification of Protein Interactions Involved in Cellular Signaling. *Mol. Cell. Proteom*. **2013**, *12* (7), 1752-1763.

(5) He, Y.; Sun, M. M.; Zhang, G. G.; Yang, J.; Chen, K. S.; Xu, W. W.; Li, B. Targeting PI3K/Akt Signal Transduction for Cancer Therapy. *Signal Transduct. Target. Ther.* **2021**, *6* (425), 1-17.

(6) Hennessy, B. T.; Smith, D. L.; Ram, P. T.; Lu, Y.; Mills, G. B. Exploiting the PI3K/AKT Pathway for Cancer Drug Discovery. *Nat. Rev. Drug Discov.* **2005**, *4*, 988-1004.

(7) Wu, D.; Li, Y.; Zheng, L.; Xiao, H.; Ouyang, L.; Wang, G.; Sun, Q. Small Molecules Targeting Protein–Protein Interactions for Cancer Therapy. *Acta Pharm. Sin. B.* **2023**, *13* (10), 4060-4088.

(8) Ni, D.; Lu, S.; Zhang, J. Emerging Roles of Allosteric Modulators in the Regulation of Protein-Protein Interactions (PPIs): A New Paradigm for PPI Drug Discovery. *Med. Res. Rev*. **2019**, *39*, 2314-2342.

(9) Cossins, B. P.; Lawson, A. D. G. Small Molecule Targeting of Protein-Protein Interactions through Allosteric Modulation of Dynamics. *Molecules* **2015**, *20* (9), 16435-16445.

(10) Lu, H.; Zhou, Q.; He, J.; Jiang, Z.; Peng, C.; Tong, R.; Shi, J. Recent Advances in the Development of Protein–Protein Interactions Modulators: Mechanisms and Clinical Trials. *Signal Transduct. Target Ther*. **2020**, *5* (213), 1-23.

(11) Lu, R. M.; Hwang, Y. C.; Liu, I. J.; Lee, C. C.; Tsai, H. Z.; Li, H. J.; Wu, H. C. Development of Therapeutic Antibodies for the Treatment of Diseases. *J. Biomed. Sci*. **2020**, *27* (1), 1-30.

(12) Beck, A.; Wurch, T.; Bailly, C.; Corvaia, N. Strategies and Challenges for the next Generation of Therapeutic Antibodies. *Nat. Rev. Immunol.* **2010**, *10*, 345-352.

(13) Fosgerau, K.; Hoffmann, T. Peptide Therapeutics: Current Status and Future Directions. *Drug Discov. Today* **2015**, *20* (1), 122-128.

(14) Jesús Pérez De Vega, M.; Martín-Martínez, M.; González-Muñiz, R. Modulation of Protein-Protein Interactions by Stabilizing/Mimicking Protein Secondary Structure Elements; *Curr. Top. Med. Chem.* **2007**, *7* (1), 33-62.

(15) Nero, T. L.; Morton, C. J.; Holien, J. K.; Wielens, J.; Parker, M. W. Oncogenic Protein Interfaces: Small Molecules, Big Challenges. *Nat. Rev. Cancer* **2014**, *14*, 248-262.

(16) Sheng, C.; Dong, G.; Miao, Z.; Zhang, W.; Wang, W. State-of-the-Art Strategies for Targeting Protein-Protein Interactions by Small-Molecule Inhibitors. *Chem. Soc. Rev.* **2015**, *44*, 8238-8259.

(17) Jones, S.; Thornton, J. M. Principles of Protein-Protein Interactions. *Proc. Natl. Acad. Sci. U S A* **1996**, *93*, 13-20.

(18) Smith, M. C.; Gestwicki, J. E. Features of Protein-Protein Interactions That Translate into Potent Inhibitors: Topology, Surface Area and Affinity. *Expert. Rev. Mol. Med.* **2012**, *14*, 1-20.

(19) Jochim, A. L.; Arora, P. S. Systematic Analysis of Helical Protein Interfaces Reveals Targets for Synthetic Inhibitors. *ACS Chem. Biol.* **2010**, *5* (10), 919-923.

(20) Ivanov, A. A.; Khuri, F. R.; Fu, H. Targeting Protein-Protein Interactions as an Anticancer Strategy. *Trends Pharmacol. Sci.* **2013**, *34* (7), 393-400.

(21) Arkin, M. M. R.; Wells, J. A. Small-Molecule Inhibitors of Protein-Protein Interactions: Progressing towards the Dream. *Nat Rev Drug Discov.* **2004**, *3* (4), 301-317.

(22) Wells, J. A.; McClendon, C. L. Reaching for High-Hanging Fruit in Drug Discovery at Protein-Protein Interfaces. *Nature* **2007**, *450* (7172), 1001-1009.

(23) Birkinshaw, R. W.; Gong, J. nan; Luo, C. S.; Lio, D.; White, C. A.; Anderson, M. A.; Blombery, P.; Lessene, G.; Majewski, I. J.; Thijssen, R.; Roberts, A. W.; Huang, D. C. S.; Colman, P. M.; Czabotar, P. E. Structures of BCL-2 in Complex with Venetoclax Reveal the Molecular Basis of Resistance Mutations. *Nat. Commun.* **2019**, *10* (1), 1-10.

(24) Khurana, A.; Shafer, D. A. MDM2 Antagonists as a Novel Treatment Option for Acute Myeloid Leukemia: Perspectives on the Therapeutic Potential of Idasanutlin (RG7388). *Onco. Targets Ther.* **2019**, *12*, 2903-2910.

(25) Huang, L. E.; Gu, J.; Schau, M.; Franklin Bunn, H. Regulation of Hypoxia-Inducible Factor 1 Is Mediated by an O 2-Dependent Degradation Domain via the Ubiquitin-Proteasome Pathway. *Proc. Natl. Acad. Sci. U S A* **1998**, *95* (14), 7987-7992.

(26) Mole, D. R.; Maxwell, P. H.; Pugh, C. W.; Ratcliffe, P. J. Regulation of HIF by the von Hippel-Lindau Tumour Suppressor: Implications for Cellular Oxygen Sensing. *IUBMB Life* **2001**, *52*, 43-47.

(27) Semenzas, G. L.; Roth, P. H.; Fang, H.-M.; Wang, G. L. Transcriptional Regulation of Genes Encoding Glycolytic Enzymes by Hypoxia-Inducible Factor 1. *J. Biol. Chem.* **1994**, *269* (38), 23757-23763.

(28) Wang, G. L.; Semenzas, G. L. Characterization of Hypoxia-Inducible Factor 1 and Regulation of DNA Binding Activity by Hypoxia. *J. Biol. Chem.* **1993**, *268* (29), 21513-21518.

(29) Jiang, B. H.; Rue, E.; Wang, G. L.; Roe, R.; Semenza, G. L. Dimerization, DNA Binding, and Transactivation Properties of Hypoxia- Inducible Factor 1. *J. Biol. Chem.* **1996**, *271* (30), 17771-17778.

(30) Wicks, E. E.; Semenza, G. L. Hypoxia-Inducible Factors: Cancer Progression and Clinical Translation. *J. Clin. Investig.* **2022**, *132* (11), e159839.

(31) Lee, C. C.; Wu, C. Y.; Yang, H. Y. Discoveries of How Cells Sense Oxygen Win the 2019 Nobel Prize in Physiology or Medicine. *Biomed. J.* **2020**, *43* (5), 434-437.

(32) Ratcliffe, P. J. Oxygen Sensing and Hypoxia Signalling Pathways in Animals: The Implications of Physiology for Cancer. *J. Physiol.* **2013**, *591* (8), 2027-2042.

(33) Kaelin, W. G.; Ratcliffe, P. J. Oxygen Sensing by Metazoans: The Central Role of the HIF Hydroxylase Pathway. *Mol. Cell.* **2008**, *30* (4), 393-402.

(34) Pugh, C. W.; O'Rourke, J. F.; Nagao, M.; Gleadle, J. M.; Ratcliffe, P. J. Activation of Hypoxia-Inducible Factor-1; Definition of Regulatory Domains within the α Subunit. *J. Biol. Chem.* **1997**, *272* (17), 11205-11214.

(35) Jiang, B. H.; Zheng, J. Z.; Leung, S. W.; Roe, R.; Semenza, G. L. Transactivation and Inhibitory Domains of Hypoxia-Inducible Factor 1α: Modulation of Transcriptional Activity by Oxygen Tension. *J. Biol. Chem.* **1997**, *272* (31), 19253-19260.

(36) Carrero, P.; Okamoto, K.; Coumailleau, P.; O'Brien, S.; Tanaka, H.; Poellinger, L. Redox-Regulated Recruitment of the Transcriptional Coactivators CREB-Binding Protein and SRC-1 to Hypoxia-Inducible Factor 1α. *Mol. Cell. Biol.* **2000**, *20* (1), 402-415.

(37) Ema, M.; Hirota, K.; Mimura, J.; Abe, H.; Yodoi, J.; Sogawa, K.; Poellinger, L.; Fujii-Kuriyama, Y. Molecular Mechanisms of Transcription Activation by HLF and HIF1α in Response to Hypoxia: Their Stabilization and Redox Signal-Induced Interaction with CBP/p300. *EMBO J.* **1999**, *18* (7),1905-1914.

(38) Ruas, J. L.; Berchner-Pfannschmidt, U.; Malik, S.; Gradin, K.; Fandrey, J.; Roeder, R. G.; Pereira, T.; Poellinger, L. Complex Regulation of the Transactivation Function of Hypoxia-Inducible Factor-1αby Direct Interaction with Two Distinct Domains of the Creb-Binding Protein/p300. *J. Biol. Chem.* **2010**, *285* (4), 2601-2609.

(39) Freedman, S. J.; Sun, Z.-Y. J.; Poy, F.; Kung, A. L.; Livingston, D. M.; Wagner, G.; Eck, M. J. Structural Basis for Recruitment of CBPp300 by Hypoxia-Inducible Factor-1. *Proc. Natl. Acad. Sci. U S A.* **2002**, *99* (8), 5367-5372.

(40) Lao, B. B.; Grishagin, I.; Mesallati, H.; Brewer, T. F.; Olenyuk, B. Z.; Arora, P. S. In Vivo Modulation of Hypoxia-Inducible Signaling by Topographical Helix Mimetics. *Proc. Natl. Acad. Sci. U S A.* **2014**, *111* (21), 7531-7536.

(41) Kushal, S.; Lao, B. B.; Henchey, L. K.; Dubey, R.; Mesallati, H.; Traaseth, N. J.; Olenyuk, B. Z.; Arora, P. S. Protein Domain Mimetics as in Vivo Modulators of Hypoxia-Inducible Factor Signaling. *Proc. Natl. Acad. Sci. U S A.* **2013**, *110* (39), 15602-15607.

(42) Henchey, L. K.; Kushal, S.; Dubey, R.; Chapman, R. N.; Olenyuk, B. Z.; Arora, P. S. Inhibition of Hypoxia Inducible Factor 1-Transcription Coactivator Interaction by a Hydrogen Bond Surrogate α-Helix. *J. Am. Chem. Soc.* **2010**, *132* (3), 941-943.

(43) Burslem, G. M.; Kyle, H. F.; Breeze, A. L.; Edwards, T. A.; Nelson, A.; Warriner, S. L.; Wilson, A. J. Small-Molecule Proteomimetic Inhibitors of the HIF-1α-p300 Protein-Protein Interaction. *ChemBioChem.* **2014**, *15* (8), 1083-1087.

(44) Qin, X.; Chen, H.; Tu, L.; Ma, Y.; Liu, N.; Zhang, H.; Li, D.; Riedl, B.; Bierer, D.; Yin, F.; Li, Z. Potent Inhibition of HIF1α and p300 Interaction by a Constrained Peptide Derived from CITED2. *J. Med. Chem.* **2021**, *64* (18), 13693-13703.

(45) Qannita, R. A.; Alalami, A. I.; Harb, A. A.; Aleidi, S. M.; Taneera, J.; Abu-Gharbieh, E.; El-Huneidi, W.; Saleh, M. A.; Alzoubi, K. H.; Semreen, M. H.; Hudaib, M.; Bustanji, Y. Targeting Hypoxia-Inducible Factor-1 (HIF-1) in Cancer: Emerging Therapeutic Strategies and Pathway Regulation. *Pharmaceuticals* **2024**, *17* (2), 195.

(46) Viziteu, E.; Grandmougin, C.; Goldschmidt, H.; Seckinger, A.; Hose, D.; Klein, B.; Moreaux, J. Chetomin, Targeting HIF-1α/p300 Complex, Exhibits Antitumour Activity in Multiple Myeloma. *Br. J. Cancer* **2016**, *114* (5), 519-523.

(47) Shan, H. L.; Dong, H. S.; Chun, Y. S.; Myung, K. L.; Kim, M. S.; Park, J. W. A Novel Mode of Action of YC-1 in HIF Inhibition: Stimulation of FIH-Dependent p300 Dissociation from HIF-1α. *Mol. Cancer Ther.* **2008**, *7* (12), 3729–3738.

(48) Kung, A. L.; Zabludoff, S. D.; France, D. S.; Freedman, S. J.; Tanner, E. A.; Vieira, A.; Cornell-Kennon, S.; Lee, J.; Wang, B.; Wang, J.; Memmert, K.; Naegeli, H.-U.; Petersen, F.; Eck, M. J.; Bair, K. W.; Wood, A. W.; Livingston, D. M. Small Molecule Blockade of Transcriptional Coactivation of the Hypoxia-Inducible Factor Pathway. *Cancer Cell.* **2004**, *6*, 33-43.

(49) Lee, J. Y.; Lee, K.; Lee, K.; Kang, J. S.; Kim, M. J.; Yoo, D. G.; Kim, J. A.; Shin, E. J.; Oh, S. J. Pharmacokinetic Characterization of Lw6, a Novel Hypoxia-Inducible Factor-1α (HIF-1α) Inhibitor in Mice. *Molecules* **2021**, *26* (8), 2608-2226.

(50) Jayatunga, M. K. P.; Thompson, S.; McKee, T. C.; Chan, M. C.; Reece, K. M.; Hardy, A. P.; Sekirnik, R.; Seden, P. T.; Cook, K. M.; McMahon, J. B.; Figg, W. D.; Schofield, C. J.; Hamilton, A. D. Inhibition of the HIF1α-p300 Interaction by Quinone- and Indandione-Mediated Ejection of Structural Zn(II). *Eur. J. Med. Chem.* **2015**, *94*, 509-516.

(51) Tsujita, T.; Kawaguchi, S. I.; Dan, T.; Baird, L.; Miyata, T.; Yamamoto, M. Hypoxia-Sensitive Reporter System for High-Throughput Screening. *Tohoku J. Exp. Med.* **2015**, *235* (2), 151-159.

(52) Lu, Y.; Madu, C.; Masters, J.; Lu, A.; Li, L. Development of a Novel Anti-HIF-Lα Screening System Coupled with Biochemical and Biological Validation for Rapidly Selecting Potent Anti-Cancer Compounds. *J. Cancer* **2014**, *5* (6), 417-424.

(53) Tan, C.; De Noronha, R. G.; Devi, N. S.; Jabbar, A. A.; Kaluz, S.; Liu, Y.; Mooring, S. R.; Nicolaou, K. C.; Wang, B.; Van Meir, E. G. Sulfonamides as a New Scaffold for Hypoxia Inducible Factor Pathway Inhibitors. *Bioorg. Med. Chem. Lett.* **2011**, *21* (18), 5528-5532.

(54) Park, S. R.; Kinders, R. J.; Khin, S.; Hollingshead, M.; Antony, S.; Parchment, R. E.; Tomaszewski, J. E.; Kummar, S.; Doroshow, J. H. Validation of a Hypoxia-Inducible Factor-1 Alpha Specimen Collection Procedure and Quantitative Enzyme-Linked Immunosorbent Assay in Solid Tumor Tissues. *Anal. Biochem.* **2014**, *459*, 1-11.

(55) Chowdhury, R.; Candela-Lena, J. I.; Chan, M. C.; Greenald, D. J.; Yeoh, K. K.; Tian, Y. M.; McDonough, M. A.; Tumber, A.; Rose, N. R.; Conejo-Garcia, A.; Demetriades, M.; Mathavan, S.; Kawamura, A.; Lee, M. K.; Van Eeden, F.; Pugh, C. W.; Ratcliffe, P. J.; Schofield, C. J. Selective Small Molecule Probes for the Hypoxia Inducible Factor (HIF) Prolyl Hydroxylases. *ACS Chem. Biol.* **2013**, *8* (7), 1488-1496.

(56) Dao, J. H.; Kurzeja, R. J. M.; Morachis, J. M.; Veith, H.; Lewis, J.; Yu, V.; Tegley, C. M.; Tagari, P. Kinetic Characterization and Identification of a Novel Inhibitor of Hypoxia-Inducible Factor Prolyl Hydroxylase 2 Using a Time-Resolved Fluorescence Resonance Energy Transfer-Based Assay Technology. *Anal. Biochem.* **2009**, *384* (2), 213-223.

(57) Youssef, S.; Ren, W.; Ai, H. W. A Genetically Encoded FRET Sensor for Hypoxia and Prolyl Hydroxylases. *ACS Chem. Biol.* **2016**, *11* (9), 2492-2498.

(58) Lee, M. J.; Kim, J. W.; Yang, E. G. Hinokitiol Activates the Hypoxia-Inducible Factor (HIF) Pathway through Inhibition of HIF Hydroxylases. *Biochem. Biophys. Res. Commun.* **2010**, *396* (2), 370-375.

(59) Weber, G. Polarization of the fluorescence of macromolecules. 1. Theory and experimental method. *Biochem. J.* **1952**, *51* (2), 145-155.

(60) Weber, G. Polarization of the fluorescence of macromolecules 2. Fluorescent Conjugates of Ovalbumin And Bovine Serum Albumin, *Biochem. J* **1952**, *51* (2), 155-167.

(61) Weber, G. Photoelectric Method for the Measurement of the Polarization of the Fluorescence of Solutions. *J. Opt. Soc. Am.* **1956**, *46* (11), 962-970.

(62) Jameson, D. M.; Mocz, G. Fluorescence Polarization/Anisotropy Approaches to Study Protein-Ligand Interactions: Effects of Errors and Uncertainties. *Methods Mol. Biol.* **2005**, *305*, 301-322.

(63) Inoyama, D.; Chen, Y.; Huang, X.; Beamer, L. J.; Kong, A. N. T.; Hu, L. Optimization of Fluorescently Labeled Nrf2 Peptide Probes and the Development of a Fluorescence Polarization Assay for the Discovery of Inhibitors of Keap1-Nrf2 Interaction. *J. Biomol. Screen.* **2012**, *17* (4), 435-447.

(64) Lea, W. A.; Simeonov, A. Fluorescence Polarization Assays in Small Molecule Screening. *Expert. Opin. Drug Discov.* **2011**, *6* (1), 17-32.

(65) Cisneros, J. A.; Robertson, M. J.; Valhondo, M.; Jorgensen, W. L. A Fluorescence Polarization Assay for Binding to Macrophage Migration Inhibitory Factor and Crystal Structures for Complexes of Two Potent Inhibitors. *J. Am. Chem. Soc.* **2016**, *138* (27), 8630-8638.

(66) Zhu, M. R.; Du, D. H.; Hu, J. C.; Li, L. C.; Liu, J. Q.; Ding, H.; Kong, X. Q.; Jiang, H. L.; Chen, K. X.; Luo, C. Development of a High-Throughput Fluorescence

Polarization Assay for the Discovery of EZH2-EED Interaction Inhibitors. *Acta Pharmacol. Sin.* **2018**, *39* (2), 302-310.

(67) Boes, A.; Olatunji, S.; Mohammadi, T.; Breukink, E.; Terrak, M. Fluorescence Anisotropy Assays for High Throughput Screening of Compounds Binding to Lipid II, PBP1b, FtsW and MurJ. *Sci. Rep.* **2020**, *10* (1), 1-8.

(68) Nikolovska-Coleska, Z.; Wang, R.; Fang, X.; Pan, H.; Tomita, Y.; Li, P.; Roller, P. P.; Krajewski, K.; Saito, N. G.; Stuckey, J. A.; Wang, S. Development and Optimization of a Binding Assay for the XIAP BIR3 Domain Using Fluorescence Polarization. *Anal. Biochem.* **2004**, *332* (2), 261-273.

(69) Zhou, W.; You, B.; Zhao, X.; Si, S.; Li, Y.; Zhang, J. Establishment, Optimization and Validation of a Fluorescence Polarization-Based High-Throughput Screening Assay Targeting Cathepsin L Inhibitors. *SLAS Discov.* **2024**, *29* (3), 100153.

(70) Harris, C. J.; Hill, R. D.; Sheppard, D. W.; Slater, M. J.; Stouten, P. F. W. The Design and Application of Target-Focused Compound Libraries. *Comb. Chem. High Throughput Screen.* **2011**, *14* (6), 521-531.

(71) Erlanson, D. A.; Fesik, S. W.; Hubbard, R. E.; Jahnke, W.; Jhoti, H. Twenty Years on: The Impact of Fragments on Drug Discovery. *Nat. Rev. Drug Discov.* **2016**, *15*, 605-619.

(72) Wilson, B. A. P.; Thornburg, C. C.; Henrich, C. J.; Grkovic, T.; O'Keefe, B. R. Creating and Screening Natural Product Libraries. *Nat. Prod. Rep.* **2020**, *37* (7), 893-918.

(73) Van Hilten, N.; Chevillard, F.; Kolb, P. Virtual Compound Libraries in Computer-Assisted Drug Discovery. *J. Chem. Inf. Model.* **2019**, *59* (2), 644-651.

(74) Scholz, M.; Hey-Hawkins, E. Carbaboranes as Pharmacophores: Properties, Synthesis, and Application Strategies. *Chem. Rev.* **2011**, *111* (11), 7035-7062.

(75) Leśnikowski, Z. J. Challenges and Opportunities for the Application of Boron Clusters in Drug Design. *J. Med. Chem.* **2016**, *59* (17), 7738-7758.

(76) Stockmann, P.; Gozzi, M.; Kuhnert, R.; Sárosi, M. B.; Hey-Hawkins, E. New Keys for Old Locks: Carborane-Containing Drugs as Platforms for Mechanism-Based Therapies. *Chem. Soc. Rev.* **2019**, *48*, 3497-3512.

(77) Asawa, Y.; Hatsuzawa, S.; Yoshimori, A.; Yamada, K.; Katoh, A.; Kouji, H.; Nakamura, H. Comprehensive Exploration of Chemical Space Using Trisubstituted Carboranes. *Sci. Rep.* **2021**, *11* (1).

(78) Tajabadi, F. M.; Pouwer, R. H.; Liu, M.; Dashti, Y.; Campitelli, M. R.; Murtaza, M.; Mellick, G. D.; Wood, S. A.; Jenkins, I. D.; Quinn, R. J. Design and Synthesis of Natural Product Inspired Libraries Based on the Three-Dimensional (3D) Cedrane Scaffold: Toward the Exploration of 3D Biological Space. *J. Med. Chem.* **2018**, *61* (15), 6609-6628.

(79) Umedera, K.; Morita, T.; Yoshimori, A.; Yamada, K.; Katoh, A.; Kouji, H.; Nakamura, H. Synthesis of Three-Dimensional (Di)Azatricyclododecene Scaffold and Its Application to Peptidomimetics. *Chem. - Eur. J.* **2021**, *27* (46), 11888-11894.

Chapter 2

Construction of Fluorescence Anisotropy Screening Assay System for the Discovery of HIF-1α/p300 PPI Inhibitors

2.1 Introduction

As mentioned in chapter 1, the HIF-1α/p300 interaction is one of many PPIs that represent a promising drug target. The identification of small molecules that can selectively disrupt this interaction holds immense promise for cancer therapy. To date, there are several small molecules reported as HIF-1α/p300 inhibitors, such as chetomin and YC-1.[1,2] However, chetomin has been found to have local toxicity, and the specificity of YC-1 for HIF-1α is not high, limiting its clinical application.[2,3] OHM 1, an analogue of HIF-1α CTAD, is reported to inhibit its binding with p300/CBP, and the *in vivo* study shows that the compound can reduce the median tumor volume by roughly 50% compared to the untreated group.[4] Although the HIF-1α/p300 interaction is a promising drug target, there are no approved HIF-1α/p300 inhibitors to date.

FA-based assay systems are excellent methods for measuring interactions between proteins and peptides. The concept asserts that a fluorophore stimulated by polarised light produces partially polarised emission.[5] Kushal et al. reported FA-based assays for detecting HIF-1α/p300 inhibitors using p300 CH1 protein (~12 kDa) with fluorescein-labeled CTAD (41 amino acid residues) and identified protein domain mimetic peptides.[6] Although this method could detect the HIF-1α/p300 interaction, the fluorophore is limited by its high photobleaching rate and noise background.

In this study, the FA-based screening system using a dansyl group as a fluorophore were designed to improve photostability[7,8] and reduce interference from the excitation source and background autofluorescence.[9] The peptides based on the CTAD (45 amino acid residues) and HIF-1α α_B (15 amino acid residues) regions of HIF-1α were synthesized using Fmoc solid-phase synthesis. CTAD and HIF-1α α_B's N-terminus were labeled with a dansyl fluorophore. The screening assay system was validated using competitive binding to the p300 CH1 protein with an unlabeled peptide, reported HIF-1α/p300 inhibitors, and the determination of statistical criteria Z' factor.

2.2 Vector construction for overexpression of human p300 CH1 protein

Protein expression was achieved by a recombinant expression system in *E. coli*. In this research, human p300 CH1 domain (amino acid residues 323-423) gene was amplified from the HeLa cell cDNA library by PCR (Figure 2-1, Lane 3). The p300 CH1 gene and pGEX-6p-1 vectors were treated with restriction enzymes (XhoI and EcoRI) (Figure 2-1, Lane 2 and 3). The pGEX-6p-1 vector was treated with CIAP (Calf-intestinal alkaline phosphatase) to dephosphorylate it and prevent self-ligation prior to ligation.

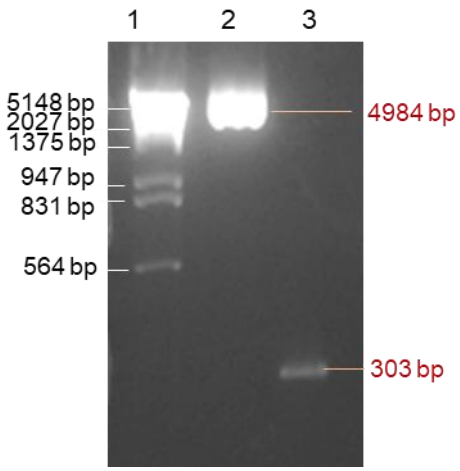

Figure 2-1. Electrophoresis result of amplified p300 CH1 gene and pGEX-6p-1 vector with restriction enzymes treatment. (4% agarose gel, 100 V, 45 min, stained by EtBr). Lane 1: DNA ladder; Lane 2: restriction enzyme treated pGEX-6p-1 vector; Lane 3: amplified p300 CH1 gene.

After vector preparation, the pGEX-6p-1 vector and the p300 CH1 gene were ligated and transformed into *E. coli* JM 109 strain. The recombinant vector was re-transformed into *E. coli* (SHuffle T7 Express) competent cell and verified by performing EcoRI and XhoI restriction enzymes (Figure 2-2). It is shown that the band intensity of the pGEX-6p-1 vector has high intensity while the p300 CH1 gene showed a low-intensity band. The recombinant vector was confirmed by DNA sequence analysis.

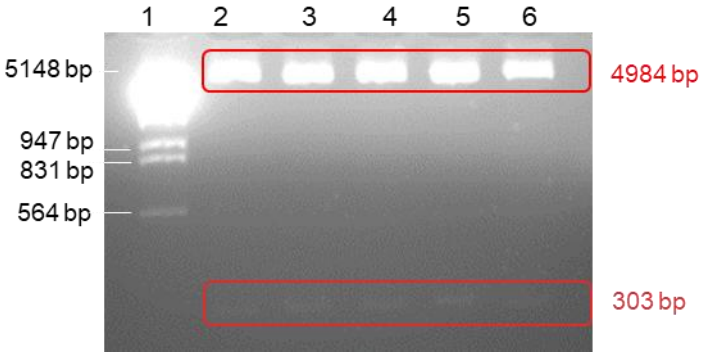

Figure 2-2. Electrophoresis result of digestion of pGEX-6P-1 plasmid (4,984 bp) containing p300 CH1 gene (303 bp) by EcoRI and XhoI restriction enzymes (4% agarose gel, 100 V, 45 min, stained by EtBr). Lane 1: DNA ladder; Lane 2-6: Cut check 1-5 (recombinant vector with enzyme, pGEX-6p-1 vector (4,984 bp) and p300 CH1 gene (303 bp)).

2.3 Protein expression and purification of human p300 CH1 protein from *E. coli*

Protein expression and purification of recombinant human p300 CH1 protein from *E coli* were performed according to previous report.[10] The p300 CH1 protein contains three zinc finger structures and nine total cysteine residues, presenting many challenges for recombinant protein purification. The p300 CH1 has been reported to be structurally compromised without a 3:1 stoichiometric ratio of Zn.[11] Without Zn ion, cysteine residues typically found at Zn fingers can form unwanted disulfide linkages that are thermodynamically more stable than cysteine-Zn ion interactions, resulting in unwanted protein conformations and aggregation.[10] Thus, protein expression and purification of recombinant human p300 CH1 protein from *E. coli* was conducted in the presence of Zn ion.

In this work, as much as 0.394 mg of purified recombinant p300 CH1 protein was successfully produced from a 200 mL bacterial culture. This work was confirmed by SDS-PAGE, as shown in Figure 2-3. The purified protein was shown in lanes 10 and 11 at 11 kDa. The protein was stored in a solution of 50 mM Tris-HCl (pH = 8.0), 150 mM NaCl, and 25% glycerol at -80 °C.

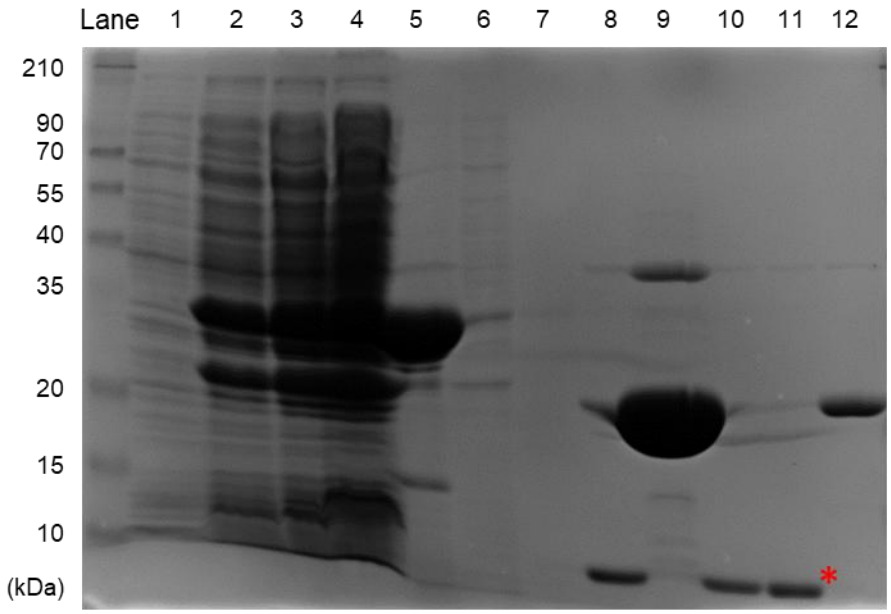

Figure 2-3. Purification of recombinant human p300 CH1 protein from *E. coli* and coomassie staining of purified recombinant human p300 CH1 protein after SDS-PAGE. Lane 1: *E. coli* total protein (No stimulation with IPTG); Lane 2: *E. coli* total protein (Stimulation with IPTG before lysis); Lane 3: *E. coli* lysate (Stimulation with IPTG after

lysis); Lane 4: Clarified bacterial lysate after capture; Lane 5: Beads fraction (GST-proteins including GST-conjugated p300 CH1 protein = 36 kDa); Lane 6-7: Beads wash fraction; Lane 8: Protease-treated fractions for GST cleavage (p300 CH1 protein and free GST); Lane 9: Bead fraction with p300 CH1 protein released (GST=25 kDa and Protease= ~40 kDa); 10-11: Purified p300 CH1 protein (11 kDa); 12: Bead fractions with captured free GST. Recombinant human p300 CH1 protein is shown with an asterisk.

2.4 Synthesis of dansyl-labeled peptides using Fmoc solid-phase peptide synthesis

Based on the CTAD and HIF-1α α_B regions, the peptides were synthesized using the Fmoc solid-phase synthesis (Schemes 2-1 – 2-4). The *N*-terminus of both CTAD and HIF-1α α_B were labeled with a dansyl fluorophore. The synthesized peptides were characterized by MALDI-TOF MS (Table 2-1).

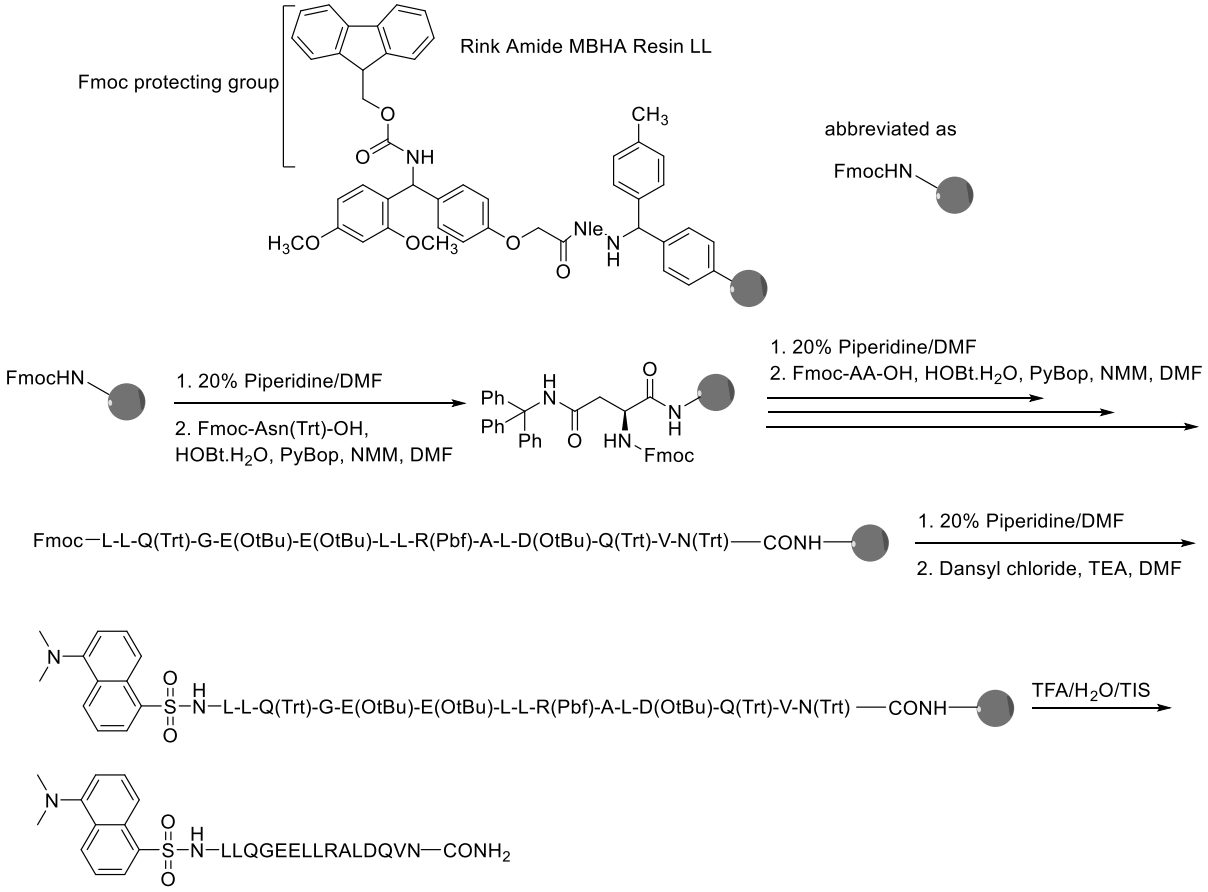

Scheme 2-1. Synthesis of dansyl-labeled HIF-1α α_B peptide

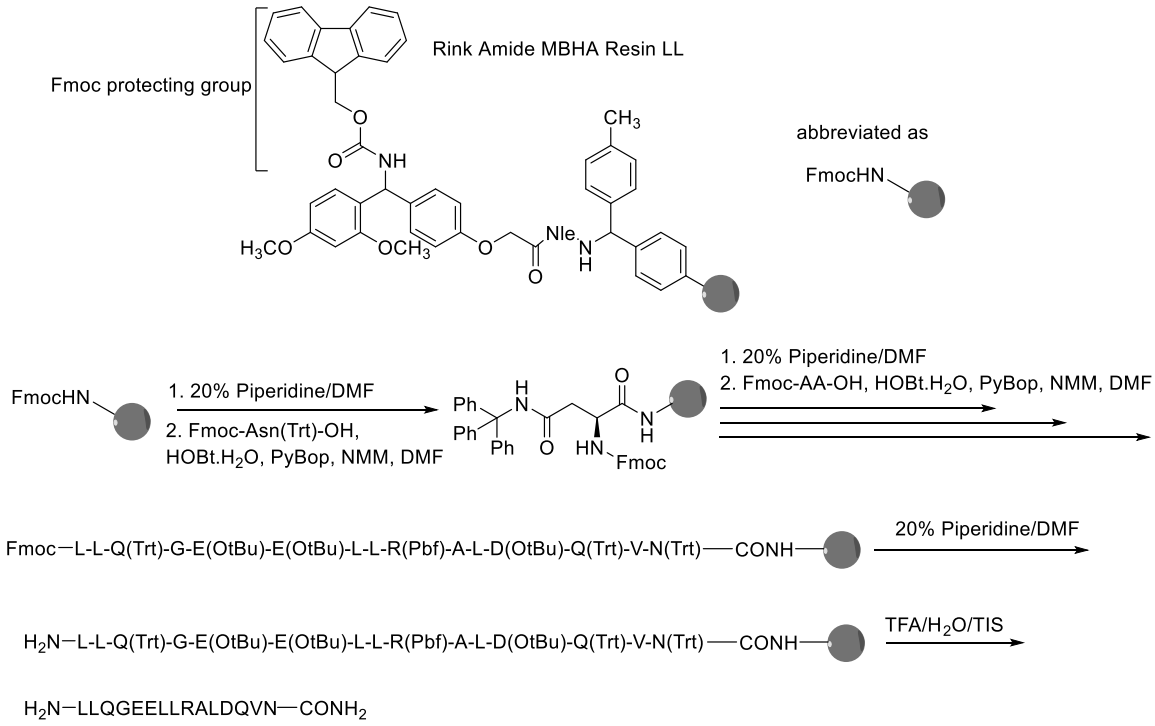

Scheme 2-2. Synthesis of HIF-1α α_B peptide

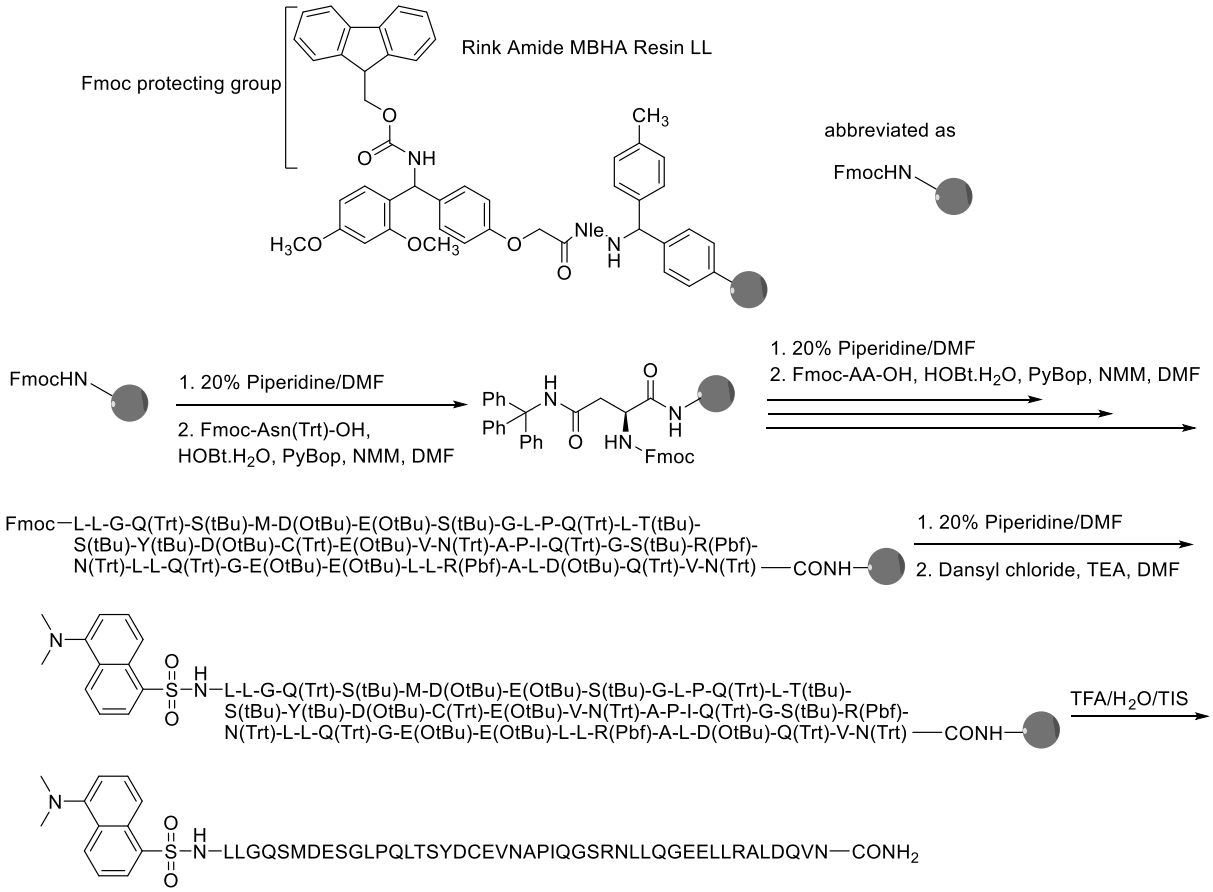

Scheme 2-3. Synthesis of dansyl-labeled CTAD peptide

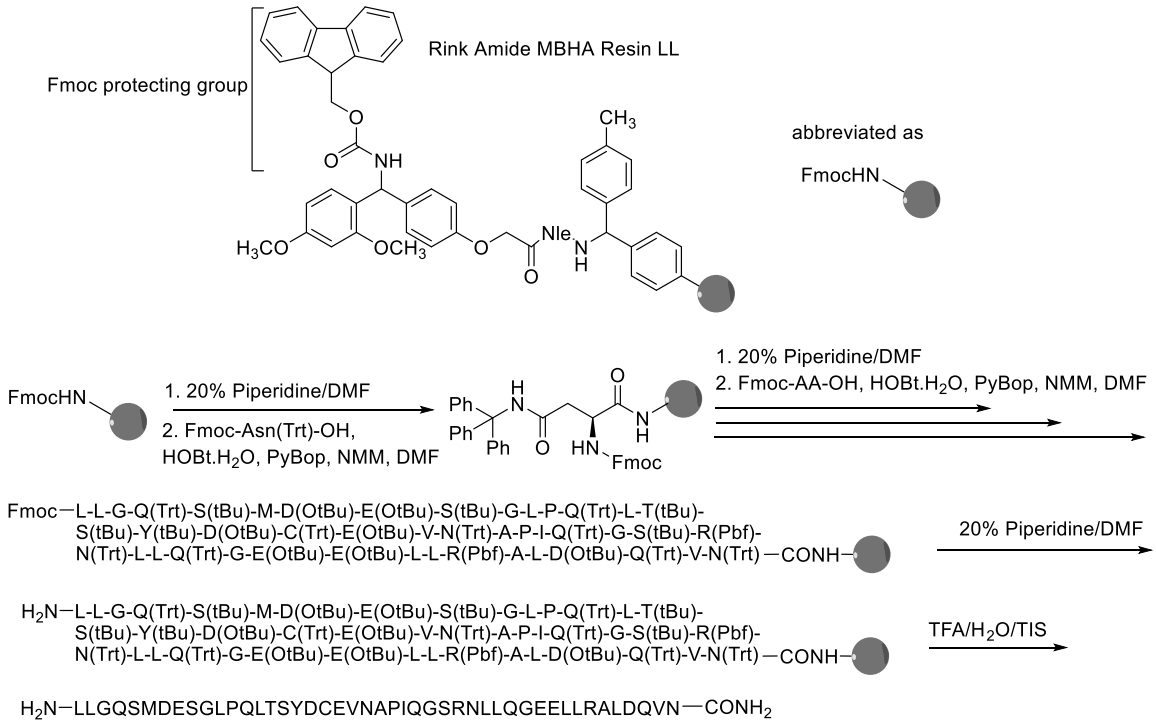

Scheme 2-4. Synthesis of CTAD peptide

Table 2-1. Sequence and MALDI-TOF MS analysis of the synthesized peptides

Peptide	Sequence	Calcd. for $[M+H]^+$/found
CTAD	H_2N-LLGQSMDESGLPQLTSYDCEVNAPIQGSRN LLQGEELLRALDQVN-CONH$_2$	4915.40/4915.923
Dansyl-labeled CTAD	Dan-LLGQSMDESGLPQLTSYDCEVNAPIQGSRN LLQGEELLRALDQVN-CONH$_2$	5149.69/5149.906
HIF-1α α_B	H_2N-LLQGEELLRALDQVN-CONH$_2$	1710.93/1710.442
Dansyl-labeled HIF-1α α_B	Dan-LLQGEELLRALDQVN-CONH$_2$	1944.22/1944.093

2.5 Synthesis of OHM 1 as HIF-1α/p300 interaction inhibitor

OHMs are assembled from naturally occurring amino acids with the nitrogen atoms of neighboring backbone amides constrained with ethylene bridges to afford a nonpeptidic chiral scaffold displaying protein-like functionality. The strategy of Arora's group is to mimic the α-helix structure important for the HIF-1α/p300 interaction on a small molecule oxopiperazine scaffold and deploy it as a novel PPI inhibitor.[4] OHM 1 mimics three amino

acid residues (Leu^{818}, Leu^{822}, and Gln^{824}) in the α-helical structure of HIF-1α that are important for interaction with p300. OHM 1 was synthesized using standard Fmoc amino acids and coupling reagents on Rink amide resin. The oxopiperazine ring is obtained via the application of the Fukuyama–Mitsunobu strategy, which involves activating the amine functionality by reaction with *o*-nitrobenzenesulfonyl chloride followed by N-alkylation with 2-bromoethanol. The synthesis scheme of OHM 1 is shown in Scheme 2-5. This compound will be used in this research as a positive control for the FA assay.

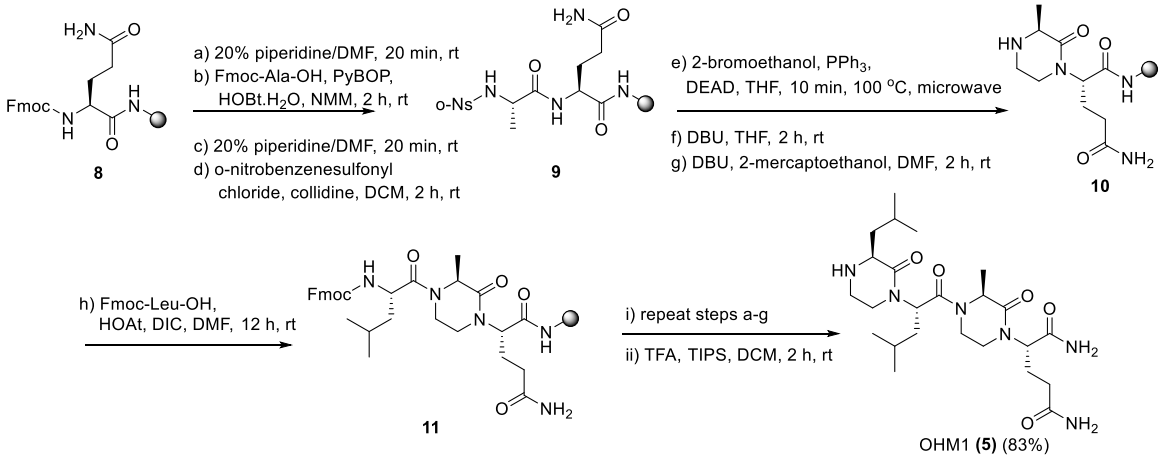

Scheme 2-5. Synthesis of OHM 1

2.6 Evaluation of the binding affinity of each synthesized peptide for p300 CH1 protein

The binding affinity of dansyl-labeled CTAD and HIF-1α α_B peptides to human p300 CH1 protein was determined (Figure 2-4). The binding affinity of HIF-1α α_B to p300 CH1 protein in this assay was found to have a K_d value of 55.85 ± 3.19 nM. The binding affinity of CTAD to p300 CH1 protein in this assay was consistent with previous results obtained using fluorescein-labeled CTAD and isothermal titration microcalorimetry with K_d value of 29.54 ± 1.73 nM.[5,6,12] Comparing the binding affinity of the dansyl-labeled peptides to the p300 CH1 protein, the CTAD peptide showed more than twice as strong binding affinity as HIF-1α α_B peptide.

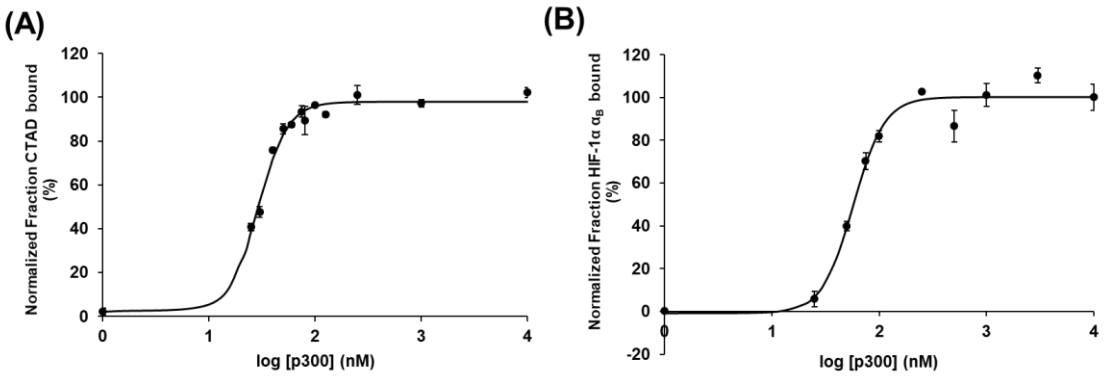

Figure 2-4. Evaluation of the binding affinity of each synthesized peptide for human p300 CH1 protein. p300 CH1 protein was incubated with dansyl-labeled CTAD (A) and HIF-1α α_B (B). Fluorescence anisotropy measured using SpectraMax iD5 Multi-Mode Microplate Reader (Molecular Devices, USA) with 330 nm of excitation wavelength and 510 nm of emission wavelength. All assays were performed in 125 nM dansyl-labeled CTAD or HIF-1α α_B peptide, 0-10 μM recombinant p300 CH1 protein, 20 mM Tris-HCl (pH = 8.0), 60 mM NaCl, 2 mM DTT, 1.5 μM $ZnCl_2$, and 0.5% DMSO in phosphate buffered saline (PBS). K_d values of CTAD and HIF-1α α_B on p300 CH1 protein was calculated 29.54 ± 1.73 nM and 55.85 ± 3.19 nM, respectively. Data are presented as means ± S.D. of three separate experiments. Error bars, S.D.

The screening assay system was developed using the dansyl-labeled HIF-1α α_B peptide with the purified p300 CH1 protein. Because HIF-1α α_B plays a crucial role in the CTAD/CH1 domain interactions in the HIF-1α/p300 complex, FA is well-suited for studying the binding between molecules with significantly different masses.[13] To validate the screening assay system, a competition assay was conducted using unlabeled peptides and reported HIF-1α/p300 inhibitors.

2.7 Validation of screening assay system

A competition assay using unlabeled HIF-1α peptides and known HIF-1α/p300 inhibitors was conducted to validate the established screening assay system. First, a competition assay was performed using unlabeled HIF-1α α_B and CTAD peptides. The decreases in anisotropy associated with disruption of the interaction upon titration with the unlabeled peptides were observed. In the FA assay, the IC_{50} value of the unlabeled HIF-1α α_B peptide was 57.2 ± 4.55 nM, while the IC_{50} value of the unlabeled CTAD peptide was

42.3 ± 5.10 nM (Figure 2-5). These results indicated that the unlabeled CTAD peptide disrupts the interaction more effectively than the unlabeled HIF-1α α_B peptide.

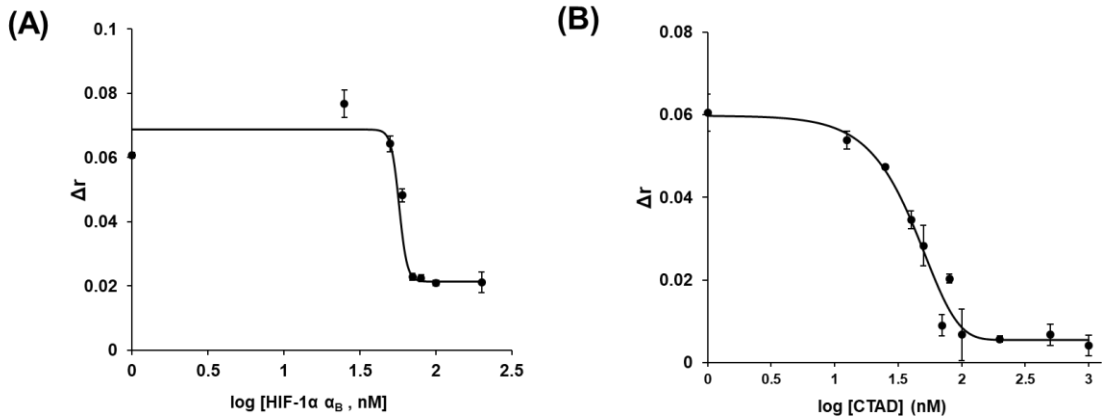

Figure 2-5. Competition assay of each synthesized unlabeled peptide for p300 CH1 protein. p300 CH1 protein was incubated with dansyl-labeled HIF-1α α_B and addition of unlabeled peptide HIF-1α α_B (A) and CTAD (B). Fluorescence anisotropy was measured using SpectraMax iD5 Multi-Mode Microplate Reader (Molecular Devices, USA) with 330 nm of excitation wavelength and 510 nm of emission wavelength. All assays were performed in 125 nM dansyl-labeled HIF-1α α_B peptide, 200 nM recombinant p300 CH1 protein, 20 mM Tris-HCl (pH = 8.0), 60 mM NaCl, 2 mM DTT, 1.5 μM $ZnCl_2$, and 0.5% DMSO in PBS. IC_{50} values competition assay of HIF-1α α_B and CTAD on p300 CH1 protein and N-Dan-HIF-1α α_B PPI was calculated 57.2 ± 4.55 nM and 42.3 ± 5.10 nM, respectively. Data are presented as means ± S.D. of three separate experiments. Error bars, S.D.

Next, a competition assay with known HIF-1α/p300 PPI inhibitors, OHM 1, and streptonigrin was performed to validate the screening assay system. As shown in Figure 2-6, a decrease in anisotropy associated with the interaction disruption was observed upon the addition of OHM 1 and streptonigrin. OHM 1 exhibited an IC_{50} value of 51.3 nM, while streptonigrin had an IC_{50} value of 1.38 μM. The previous reports showed that a known inhibitor for HIF-1α/p300, OHM 1, has an IC_{50} value of 530 nM as determined by tryptophan fluorescence spectroscopy, while streptonigrin has an IC_{50} value of 3 μM through an ELISA competition assay.[4,14] These results are consistent with the IC_{50} values of the HIF-1α/p300 PPI inhibitors and confirm that the established assay system has been validated as an effective screening assay for HIF-1α/p300 PPI inhibitors.

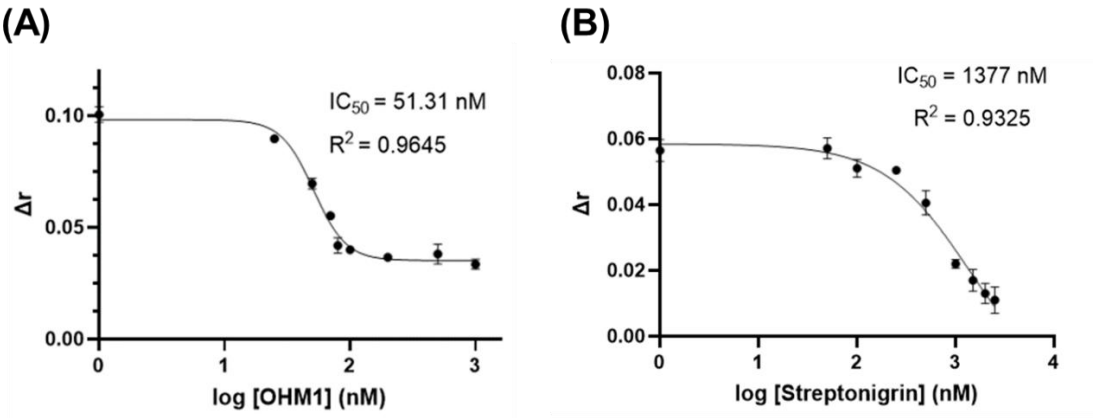

Figure 2-6. Competition assay of reported HIF-1α/p300 inhibitors for p300 CH1 protein. p300 CH1 protein was incubated with dansyl-labeled HIF-1α α_B and addition of OHM 1 (A) and streptonigrin (B). Fluorescence anisotropy was measured using SpectraMax iD5 Multi-Mode Microplate Reader (Molecular Devices, USA) with 330 nm excitation wavelength and 510 nm emission wavelength. All assays were performed in 125 nM dansyl-labeled HIF-1α α_B peptide, 200 nM recombinant p300 CH1 protein, 20 mM Tris-HCl (pH = 8.0), 60 mM NaCl, 2 mM DTT, 1.5 μM $ZnCl_2$, and 0.5% DMSO in PBS. Data are presented as means ± S.D. of three separate experiments. Error bars, S.D.

In order to evaluate the quality of screening assays, Zhang et al. introduced a statistical criteria "Z′ factor", which is calculated from the mean signals of the positive and negative controls (μ_{c+} and μ_{c-}) and their standard deviations (σ_{c+} and σ_{c-}) using the equation (3).[15]

$$Z' = 1 - \frac{3(\sigma_{C+} + \sigma_{C-})}{|\mu_{C+} + \mu_{C-}|} \qquad (3)$$

As the signal range increases and the variations decrease, Z′ tends to the ideal limit of 1, while Z′ values above 0.5 are considered "excellent" which means the assay system is statically robust and reliable.[15] In the established FA assay system, the Z′-factor is calculated as 0.54 from four independent measurements of the positive (p300 CH1/N-Dan-HIF-1α α_B with addition of OHM 1) and negative (p300 CH1/N-Dan-HIF-1α α_B with 0.5% of DMSO) controls (Figure 2-7). These results demonstrated that the FA competitive measurement is robust and suitable for screening assay.

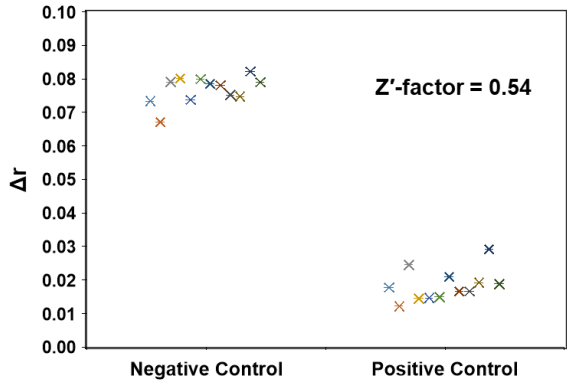

Figure 2-7. *Z′*-factor determination of four independent measurements of the negative (p300 CH1/N-Dan-HIF-1α α_B with 0.5% of DMSO) and positive (p300 CH1/N-Dan-HIF-1α α_B with addition of OHM 1 (10 μM)) controls.

2.8 Summary

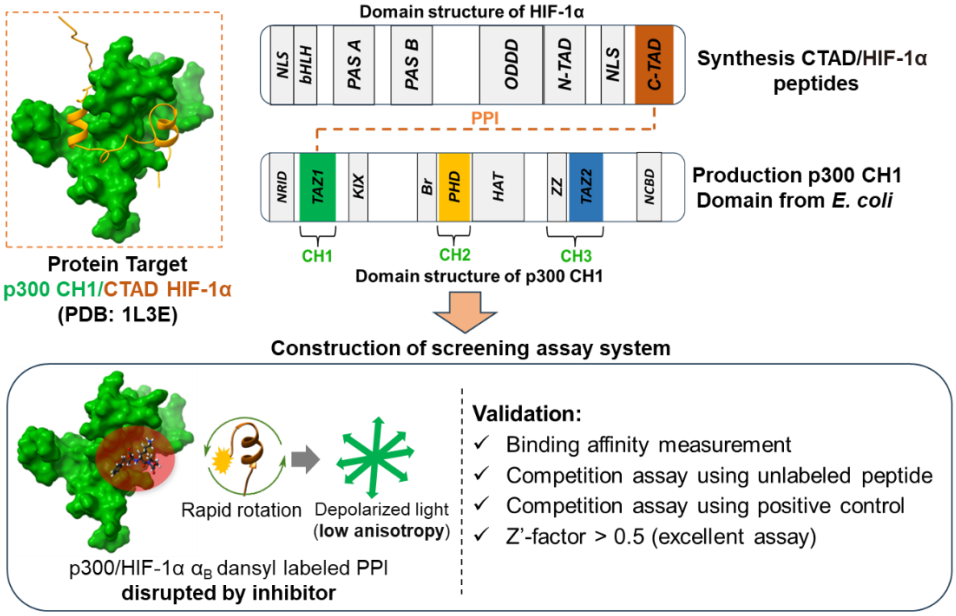

Figure 2-8. Summary of chapter 2

In chapter 2, the p300 CH1 protein was produced from *E. coli*. Labeled and unlabeled CTAD and HIF-1α α_B peptides were synthesized. The FA screening system was established for HIF-1α/p300 PPI inhibitor discovery using the p300 CH1 protein and dansyl-labeled HIF-1α α_B. This system was validated using an unlabeled peptide and a known inhibitor, demonstrating its effectiveness for screening. The *Z′*-factor value showed that the FA competitive assay is robust and suitable for screening assay.

2.9 References

(1) Viziteu, E.; Grandmougin, C.; Goldschmidt, H.; Seckinger, A.; Hose, D.; Klein, B.; Moreaux, J. Chetomin, Targeting HIF-1α/p300 Complex, Exhibits Antitumour Activity in Multiple Myeloma. *Br. J. Cancer* **2016**, *114*, 519–523.

(2) Shan, H. L.; Dong, H. S.; Chun, Y. S.; Myung, K. L.; Kim, M. S.; Park, J. W. A Novel Mode of Action of YC-1 in HIF Inhibition: Stimulation of FIH-Dependent p300 Dissociation from HIF-1α. *Mol. Cancer Ther.* **2008**, *7*, 3729–3738.

(3) Kung, A. L.; Zabludoff, S. D.; France, D. S.; Freedman, S. J.; Tanner, E. A.; Vieira, A.; Cornell-Kennon, S.; Lee, J.; Wang, B.; Wang, J.; Memmert, K.; Naegeli, H.-U.; Petersen, F.; Eck, M. J.; Bair, K. W.; Wood, A. W.; Livingston, D. M. Small Molecule Blockade of Transcriptional Coactivation of the Hypoxia-Inducible Factor Pathway. *Cancer Cell* **2004**, *6*, 33-43.

(4) Lao, B. B.; Grishagin, I.; Mesallati, H.; Brewer, T. F.; Olenyuk, B. Z.; Arora, P. S. In Vivo Modulation of Hypoxia-Inducible Signaling by Topographical Helix Mimetics. *Proc. Natl. Acad. Sci. USA* **2014**, *111*, 7531–7536.

(5) Burslem, G. M.; Kyle, H. F.; Breeze, A. L.; Edwards, T. A.; Nelson, A.; Warriner, S. L.; Wilson, A. J. Small-Molecule Proteomimetic Inhibitors of the HIF-1α-p300 Protein-Protein Interaction. *ChemBioChem.* **2014**, *15*, 1083–1087.

(6) Kushal, S.; Lao, B. B.; Henchey, L. K.; Dubey, R.; Mesallati, H.; Traaseth, N. J.; Olenyuk, B. Z.; Arora, P. S. Protein Domain Mimetics as in Vivo Modulators of Hypoxia-Inducible Factor Signaling. *Proc. Natl. Acad. Sci. USA* **2013**, *110*, 15602–15607.

(7) Uygun, M.; Doganci, E.; Tasdelen, M. A.; Gurek, A. G. One-Pot Photoinduced Synthesis of Dansyl Containing Acrylamide Hydrogels and Their Chemosensing Properties. *J. Appl. Polym. Sci.* **2019**, *136*, 47096.

(8) Song, L.; Hennink, E. J.; Young, I. T.; Tanke, H. J. Photobleaching Kinetics of Fluorescein in Quantitative Fluorescence Microscopy. *Biophys. J.* **1995**, *68*, 2588–2600.

(9) Yang, J.; Xu, Z.; Yu, L.; Wang, B.; Hu, R.; Tang, J.; Lv, J.; Xiao, H.; Tan, X.; Wang, G.; Li, J. X.; Liu, Y.; Shao, P. L.; Zhang, B. Organic Fluorophores with Large Stokes Shift for the Visualization of Rapid Protein and Nucleic Acid Assays. *Angew. Chem. Int. Ed.* **2024**, *63*, e202318800.

(10) Kim, Y.; Kaluz, S.; Mehta, A.; Weinert, E.; Rivera, S.; Van Meir, E. Purifying Properly Folded Cysteine-Rich, Zinc Finger Containing Recombinant Proteins for Structural Drug Targeting Studies: The CH1 Domain of p300 as a Case Example. *Bio. Protoc.* **2017**, *7*, 17.

(11) De Guzman, R. N.; Wojciak, J. M.; Martinez-Yamout, M. A.; Dyson, H. J.; Wright, P. E. CBP/p300 TAZ1 Domain Forms a Structured Scaffold for Ligand Binding. *Biochemistry* **2005**, *44*, 490–497.

(12) Dames, S. A.; Martinez-Yamout, M.; De Guzman, R. N.; Dyson, H. J.; Wright, P. E. Structural Basis for Hif-1CBP Recognition in Thecellular Hypoxic Response. *Proc. Natl. Acad. Sci. USA,* **2002**, *99*, 5271-5276.
(13) Blay, V.; Tolani, B.; Ho, S. P.; Arkin, M. R. High-Throughput Screening: Today's Biochemical and Cell-Based Approaches. *Drug Discov. Today* **2020**, *25*, 1807–1821.
(14) Jayatunga, M. K. P.; Thompson, S.; McKee, T. C.; Chan, M. C.; Reece, K. M.; Hardy, A. P.; Sekirnik, R.; Seden, P. T.; Cook, K. M.; McMahon, J. B.; Figg, W. D.; Schofield, C. J.; Hamilton, A. D. Inhibition of the HIF1α-p300 Interaction by Quinone- and Indandione-Mediated Ejection of Structural Zn(II). *Eur. J. Med. Chem.* **2015**, *94*, 509–516.
(15) Zhang, J.-H.; Chung, T. D. Y.; Oldenburg, K. R. A Simple Statistical Parameter for Use in Evaluation and Validation of High Throughput Screening Assays. *J. Biomol. Screen.* **1999**, *4*, 67–73.
(16) Okada, S.; Muto, Y.; Zhu, B.; Ueda, H.; Nakamura, H. Development of a Peptide Sensor Derived from Human ACE2 for Fluorescence Polarization Assays of the SARS-CoV-2 Receptor Binding Domain. *Anal. Chem.* **2023**, *95*, 6198–6202.

2.10 Experimental section

Biology

Vector construction for overexpression of human p300 CH1 domain protein

Human p300 CH1 domain (amino acid residues 323-423) cDNA was amplified from the HeLa cell cDNA library by PCR. The primer sequences used to amplify the p300 CH1 domain cDNA were as follows: 5′-TTTTGAATTCATGGGTTCTGGAGCACATACAGCT-3′ (forward) and 5′-TTTTCTCGAGCTTATCACCAGCATTTTTGAGGGGG-3′ (reverse). The PCR obtained product was subcloned into *EcoRI*/*XhoI* sites of the pGEX-6P-1 vector (Thermo Fisher Scientific, Inc., USA). The constructed vector (pGEX-6P-1-p300/CH1 vector) was transformed into SHuffle® T7 Express Competent *E. coli* (New England Biolabs, MA, USA).

Protein expression and purification of p300 CH1 domain protein

The pGEX-6P-1-p300/CH1 vector was transformed into SHuffle® T7 Express Competent *E. coli* (New England Biolabs, MA, USA) and incubated at 37 °C with aeration to an OD_{600} of 0.6-0.8. Protein expression was induced by the addition of 1 mM isopropyl β-D-thiogalactopyranoside (IPTG) and incubated for 16-20 h at 16 °C in the presence of 100 μM zinc chloride ($ZnCl_2$). The *E. coli* was collected by centrifuging at 4,000 x *g* for 15 min at 4 °C, and the obtained pellets were resuspended in BugBuster® protein extraction reagent (Merck Millipore, MA, USA) containing Lysonase™ bioprocessing reagent (Merck Millipore, MA, USA) and protease inhibitor cocktail (Promega, Madison, WI, USA) and shaken at 4 °C for 1 h. The lysate was collected by centrifugation (10,000 x *g*, 4 °C, 15 min) and then incubated with GSH-agarose beads (Thermo Fisher Scientific, Inc., MA, USA) for 3-4 h at 4 °C. The recombinant GST-p300/CH1 protein bound beads were washed five times with prechilled acidic resuspension buffer (50 mM Tris-HCl (pH = 6.3) and 150 mM NaCl) and prechilled alkaline resuspension buffer (50 mM Tris-HCl (pH = 8.0) and 150 mM NaCl), respectively. Recombinant GST-p300/CH1 was eluted with elution buffer (50 mM Tris-HCl (pH = 8.0), 150 mM NaCl, and 10 mM reduced gluthatione (FUJIFILM Wako Pure Chemical Corporation, Japan)). Recombinant p300/CH1 was eluted by incubation with cleavage buffer (50 mM Tris-HCl (pH = 8.0), 150 mM NaCl, 1 mM ethylenediaminetetraacetic acid (EDTA), and 1 mM dithiothreitol (DTT)) for 16-18 h

at 4 °C and purified by incubating the resulting eluate with GSH-agarose beads for 3-4 h at 4 °C. Each protein was confirmed with sodium dodecyl sulfate–polyacrylamide gel electrophoresis (SDS-PAGE).

FA measurement

The FA assay was performed with reference to previously reported literature[82]. Protein was serially diluted into a solution of labeled peptide (125 nM) and the plates were incubated for 30 min at room temperature. Each experiment was run in triplicate and the anisotropy was measured using SpectraMax iD5 Multi-Mode Microplate Reader (Molecular Devices, USA) with 330 nm of excitation wavelength and 510 nm of emission wavelength. All assays were performed in 20 mM Tris-HCl (pH = 8.0), 60 mM NaCl, 2 mM DTT, 1.5 μM $ZnCl_2$, and 0.5% dimethyl sulfoxide (DMSO) in PBS. The anisotropy data from this measurement were corrected by subtracting the corresponding control wells and were used to calculate the amount of bound labeled peptide using equation 4. This data was then fitted using equation 5 in OriginPro 2023 to determine the dissociation constant, K_d.

$$L_b = \frac{r - r_{min}}{\lambda(r_{max} - r) + r - r_{min}} \quad (4)$$

$$y = \frac{(K_d + x + [\mathrm{FL}]) - \sqrt{[\{(K_d + x + [\mathrm{FL}])]^2 - 4x[FL]\}}}{2} \quad (5)$$

where r = anisotropy, L_b = fraction ligand bound, $\lambda = I_{bound}/I_{unbound} = 1$, [FL] = concentration of fluorescent peptide, K_d = dissociation constant, y = L_b multiplied by [FL], x = protein concentration. The competitive inhibition assay was performed using solution of 200 nM p300 CH1 protein and 125 nM labeled peptide which was incubated at 25 °C. After 1 h, unlabeled peptides, OHM1 or streptonigrin were added with final concentrations ranging from 0 to 200 nM, 1 μM, or 5 μM, respectively. After 1 h, the amount of dissociated fluorescent probe was determined. The IC_{50} values were determined for each peptide by fitting the averages of three individual measurements to a sigmoidal dose-response curve using a nonlinear regression model with OriginPro 2023.

DNA Sequence Analysis of pGEX-6P-1-p300/CH1 Vector

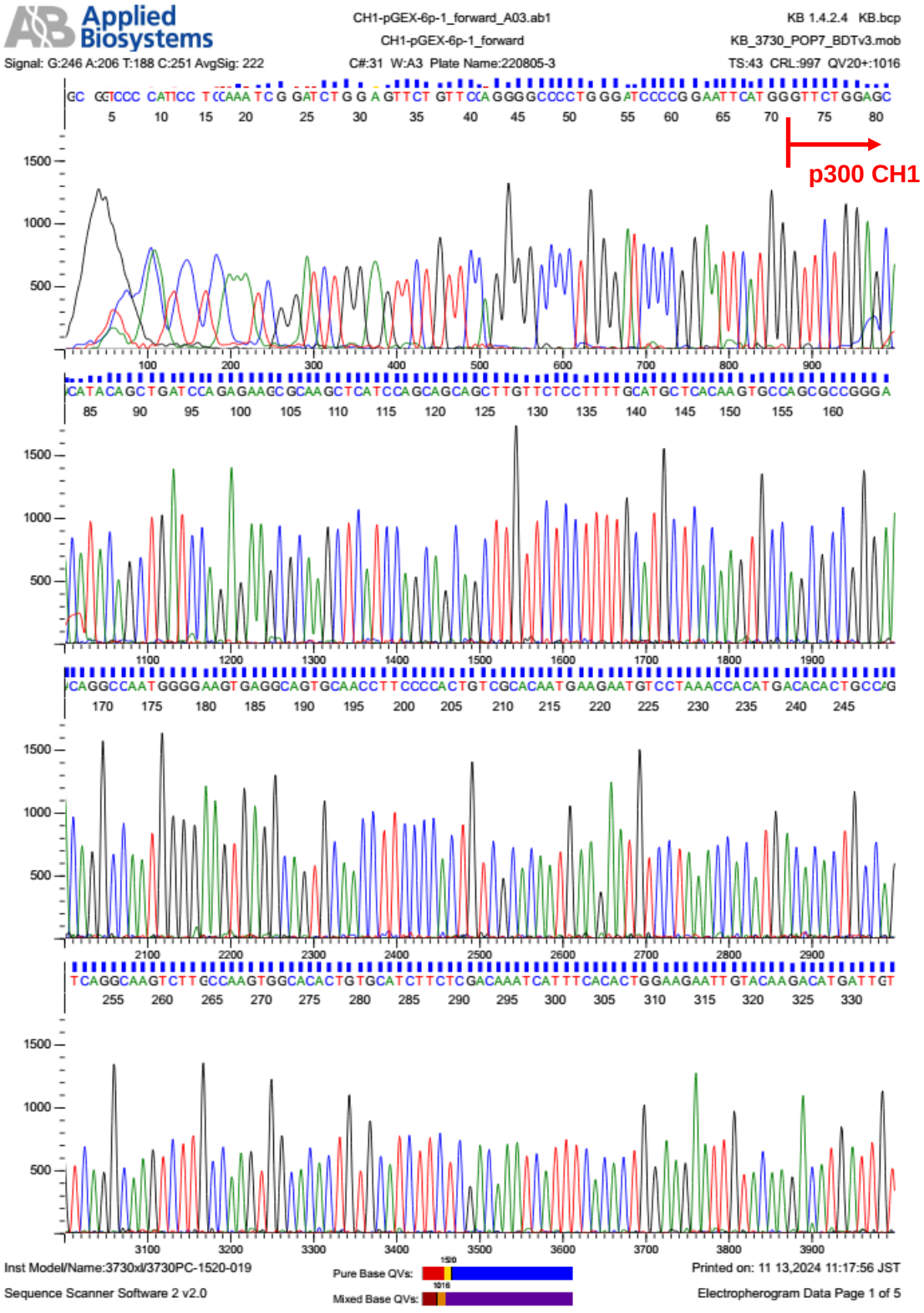

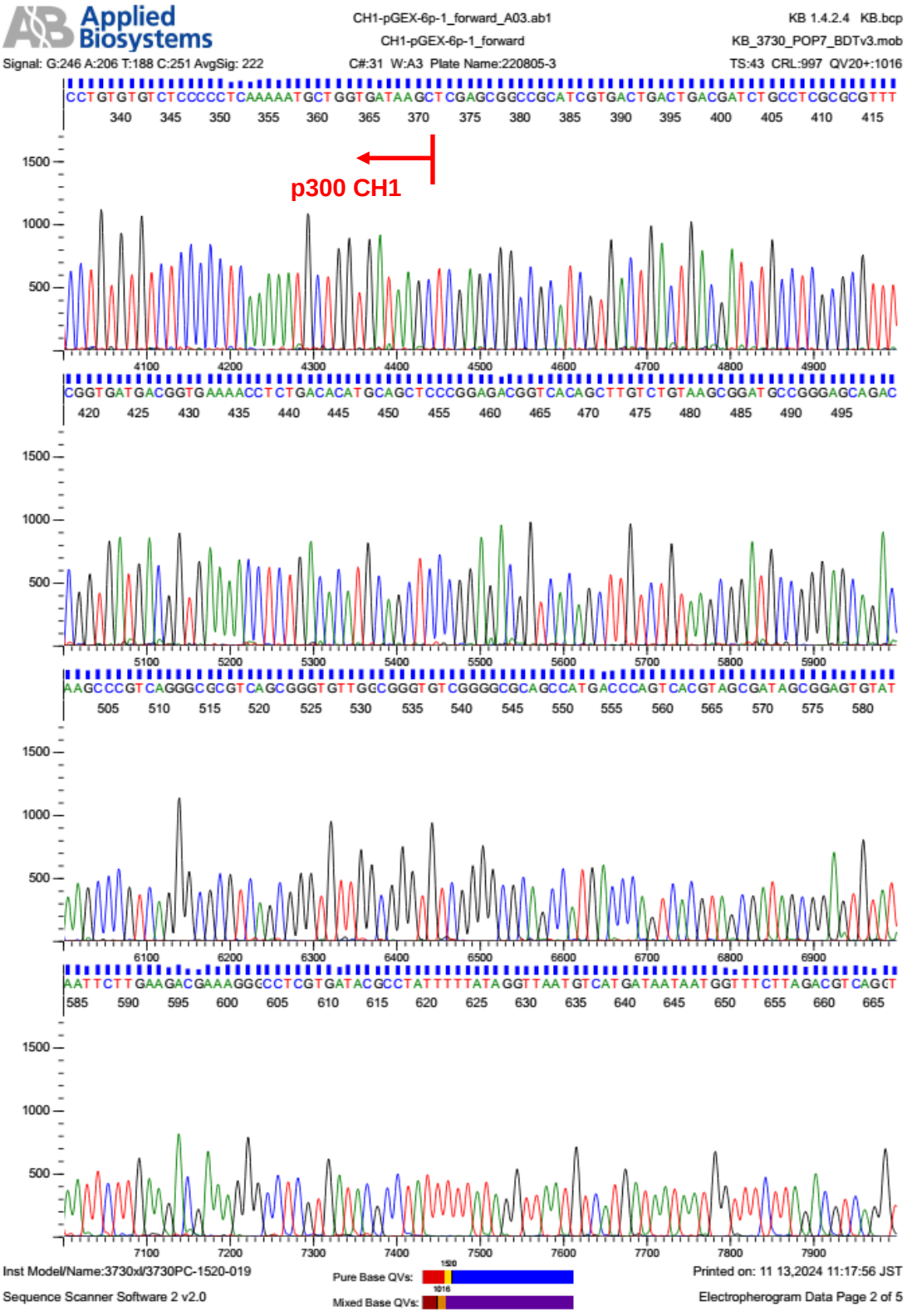
Applied Biosystems
CH1-pGEX-6p-1_forward_A03.ab1
CH1-pGEX-6p-1_forward
C#:31 W:A3 Plate Name:220805-3
KB 1.4.2.4 KB.bcp
KB_3730_POP7_BDTv3.mob
TS:43 CRL:997 QV20+:1016
Signal: G:246 A:206 T:188 C:251 AvgSig: 222
p300 CH1
Inst Model/Name:3730xl/3730PC-1520-019
Sequence Scanner Software 2 v2.0
Pure Base QVs:
Mixed Base QVs:
Printed on: 11 13,2024 11:17:56 JST
Electropherogram Data Page 2 of 5

Chemistry

General Information

NMR spectra were recorded on a Bruker biospin AVANCE II (400 MHz for ^{1}H) instrument in the indicated solvent. Chemical shifts are reported in parts per million (ppm) relative to DMSO-d_6 (2.50 ppm for ^{1}H NMR) of the standard. Multiplicities are reported using the following abbreviations: s, singlet; d, doublet; dd, doublet of doublets; t, triplet; q, quartet; m, multiplet; brs, broad; *J*, coupling constants in Hertz. High-resolution mass spectra (HRMS) were recorded on a Bruker electrospray ionization (ESI)–time of flight (TOF)–mass spectrometer (micrOTOF II). Analytical thin-layer chromatography (TLC) was performed on a glass plate of silica gel 60 GF254 (Merck). All chemicals and reagents for biological experiments were obtained from commercial sources and used without further purification. The purity of all assayed compounds was determined by a reverse-phase HPLC system (JASCO Corporation, Japan) equipped with a C18 column (Finepak SIL C18S (4.6 x 75 mm), JASCO Corporation, Japan). All synthesized compounds were detected using a UV detector at 215 nm with 0.1% formic acid in H_2O: 0.1% formic acid in MeCN from 0-100% of solvent B for 20 min; flow rate 1.0 mL/min). All organic synthesis experiments encountered no unexpected or unusually high safety hazards.

Synthesis of dansyl-labeled HIF-1α C-terminal fragment

Peptides synthesis was performed according to previously reported literature[16]. Peptides were manually synthesized using a standard Fmoc solid-phase synthesis on Rink Amide MBHA resin LL (0.30–0.45 mmol/g). The resin (100 mg, 0.03 mmol) was swelled overnight in *N*,*N*-dimethylformamide (DMF). DMF was removed and followed by addition of 7 mL of 20% piperidine in DMF to deprotect a Fmoc group. The solution was removed 20 min after shaking at room temperature. The deprotected Fmoc groups were quantified by measuring the absorbance of the solution at 301 nm using $\varepsilon_{301\ nm} = 7800\ M^{-1}\ cm^{-1}$ to determine the loading number of amino acids. The resin was washed by DMF five times and 2,4,6-trinitrobenzene sulfonic acid (TNBS) test was conducted to confirm the deprotection. To the filtrated resin was added 1 mL of DMF, 1 mL of DMF solution containing Fmoc-amino acid (0.09 mmol), *1H*-Benzotriazole-1-yloxytris(pyrrolidine-1-yl)phosphonium hexafluorophosphate (PyBOP; 47.8 mg, 0.09 mmol) and 1-hydroxybenzotriazole monohydrate ($HOBt{\cdot}H_2O$; 13.8 mg, 0.09 mmol) and 1 mL of DMF solution containing *N*-methylmorpholine (NMM; 15 μL, 0.14 mmol). The mixture was

shaken for 1 h at room temperature and washed by DMF. After confirming the amino acid coupling by TNBS test, the peptide chain was deprotected and elongated in the same way. For the synthesis of N-Dan, the dansyl chloride was directly conjugated to the N-terminal amine after Fmoc deprotection. The peptides were cleaved from the resin in cold trifluoroacetic acid: triisopropylsilane: 1,2-ethanedithiol : H_2O = 94 : 1 : 2.5 : 2.5 for 2 h and 5 h for short and long peptides, respectively. The crude peptide was precipitated by adding cold diethyl ether (Et_2O), collected by centrifuge, and washed by Et_2O three times. The purity of all peptides was determined by a reverse-phase HPLC system (JASCO Corporation, Japan) equipped with a C18 column (Finepak SIL C18S (4.6 x 75 mm), JASCO Corporation, Japan). All synthesized compounds were detected using a UV detector at 215 nm with 0.1% formic acid in H_2O: 0.1% formic acid in MeCN from 0-100% of solvent B for 20 min; flow rate 1.0 mL/min). The characterization of the peptides was confirmed by matrix-assisted laser desorption ionization-time of flight mass spectrometry (MALDI-TOF-MS; ultrafleXtreme, Bruker, Billerica, USA).

Synthesis of OHM 1

Synthesis of OHM 1 was performed according to previous reported literature[4]. Peptides were manually synthesized using a standard Fmoc solid-phase synthesis on Rink Amide MBHA resin LL. The resin (200 mg, 0.06 mmol) was swelled overnight in DMF. DMF was removed and followed by adding 7 mL of 20% piperidine in DMF to deprotect a Fmoc group. The solution was removed 20 min after shaking at room temperature. The deprotected Fmoc groups were quantified by measuring the absorbance of the solution at 301 nm using $\varepsilon_{301\ nm} = 7800\ M^{-1}\ cm^{-1}$ to determine the loading number of amino acids. The resin was washed by DMF five times and TNBS test was conducted to confirm the deprotection. To the filtrated resin was added 1 mL of DMF, 1 mL of DMF solution containing Fmoc-Gln(Trt)-OH (54.9 mg, 0.09 mmol), *1H*-Benzotriazole-1-yloxytris(pyrrolidine-1-yl)phosphonium hexafluorophosphate (PyBOP; 47.8 mg, 0.09 mmol) and 1-hydroxybenzotriazole monohydrate ($HOBt \cdot H_2O$; 13.8 mg, 0.09 mmol) and 1 mL of DMF solution containing *N*-methylmorpholine (NMM; 15 μL, 0.14 mmol). The mixture was shaken for 2 h at room temperature and washed by DMF. After confirming the amino acid coupling by TNBS test, the peptide chain was deprotected and elongated in the same way using Fmoc-Ala-OH (28.1 mg, 0.09 mmol). The resultant Fmoc-Ala-Gln-resin was deprotected with 20% piperidine/DMF and resin was washed sequentially with DMF, dichloromethane (DCM), methanol (MeOH), and Et_2O and dried *in vacuo*. *O*-

Nitrobenzenesulfonyl chloride (*o*-Ns-Cl, 10 eq) and collidine (10 eq) were dissolved in dry DCM and added to the reaction vessel. After stirring for 2 h at 23 °C, the resin was washed with sequentially with DMF, DCM, MeOH, and Et_2O and dried for 12 h *in vacuo* to obtain compound **9**. The compound **9** bound resin was transferred to a glass microwave tube (CEM Corporation, USA). Triphenylphosphine (PPh_3, 10 eq) was added and the tube was flushed with nitrogen gas for 30 min. Tetrahydrofuran (THF; 5 mL), diisopropyl azodicarboxylate (DIAD, 10 eq), and 2-bromoethanol (10 eq) were added and the reaction mixture was subjected to microwave irradiation (200 watts) for 10 min at 100 °C. The resin was washed sequentially with THF, DMF, and DCM, then transferred to a solid phase vessel and 5 mL of a THF solution of 1,8-diazabicyclo[5.4.0]undec-7-ene (DBU, 5 eq) was added. After stirring for 2 h at room temperature, the resin was washed with THF, DMF, DCM, and Et_2O, allowed to dry for 30 min *in vacuo*, and then treated with DBU (5 eq) and 2-mercaptoethanol (10 eq) in 2 mL of DMF for 2 h. The obtained resin was washed with DMF, DCM, MeOH and Et_2O and for 12 h *in vacuo* to obtain compound **10**. To the filtrated resin was added 1 mL of DMF, 1 mL of DMF solution containing Fmoc-Leu-OH (31.8 mg, 0.09 mmol), 1-Hydroxy-7-aza-*1H*-benzotriazole (HOAt, 12.3 mg, 0.09 mmol), diisopropylcarbodiimide (DIC, 14 μL, 0.09 mmol) and the mixture was shaken at 23 °C for 12 h affording **11**. Nosyl protection and the ring formation steps were repeated to obtain oxopiperazine dimers **OHM 1** (**5**; 24.7 mg, 0.05 mmol, 83% yield) after cleavage from the resin with 95% trifluoroacetic acid (TFA), 2.5% water, and 2.5% triisopropylsilane (TIPS). ^{1}H-NMR (400 MHz, DMSO-d_6, 100 °C) δ 6.95 (br, 2H), 6.66 (br, 2H), 5.36 (t, J = 7.47 Hz, 1H), 4.90-4.85 (m, 1H), 4.67 (q, J = 6.88 Hz, 1H), 3.96 (br, 2H), 3.63-3.41 (m, 8H), 2.12-2.03 (m, 3H), 1.92-1.85 (m, 3H), 1.67-1.61 (m, 3H), 1.57-1.51 (m, 1H), 1.39 (s, 3H), 0.99-0.91 (m, 12H); HRMS (ESI, positive) calcd for $C_{24}H_{42}N_6O_5$ $[M+H]^+$ 495.3289, found 495.3292.

HPLC analysis of HIF-1α α_B peptide

H_2N-LLQGEELLRALDQVN-$CONH_2$

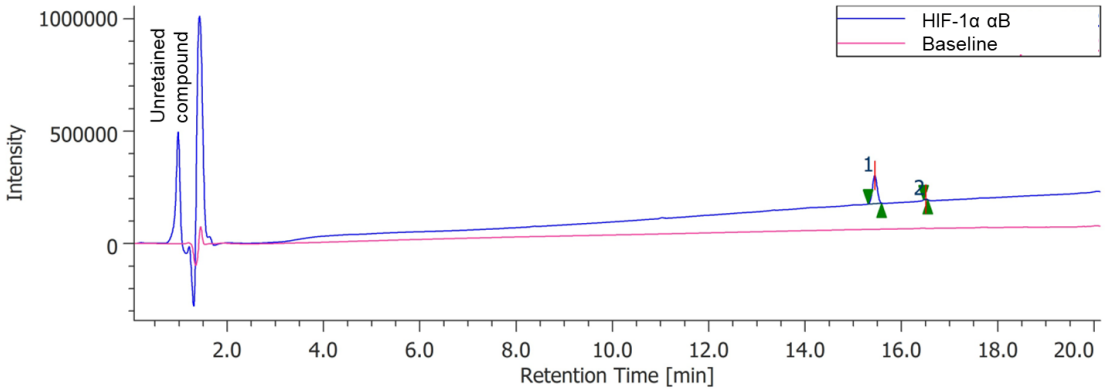

Peak	Area (%)	Retention time (min)
1	**96.892**	**15.442**
2	3.108	16.500

HPLC analysis of N-Dan-HIF-1α α_B peptide

Dan-LLQGEELLRALDQVN-$CONH_2$

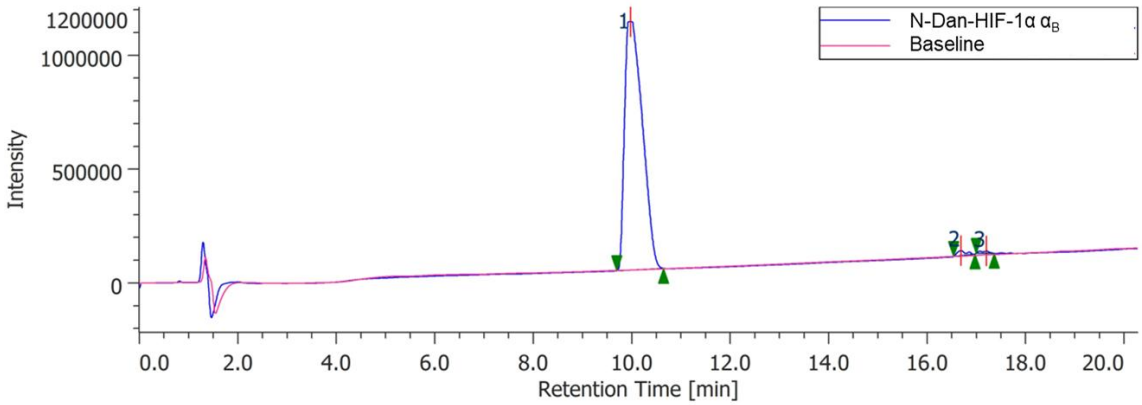

Peak	Area (%)	Retention time (min)
1	**98.544**	**9.975**
2	0.975	16.683
3	0.481	17.200

HPLC analysis of CTAD peptide

H_2N-LLGQSMDESGLPQLTSYDCEVNAPIQGSRNLLQGEELLRALDQVN-$CONH_2$

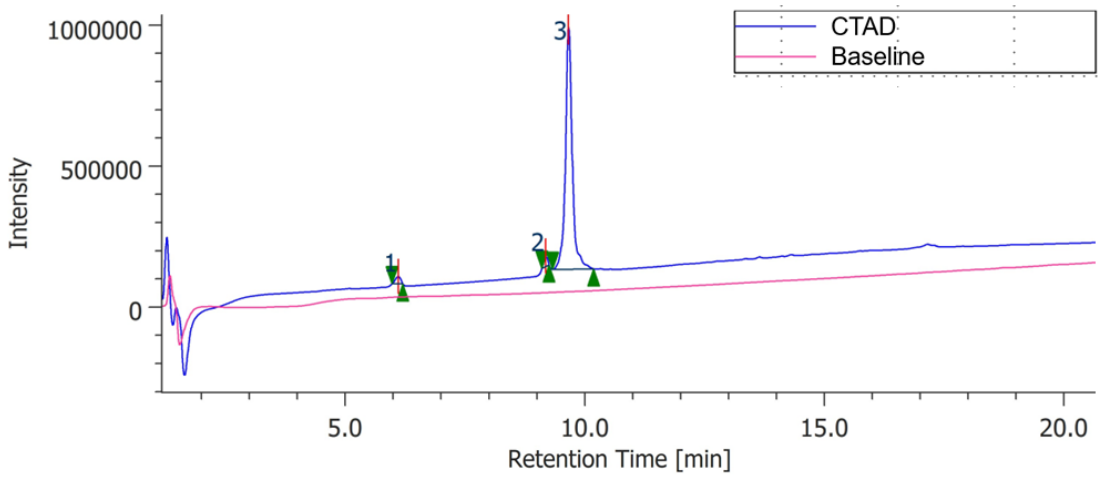

Peak	Area (%)	Retention time (min)
1	2.246	6.108
2	2.179	9.183
3	**95.574**	**9.658**

HPLC analysis of N-Dan-CTAD peptide

Dan-LLGQSMDESGLPQLTSYDCEVNAPIQGSRNLLQGEELLRALDQVN-$CONH_2$

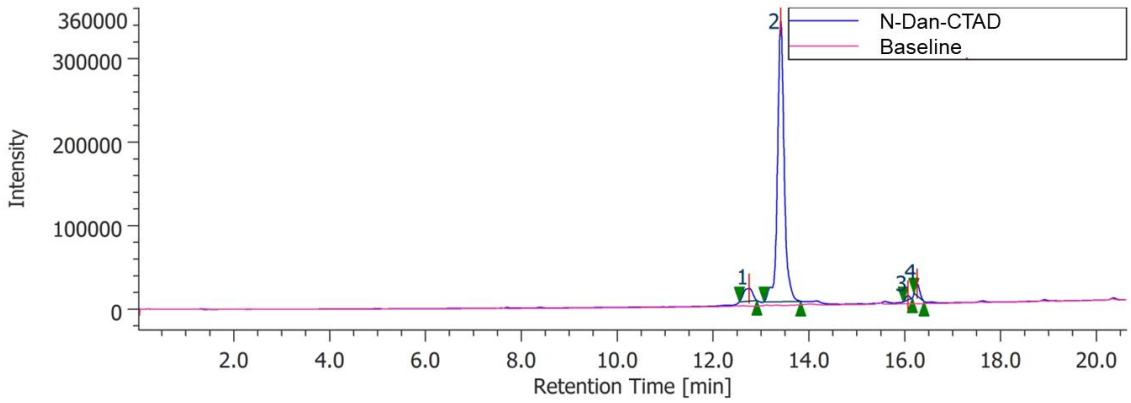

Peak	Area (%)	Retention time (min)
1	0.655	12.750
2	**95.237**	**13.408**
3	0.809	16.058
4	3.299	16.250

HPLC analysis of OHM 1

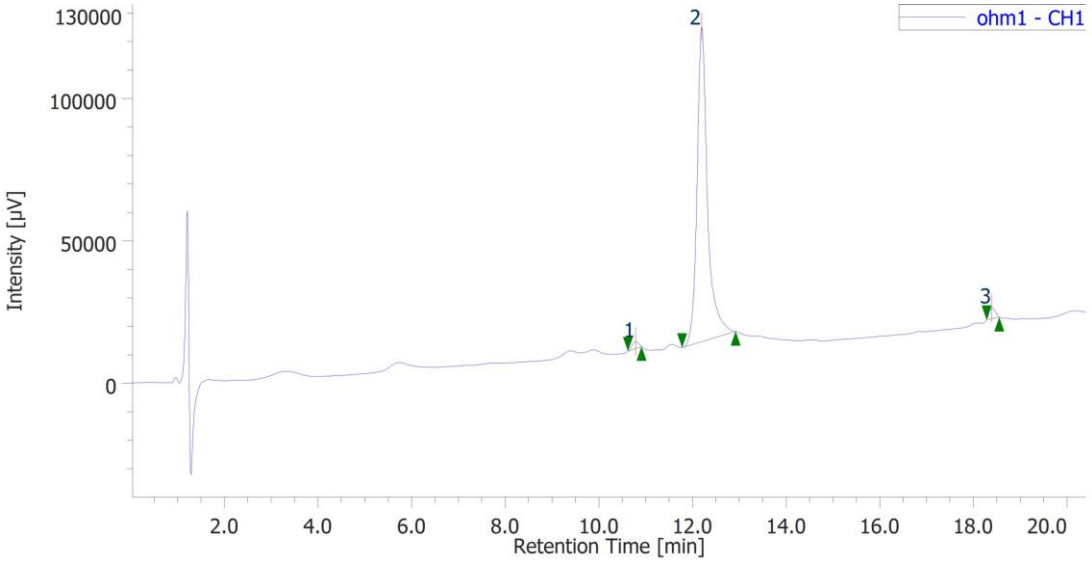

Peak	Area (%)	Retention time (min)
1	1.338	10.783
2	**96.718**	**12.192**
3	1.944	18.392

NMR spectra

OHM 1

^{1}H NMR (400 MHz, DMSO, 100 °C)

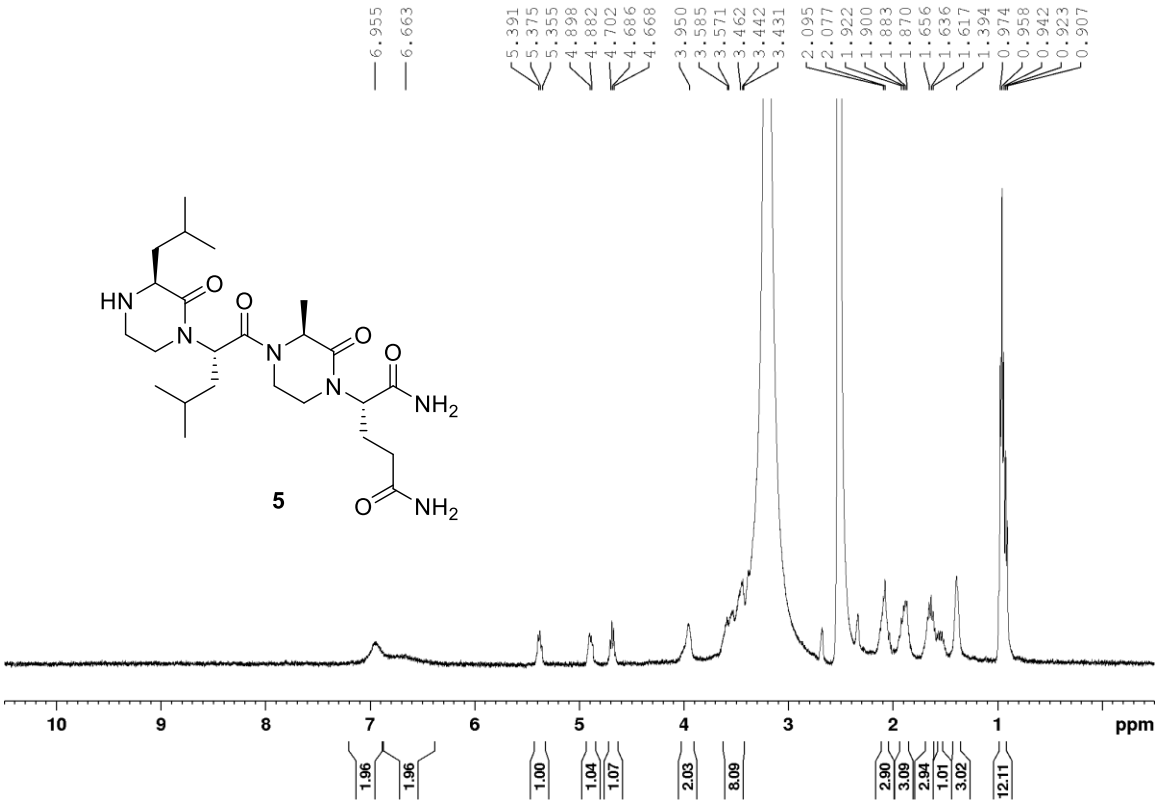

Chapter 3

Screening of Compound Library using Constructed Assay System and Validation of Lead Compounds as HIF-1α/p300 PPI Inhibitors

3.1 Introduction

HIF-1α/p300 interaction is a promising drug target. However, there are no approved HIF-1α/p300 inhibitors to date (see chapter 2.1). Despite its significance, the inhibition of HIF-1α/p300 interaction remains challenging, primarily due to the complex and dynamic nature of PPIs. PPIs are considered challenging targets for small-molecule ligands, given that the target surfaces for competitive inhibition are typically large and less well-defined than conventional small-molecule binding pockets.[1,2]

Drug development targeting PPIs is a challenging study in conventional drug discovery research and requires further research and development. Compound libraries containing diverse chemical entities serve as valuable tools in screening for potential inhibitors of protein interactions.[3] Coupled with well-designed assay systems, compound libraries can identify promising lead compounds for further development.[4]

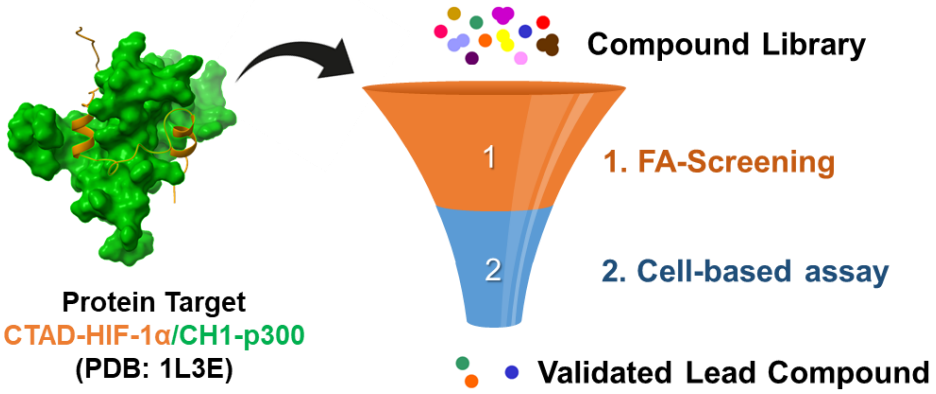

Figure 3-1. Screening of HIF-1α/p300 PPI inhibitors from compound library using constructed assay system and validation of candidate compounds.

This study focuses on screening HIF-1α/p300 PPI inhibitors from a compound library using a constructed assay system (see chapter 2) to identify novel lead compounds (Figure 3-1). Following the identification of lead compounds, the compounds are validated for their ability to inhibit the HIF-1α/p300 PPI using a cell-based assay to confirm their inhibitory activity.

3.2 NPDepo compound library

The natural product-based library offers a unique advantage due to its structural diversity, providing opportunities to uncover novel chemical scaffolds with the potential for high specificity and efficacy in targeting this important PPIs. The NPDepo authentic compound libraries are derived from natural products and drug-like synthetic compounds, resulting in a comprehensive and diverse library of bioactive molecules. The NPDepo compound library serves as a valuable resource for drug discovery and biomedical research, providing researchers worldwide with a unique tool for screening and identifying bioactive compounds. Based in Japan and managed by RIKEN, NPDepo compound library is accessible to researchers globally, facilitating advancements in pharmacology, oncology, and infectious disease research. The NPDepo compound library profile is provided in Appendix A.

3.3 Screening of HIF-1α/p300 PPI inhibitors from in-house and NPDepo compound library

Some of the in-house library compounds were screened using the established screening assay system. First, the peptidomimetic compounds (di)azatricyclododecene scaffold were screened (Figure 3-2). The reported peptidomimetics showed inhibition of HIF transcription activity which α-helix peptide mediated interaction play a pivotal role.[5] As shown in Figure 3-3, the inhibition activity of peptidomimetic compounds did not show better than that of the positive control, OHM1. Compared with the reported HIF transcriptional activity of peptidomimetic compounds in Table 3-1, compound **U-21a** is the most potent compared with other tested compounds. This result also strengthens the validation of the screening assay system.

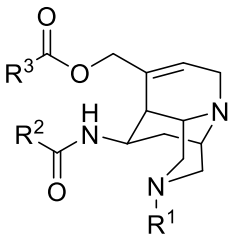

U-21a: R^1=Bn; R^2=Bn; R^3=Bn
U-21b: R^1=Bn; R^2=Bn; R^3=*i*-Bu
U-21c: R^1=Bn; R^2=*i*-Bu; R^3=Bn
U-21d: R^1=Bn; R^2=*i*-Bu; R^3=*i*-Bu
U-21f: R^1=*i*-Bu; R^2=Bn; R^3=*i*-Bu
U-21g: R^1=*i*-Bu; R^2=*i*-Bu; R^3=Bn

Figure 3-2. In-house library compounds: (di)azatricyclododecene scaffold

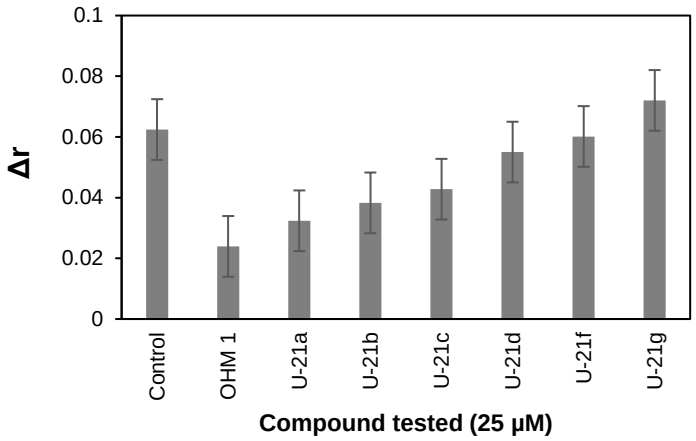

Figure 3-3. Screening of HIF-1α/p300 PPI inhibitors from in-house compound library by the established FA-assay system. p300 CH1 protein and dansyl-labeled HIF-1α α_B were incubated with compounds tested: 25 μM of peptidomimetic compounds and 10 μM of OHM1. Anisotropy was measured using SpectraMax iD5 Multi-Mode Microplate Reader (Molecular Devices, USA) with 330 nm excitation wavelength and 510 nm emission wavelength. All assays were performed in 125 nM dansyl-labeled HIF-1α α_B peptide, 200 nM recombinant p300 CH1 protein, 20 mM Tris-HCl (pH = 8.0), 60 mM NaCl, 2 mM DTT, 1.5 μM $ZnCl_2$, and 0.5% DMSO in PBS. Data are presented as means ± S.D. of three separate experiments. Error bars, S.D.

Table 3-1. Inhibition of HIF transcriptional activity of peptidomimetic compounds

Entry	Compounds	HIF-1[a, b, c] [μM]
1	**U-21a**	4.1 ± 0.8
2	**U-21b**	11.0 ± 0.1
3	**U-21c**	9.1 ± 1.8
4	**U-21d**	21.2 ± 2.2
5	**U-21f**	18.9 ± 6.0
6	**U-21g**	11.7 ± 4.2

[a] Indicated half maximal inhibitory concentration (IC_{50}) are mean ± SD of a single experiment conducted in triplicate.

[b] HRE-Luc expression was measured by luciferase reporter gene assay using HRE-dependent luciferase expression in HeLa cells (O_2 1%, CO_2 5%, 37 °C, 12 h).

[c] Measured by Umedera et al. (2021).[5]

The other in-house library compound, carborane compounds, were also screened (Figure 3-4). Using our assay system, some carborane compounds exhibited stronger inhibitory activity compared to the positive control, specifically compounds **A-Vi** and **A-Vj** (Figure 3-5). Compared with the reported HIF transcriptional activity of carborane compounds in Table 3-2, compounds **A-Vi** and **A-Vj** displayed similar activity to the screening results. Additionally, inactive compounds in HIF transcriptional activity, such as **A-Ia**, **A-IIIe**, and **A-Vn**, showed similar activity in inhibiting HIF-1α/p300 *in vitro*.

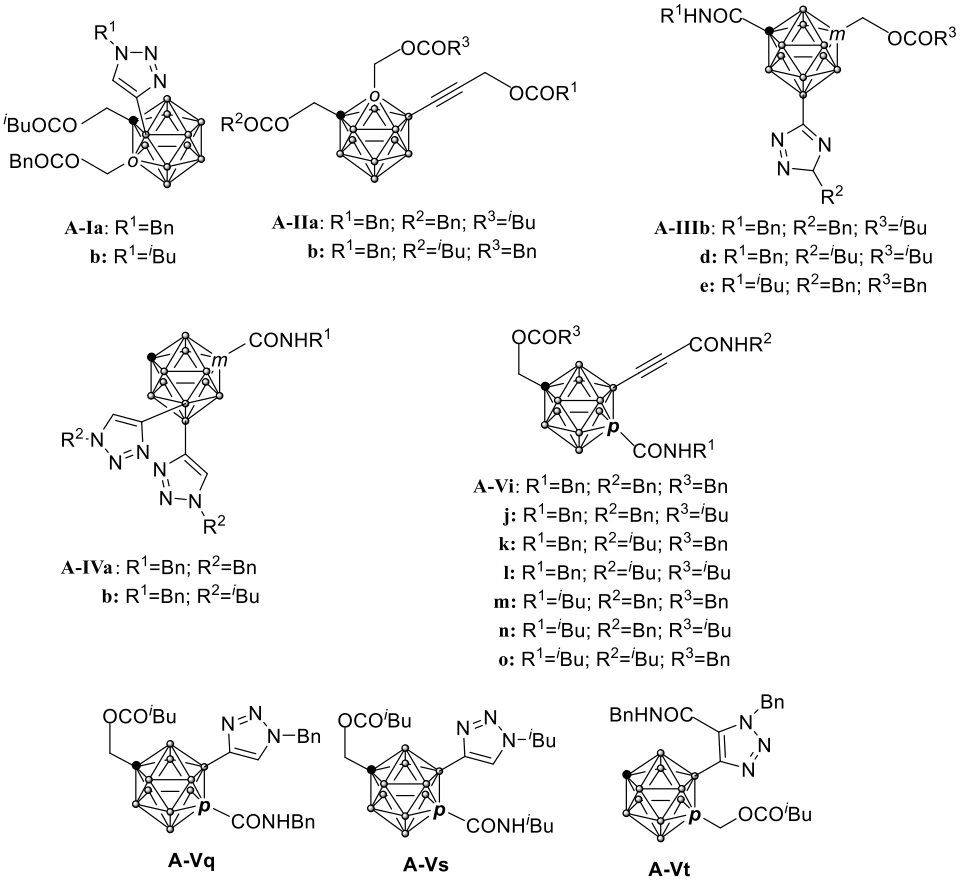

Figure 3-4. In-house library compounds: carborane compounds

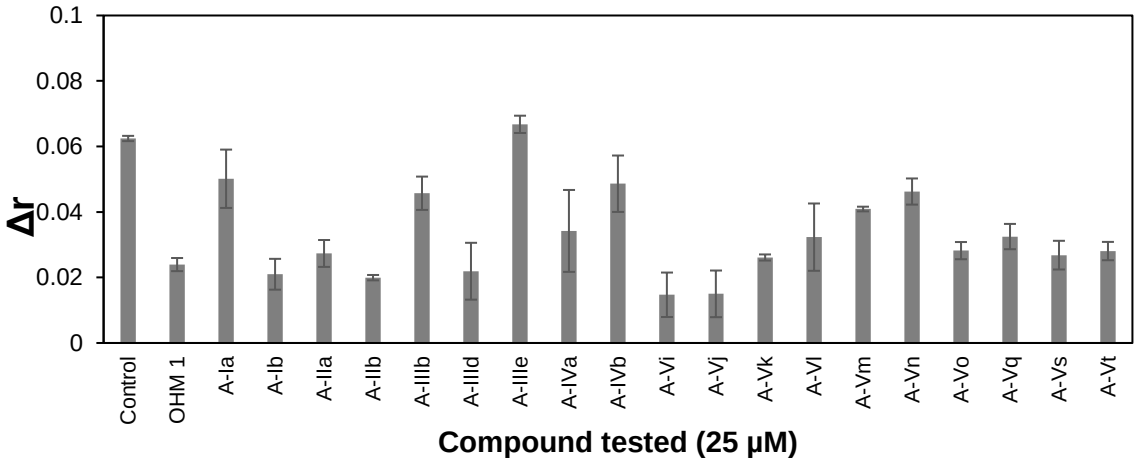

Figure 3-5. Screening of HIF-1α/p300 PPI inhibitors from in-house compound library by the established FA-assay system. p300 CH1 protein and dansyl-labeled HIF-1α α_B were incubated with compounds tested: 25 μM of carborane compounds and 10 μM of OHM1. Anisotropy was measured using SpectraMax iD5 Multi-Mode Microplate Reader (Molecular Devices, USA) with 330 nm excitation wavelength and 510 nm emission wavelength. All assays were performed in 125 nM dansyl-labeled HIF-1α α_B peptide, 200 nM recombinant p300 CH1 protein, 20 mM Tris-HCl (pH = 8.0), 60 mM NaCl, 2 mM DTT, 1.5 μM $ZnCl_2$, and 0.5% DMSO in PBS. Data are presented as means ± S.D. of three separate experiments. Error bars, S.D.

Table 3-2. Inhibition of HIF transcriptional activity of carborane compounds

Entry	Compound	HIF-1[a, b, c] [μM)[6]	Entry	Compound	HIF-1[a, b, c] [μM) [6]
1	**A-Ia**	> 30	11	**A-Vj**	3,24
2	**A-Ib**	> 30	12	**A-Vk**	3,64
3	**A-IIa**	> 30	13	**A-Vl**	18,1
4	**A-IIb**	> 30	14	**A-Vm**	23,2
5	**A-IIIb**	26,3	15	**A-Vn**	> 30
6	**A-IIId**	23,0	16	**A-Vo**	9,21
7	**A-IIIe**	> 30	17	**A-Vq**	5,59
8	**A-IVa**	> 30	18	**A-Vs**	3,24
9	**A-IVb**	17,4	19	**A-Vt**	1,34
10	**A-Vi**	5,46			

[a] Indicated half maximal inhibitory concentration (IC_{50}) are mean ± SD of a single experiment conducted in triplicate.
[b] HRE-Luc expression was measured by luciferase reporter gene assay using HRE-dependent luciferase expression in HeLa cells (O_2 1%, CO_2 5%, 37 °C, 12 h).
[c] Measured by Asawa et al. (2021).[6]

After screening the in-house library compounds, no compound exhibited significant *in vitro* HIF-1α/p300 inhibitory activity compared to OHM1. To discover a novel inhibitor for this target PPI, 80 compounds from the authentic compound library NPDepo, RIKEN, Japan, were screened using the established screening assay system. (Figure 3-6A). Each compound was tested at a concentration of 10 μM for the initial screening with OHM 1 as a positive control. Several lead compound candidates that showed better activity than OHM 1 were identified. Consequently, a second screening for the lead compound candidates at a lower concentration of 0.2 μM was conducted (Figure 3-6B). In this screening, several lead compound candidates that show HIF-1α/p300 inhibition activity better than OHM-1, e.g., ibuprofen (**S4**), naloxone (**S8**), cantharidin (**12**), flunarizine hydrochloride (**13**), perphenazine (**14**), and niclosamide (**15**) were discovered (Figure 3-7).

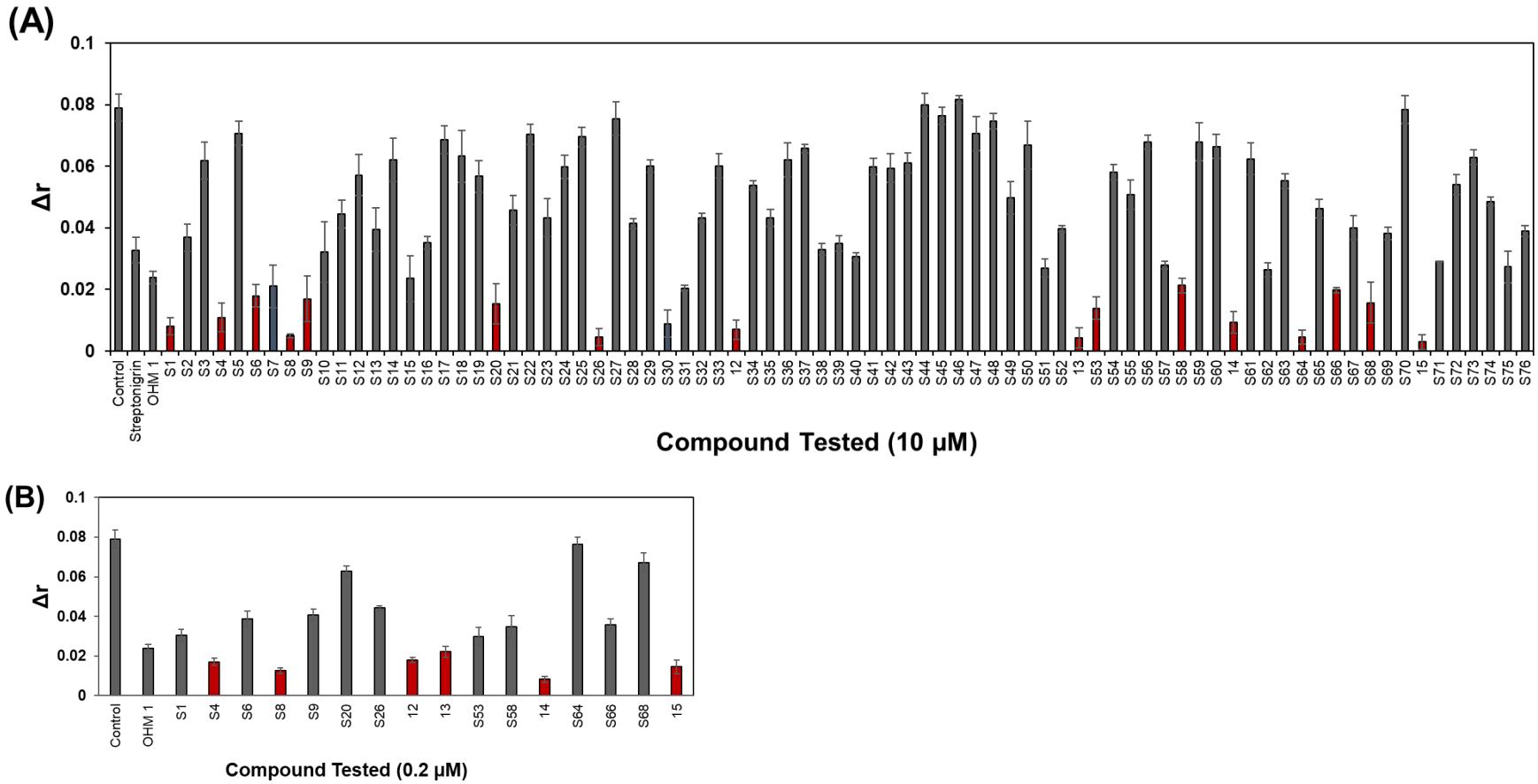

Figure 3-6. Screening of HIF-1α/p300 PPI inhibitors from NPDepo compound library by the established FA-assay system. p300 CH1 protein and dansyl-labeled HIF-1α α_B were incubated with 10 μM (A) or 0.2 μM (B) of NPDepo library compounds. Number of compounds **S1**, **S2**, **S3**, **S4**, …. **S76** are corresponding to compounds in wells A2, A3, A4, A5, …. H11 as listed in http://www.cbrg.riken.jp/auth80/list.php except for lead compound. Anisotropy was measured using SpectraMax iD5 Multi-Mode Microplate Reader (Molecular Devices, USA) with 330 nm excitation wavelength and 510 nm emission wavelength. All assays were performed in 125 nM dansyl-labeled HIF-1α α_B peptide, 200 nM recombinant p300 CH1 protein, 20 mM Tris-HCl (pH = 8.0), 60 mM NaCl, 2 mM DTT, 1.5 μM $ZnCl_2$, and 0.5% DMSO in PBS. Data are presented as means ± S.D. of three separate experiments. Error bars, S.D.

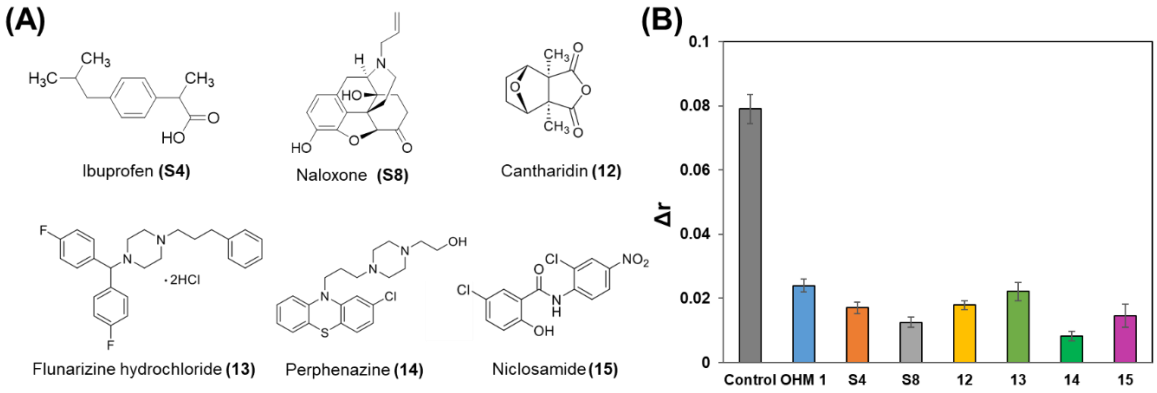

Figure 3-7. Structure of candidate lead compounds (A) and their HIF-1α/p300 PPI inhibition activity using FA assay (B). Compounds **S4, S8, 12-15** (0.2 μM) and OHM 1 (10 μM) were added to inhibit the PPI of 125 nM N-Dan-HIF-1α α_B and 200 nM recombinant p300 CH1 protein in buffer solution (20 mM Tris-HCl (pH = 8.0), 60 mM NaCl, 2 mM DTT, 1.5 μM $ZnCl_2$, 0.5% DMSO). Data are presented as means ± S.D. of three separate experiments.

3.4 Reporter gene assay for candidate HIF-1α/p300 PPI inhibitor in HeLa cells

Reporter gene assay using hypoxia response element (HRE)-luciferase-transfected HeLa cells[7,8] to evaluate compounds suggested to inhibit HIF-1α/p300 PPI, as indicated by the FA assay. LW6 was used as a positive control for HIF-1α/p300 PPI inhibition.[9] This cell line is derived from HeLa cells and is genetically engineered to express luciferase, a bioluminescent enzyme, under the control of HRE. HRE is a regulatory DNA sequence activated under low oxygen or hypoxic conditions. When cells are starved of oxygen, specific genes that allow the cells to adapt and survive are activated. One of these genes is regulated by HIF, which binds to the HRE and initiates the transcription of various adaptive genes. In this engineered cell line, luciferase under HRE control allows real-time monitoring of the hypoxic response by measuring the amount of light produced (Figure 3-8).

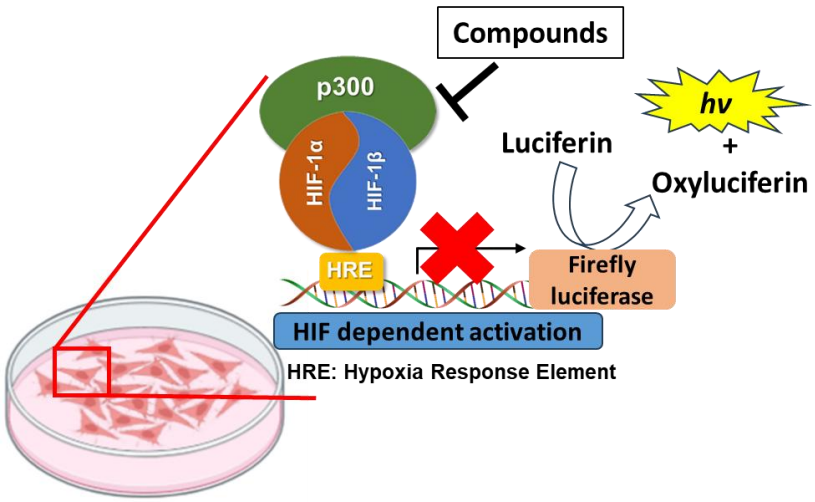

Figure 3-8. Overview of HRE-luciferase transfected HeLa cells for reporter gene assay

As shown in Table 3-3, compounds **12**-**14** inhibited HIF transcriptional activity with IC_{50} values of 5.63 ± 1.88, 9.01 ± 0.63, and 14.27 ± 1.57 μM, respectively. Compound **15** showed direct inhibition in the luciferase assay (Figure 3-9); thus, measurement of the HIF transcriptional activity of compound **15** using HRE-luciferase assay was not appropriate. Evaluation of cell growth activity of the lead compound candidates showed that compounds **12** and **15** did not have cytotoxicity in HeLa cells (> 30 μM), while compounds **13** and **14** showed cytotoxicity with IC_{50} values of 13.36 and 17.61 μM, respectively. Moreover, compounds **S4** and **S8** did not show the ability to inhibit HIF transcriptional activity (> 25 μM) and did not have cytotoxicity in HeLa cells (> 30 μM). The results indicated that these compounds **S4** and **S8** were false positives.

Table 3-3. Effects of the candidate inhibitors found by FA assay on inhibitory activities of gene transcription by HIF (HRE-Luc) and cell growth

Compounds	HIF-1[a, b] (μM)	HeLa cells[a, c] (μM)
Ibuprofen (**S4**)	> 25	> 30
Naloxone (**S8**)	> 25	> 30
Cantharidin (**12**)	5.63 ± 1.88	> 30
Flunarizine hydrochloride (**13**)	14.27 ± 1.57	13.36 ± 0.16
Perphenazine (**14**)	9.01 ± 0.63	17.61 ± 0.13
Niclosamide (**15**)	N.D.[d]	> 30
LW6 (**6**)[e]	29.1 ± 3.01	-

[a] Indicated half maximal inhibitory concentration (IC_{50}) are mean ± SD of a single experiment conducted in triplicate.

[b] HRE-Luc expression was measured by luciferase reporter gene assay using HRE-dependent luciferase expression in HeLa cells (O_2 1%, CO_2 5%, 37 °C, 8 h).

[c] Cell growth inhibitory activity was measured using MTT assay (O_2 1%, CO_2 5%, 37 °C, 8 h).

[d] Not determined (N.D.) due to direct reporter enzyme inhibition.

[e] Positive control. Reported IC_{50} = 23 μM[9]

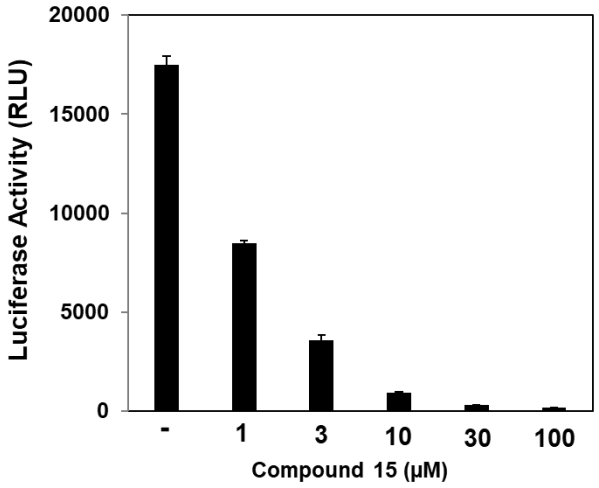

Figure 3-9. Evaluation of luciferase inhibitory activity of compound **15**. Each concentration of compound **15** and luciferase was incubated for 10 min on ice. After incubation, the luciferase activity was detected using a luciferase assay system (Promega, USA), and luminescence from luciferase was measured using a microplate reader (Infinite

F200, Tecan Japan Co., Ltd., Japan). Data are presented as means ± S.D. of three separate experiments. Error bars, S.D.

3.5 Effects of HIF-1α/p300 PPI inhibitor candidates on protein expression levels of HIF-1α and its downstream protein in HeLa cells

For further investigation, the effects of HIF-1α/p300 PPI inhibitor candidates on the expression levels of HIF-1α and its downstream protein, carbonic anhydrase IX (CAIX), were evaluated by Western blot analysis. Compound **12** (Figure 3-10A) and compound **13** (Figure 3-10B) treatments did not significantly suppress CAIX expression levels without affecting HIF-1α. In contrast, both compound **14** (Figure 3-10C) and compound **15** (Figure 3-10D) suppressed CAIX protein expression in a concentration-dependent manner without affecting HIF-1α. Due to the low cytotoxicity and its ability to suppress CAIX without affecting HIF-1α, compound **15** was selected for further experiments.

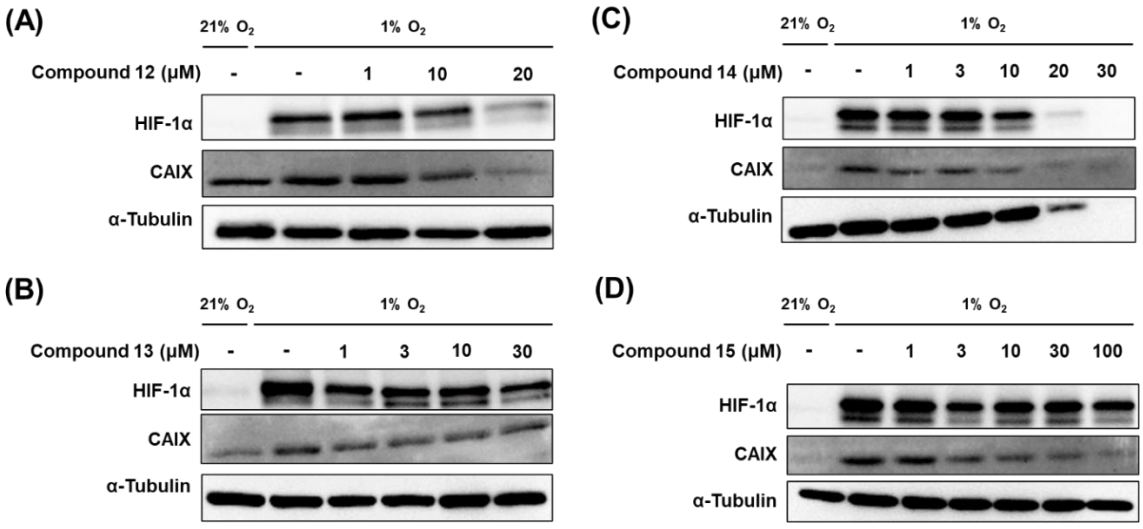

Figure 3-10. Effects of compounds **12-15** on protein expression levels of HIF-1α and its downstream protein. HeLa cells were treated with various concentrations of compounds **12-15** for 8 h under hypoxia. Cell lysates were separated by SDS-PAGE and immunoblotting was performed using HIF-1α, CAIX, and α-tubulin antibodies. α-Tubulin was used as an internal control.

3.6 Effects of niclosamide on HIF-1α and its downstream gene expressions in HeLa cells

Reverse transcription quantitative polymerase chain reaction (RT-qPCR) in combination with reverse transcription and quantitative PCR is a relatively simple, inexpensive, sensitive, and specific tool used to determine the expression level of target genes. This method requires a double-stranded DNA-specific dye that binds to newly synthesized DNA and generates fluorescence, and a special thermocycler equipped with a sensitive camera to monitor the fluorescence in each sample at frequent intervals during the PCR, respectively.[10] In this study, the RT-qPCR utilized the DNA intercalator-based (SYBR Green) method and real-time PCR system to detect of newly synthesized DNA.

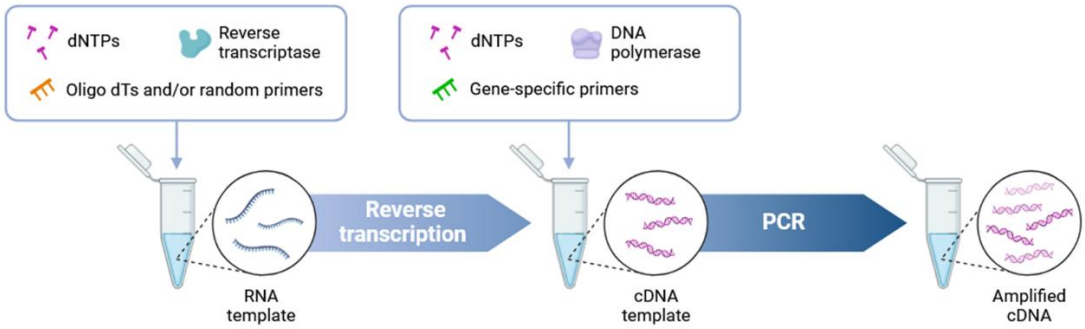

Figure 3-11. Overview of RT-qPCR workflow. This figure was created using Biorender.com.

First, RNA is isolated from cells, which includes mRNA that indicates which genes are active. The RNA is then converted into complementary DNA (cDNA) using the enzyme reverse transcriptase. The cDNA is subsequently amplified using PCR, targeting specific genes of interest. The amount of cDNA produced is directly proportional to the amount of mRNA initially present. The final step is quantification, where the amount of PCR product is measured to determine the gene expression level (Figure 3-11).

In this study, the gene expression levels of HIF-1α and its downstream signals were evaluated to confirm whether compound **15** disrupts its downstream gene expression without affecting HIF-1α levels. As shown in Figure 3-12, compound **15** did not affect HIF-1α mRNA expression but significantly suppressed the mRNA expression of CAIX. These findings suggest that compound **15** inhibits HIF-1α/p300 PPI, thereby disrupting downstream signaling pathways without directly modulating HIF-1α expression.

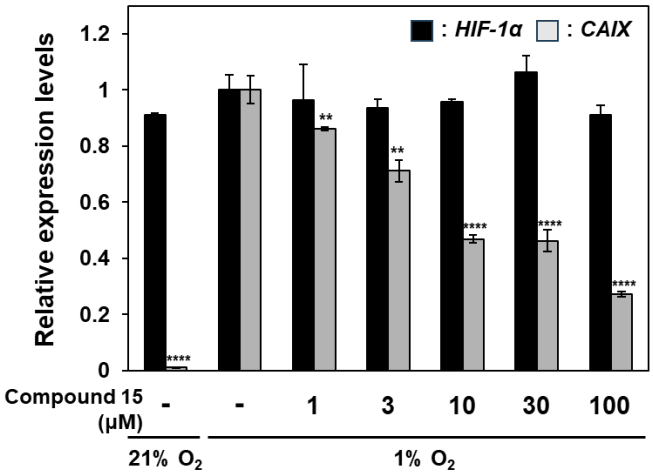

Figure 3-12. Effects of compound **15** on mRNA expression levels of HIF-1α and its downstream genes CAIX. HeLa cells were treated with various concentrations of compound **15** for 8 h under hypoxia. Total RNA was isolated from each cell, and mRNA was converted to cDNA. Gene expression levels were detected using real-time PCR. Each condition of hypoxia was defined as 1.00. Data are presented as means ± the standard deviation (SD) of three separate experiments. Error bars, SD. Significance was determined as $^{**}P < 0.01$, $^{****}P < 0.0001$ compared with sample treated without compound.

3.7 Summary

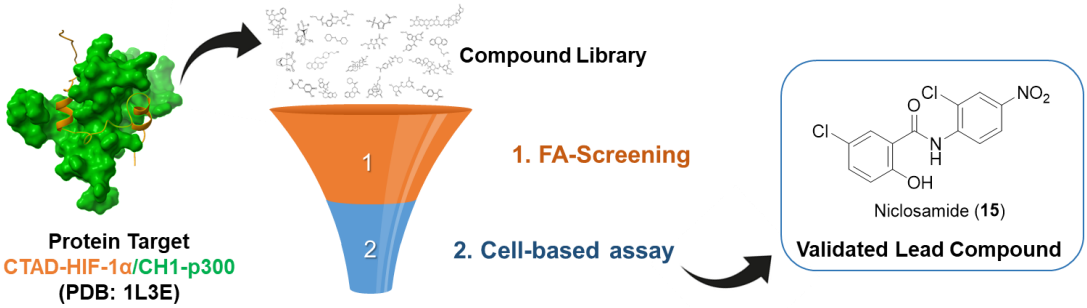

Figure 3-13. Summary of chapter 3

In chapter 3, the in-house and NPDepo compound library compounds were screened to identify several HIF-1α/p300 PPI inhibitor candidates. These lead compounds were subsequently validated in a cell-based assay (reporter gene assay, Western blot, and RT-qPCR) to confirm their inhibitory activity against the HIF-1α/p300 interaction. Among the candidates, compound **15** was identified as a promising inhibitor of the HIF-1α/p300 interaction.

3.8 References

(1) Thompson, A. D.; Dugan, A.; Gestwicki, J. E.; Mapp, A. K. Fine-Tuning Multiprotein Complexes Using Small Molecules. *ACS Chem. Biol.* **2012**, *7*, 1311–1320.

(2) Surade, S.; Blundell, T. L. Structural Biology and Drug Discovery of Difficult Targets: The Limits of Ligandability. *Chem. Biol.* **2012**, *19*, 42–50.

(3) Fox, S.; Farr-Jones, S.; Sopchak, L.; Boggs, A.; Nicely, H. W.; Khoury, R.; Biros, M. High-Throughput Screening: Update on Practices and Success. *J. Biomol. Screen.* **2006**, *11*, 864–869.

(4) Hughes, J. P.; Rees, S. S.; Kalindjian, S. B.; Philpott, K. L. Principles of Early Drug Discovery. *Br. J. Pharmacol*. **2011**, *162*, 1239–1249.

(5) Umedera, K.; Morita, T.; Yoshimori, A.; Yamada, K.; Katoh, A.; Kouji, H.; Nakamura, H. Synthesis of Three-Dimensional (Di)Azatricyclododecene Scaffold and Its Application to Peptidomimetics. *Chem. - Eur. J.* **2021**, *27* (46), 11888-11894.

(6) Asawa, Y.; Hatsuzawa, S.; Yoshimori, A.; Yamada, K.; Katoh, A.; Kouji, H.; Nakamura, H. Comprehensive Exploration of Chemical Space Using Trisubstituted Carboranes. *Sci. Rep.* **2021**, *11* (1).

(7) Miura, K.; Joshi, M.; Morita, T.; Nakamura, H. Discovery of Three-Dimensional Bicyclo[3.3.1]Nonanols as Novel Heat Shock Protein 90 Inhibitors. *Bioorg. Med. Chem.* **2023**, *93*, 1–9.

(8) Ueda, H.; Wipf, P.; Nakamura, H. Synthesis of Sp3-Rich Chiral Bicyclo[3.3.1]Nonanes for Chemical Space Expansion and Study of Biological Activities. *Bioorg. Med. Chem.* **2022**, *54*, 1–11.

(9) Nakamura, H.; Yasui, Y.; Ban, H. S. Synthesis and Biological Evaluation of Ortho-Carborane Containing Benzoxazole as an Inhibitor of Hypoxia Inducible Factor (HIF)-1 Transcriptional Activity. *J. Organomet. Chem.* **2013**, *747*, 189–194.

(10) Mo, Y.; Wan, R.; Zhang, Q. Application of Reverse Transcription-PCR and Real-Time PCR in Nanotoxicity Research; *Methods Mol. Biol.* **2012**, *926*, 99–112.

3.9 Experimental section

Screening of HIF-1α/p300 PPI inhibitor from NPDepo compounds library

A solution of 200 nM p300 CH1 protein and 125 nM dansyl-labeled HIF-1α α_B peptide was incubated at 25 °C. After 1 h, compounds with certain concentrations were added. After incubation for 1 h at room temperature, the amount of dissociated dansyl-labeled HIF-1α α_B peptide was determined by SpectraMax iD5 Multi-Mode Microplate Reader (Molecular Devices, USA) with 330 nm of excitation wavelength and 510 nm of emission wavelength. The difference anisotropy was calculated as the anisotropy of the compounds and subtracted with the buffer.

Cell culture

Human cervical carcinoma HeLa cells and HeLa cells expressing hypoxia response element-dependent firefly luciferase (HRE-Luc HeLa) were cultured in Dulbecco's modified Eagle's medium (DMEM; FUJIFILM Wako Pure Chemical Corporation, Japan) that was supplemented with 10% (v/v) heat-inactivated fetal bovine serum, 100 units/mL penicillin G potassium, and 100 μg/mL streptomycin sulfate (Thermo Fisher Scientific, Inc., MA, USA) at 37 ˚C in 5% CO_2.

Luciferase reporter gene assay

Luciferase reporter gene assay performed with reference to previously reported literature.[83,84] HRE-luc HeLa cells were seeded in a 96-well plate at a density of 2×10^4 cells/well and cultured at 37 ℃ under normoxia (21% O_2 and 5% CO_2) condition for 8 h. Then, the cells were treated with different concentrations of each compound or DMSO and incubated in normoxia for 1 h, followed by 8 h under hypoxia (1% O_2 and 5% CO_2) condition. The medium was removed and the cells were washed with cold PBS. The luciferase reporter gene assay was performed using the Luciferase Assay System (#E4550, Promega, USA) according to the manufacturer's instructions. The luminescence signals were recorded using a microplate reader (Infinite F200, Tecan group Ltd., Switzerland).

MTT assay

HeLa cells were seeded in a 96-well plate at a density of 3×10^3 cells/well and cultured at 37 ℃ under normoxia for 8 h. The cells were treated with indicated concentration of each compound or DMSO. After incubation under each condition (72 h at 37 ℃ in normoxia or 12 h at 37 ℃ in hypoxia), 0.5 mg/mL thiazolyl blue tetrazolium

bromide (MTT, diluted in PBS) was added, and incubated for 3 h at 37 ℃. Subsequently, the medium was removed and the formazan product was dissolved in 150 μL of DMSO. The absorbance at 590 nm was recorded using a microplate reader (Infinite F200, Tecan group Ltd., Switzerland).

Western Blot

HeLa cells were seeded in a 6-well plate at a density of 2×10^5 cells/well and cultured at 37 ℃ overnight. The cells were treated with different concentrations of each compound or DMSO and cultured for 8 h under hypoxia condition. The medium was removed, and the cells were washed with cold PBS and lysed with RIPA buffer (50 mM Tris-HCl (pH = 8.0), 150 mM sodium chloride, 0.5% (w/v) sodium deoxycholate, 0.1% (w/v) sodium dodecyl sulfate (SDS), 1.0% (w/v) NP-40 substitute, and protease inhibitor cocktail (Sigma-Aldrich, USA)). The obtained cell lysate was centrifuged at 16,000 x *g* for 10 min at 4 ℃. The protein concentration of each sample was determined by BCA assay. The samples were diluted in sample buffer (1 M Tris-HCl (pH = 6.8), 10% (w/w) sodium dodecyl sulfate (SDS), 500 mM DTT, 50%(v/w) glycerol, and 0.5%(w/w) bromophenol blue) and boiled for 5 min at 98 °C. Proteins in the samples were separated by SDS-PAGE and transferred to a polyvinylidene fluoride (PVDF) membrane (Merck Millipore, USA). The membrane was blocked by 5% skim milk in TTBS buffer (Tris-buffered saline containing 0.1% Tween-20) and incubated with each primary antibody (Antibody: TTBS = 1: 1000) for 12 h at 4 ℃, followed by incubation with each secondary antibody conjugated with horseradish peroxidase (Antibody: TTBS = 1: 5000). Signals were detected with ECL using ImmunoStar LD (FUJIFILM Wako Pure Chemical Corporation, Japan) or Immobilon Forte Western HRP substrates (Merck KGaA, USA). Primary antibodies were listed as follows: anti-HIF-1α (#610959, BD Biosciences, USA), anti-CAIX (#sc-365900, Santa Cruz Biotechnology, Inc., USA), and anti-α-tubulin (#013-25033, FUJIFILM Wako Pure Chemical Corporation, Japan) antibodies. The secondary antibody was used anti-mouse IgG horseradish peroxidase-linked antibody (#W4021, Promega, Madison, WI, USA).

Quantitative PCR

HeLa cells were seeded in a 6-well plate at a density of 2×10^5 cells/well and cultured at 37 ℃ overnight. Cells were treated with different concentrations of each compound or DMSO and cultured with indicated conditions. Subsequently, the medium

was removed, and the cells were washed with cold PBS. The total RNAs were extracted using TRIzol (Thermo Fisher Scientific, Inc., USA). The reverse-transcription reaction using the High-Capacity cDNA Reverse Transcription Kit (Thermo Fisher Scientific, Inc., MA, USA) was conducted according to the instructions. The obtained cDNA library was used for real-time PCR. Real-time PCR was carried out with THUNDERBIRD SYBR qPCR Mix (TOYOBO Co. LTD., Japan) using a real-time PCR system (Thermal Cycler Dice Real Time System III, Takara bio inc., Japan). The gene expression levels were analyzed by ΔΔCt method. The sequences of the primers used were shown as follows; Hypoxia-inducible factor 1-α (HIF-1α): 5'-TTTTCAAGCAGTAGGAATTGGAA-3' (forward) and 5′-GTGATG TAGTAGCTGCATGATCG-3′ (reverse); Carbonic anhydrase IX (CAIX): 5′-ACCCTCTCTGACACCCTGTG-3′ (forward) and 5′-GGCTGGCTTCTCACATTCTC-3′ (reverse); β2-microglobulin (B2M): 5′-TACATGTCTCGATCCCACTT-3′ (forward) and 5′-TACACTGAATTCACCCCCAC-3′ (reverse).

Determination of luciferase activity

Each compound and 10 nM QuantiLum recombinant luciferase (Promega, USA, diluted in stability buffer: 25 mM Tris-HCl (pH = 7.5), 8 mM $MgSO_4$, 0.1 mM EDTA, 10 mg/mL bovine serum albumin (BSA), 10% glycerol, and 0.25% Triton X-100) were incubated in reaction buffer (10 mM Tris-HCl (pH = 7.5), 3 mM $MgCl_2$, 50 mM KCl, 2 mM DTT, and 10 mM adenosine triphosphate (ATP)) for 10 min at on ice. After incubation, the luciferase activity was detected using luciferase assay system (Promega, USA), and luminescence from luciferase was measured using a microplate reader (Infinite F200, Tecan Japan Co., Ltd., Japan).

Chapter 4

Identification of the Binding Site of Niclosamide using Photoaffinity Labeling

4.1 Introduction

The identification and characterization of protein binding sites for small molecules are crucial for understanding the functions of endogenous ligands and drug molecules.[1] According to chapter 3, compound **15** has been identified as a promising inhibitor of the HIF-1α/p300 interaction. Since the binding site of compound **15** in the p300 CH1 protein remains unknown, the binding site was investigated using the photoaffinity labeling (PAL) method (Figure 4-1A). This method enables us to elucidate the interaction mechanisms between the compound and the active sites of the target protein. In order to facilitate the binding and covalent modification of the active site in proteins, a small molecule probe typically aligns photoaffinity labeling with a reactive group.[2,3]

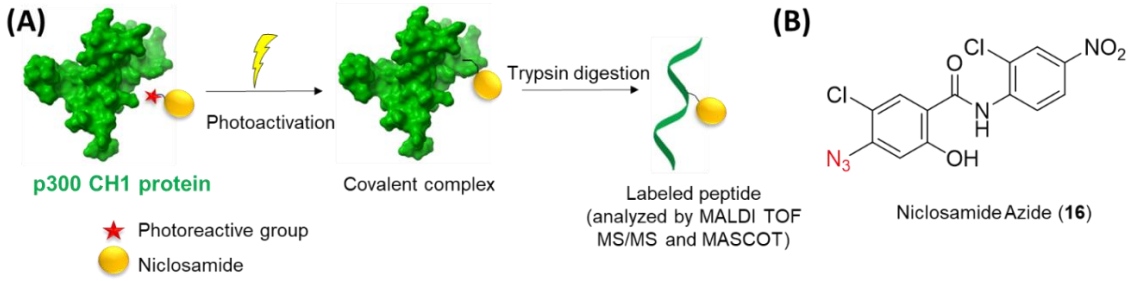

Figure 4-1. (A) Design of PAL experiment for binding site identification. (B) The chemical structure of compound **16** for PAL probe.

In this study, niclosamide azide **(16)** was designed and synthesized as a PAL probe, aiming for minimal structural changes to preserve its activity (Figure 4-1 B). Aryl azides are frequently used as photoaffinity labeling agents to investigate ligand-protein interactions.[2,3] Upon irradiation, aryl azides release N_2 to generate transient aryl nitrene intermediates[4,5], which may rapidly undergo ring expansion to form a 1,2-didehydroazepine (cyclic ketenimine) intermediate. Both the nitrene and ketenimine intermediates can insert into C–H, N–H, or O–H bonds to form covalently labeled products. For photolabeling proteins with aryl azide, the insertion reaction occurs preferentially toward nucleophilic amino acid residues in close proximity, such as lysine (K), cysteine (C), methionine (M), tyrosine (Y), and tryptophan (W).[6,7] Based on the information observed from the PAL experiment, the binding interaction between compound **16** as well as compound **15** in p300 CH1 protein was further investigated using molecular docking simulation.

4.2 Design and synthesis of niclosamide azide as photoaffinity labeling probe

Compound **16** as a PAL probe was synthesized according to Scheme 4-1. Compound **16** was synthesized through four steps. The first step is the nucleophilic substitution of 4-amino-5-chloro-2-methoxybenzoic acid (**17**) with sodium azide in aqueous media. This reaction afforded compound 4-azido-5-chloro-2-methoxybenzoic acid (**18**) in 95% of the yield. This compound was then reacted with thionyl chloride to convert the benzoic acid into acyl chloride (**19**). The acyl chloride product was used in the next step without further purification. The crude acyl chloride was reacted with 2-chloro-4-nitroaniline (**20**) and triethylamine as the base to produces condensation product 4-azido-5-chloro-*N*-(2-chloro-4-nitrophenyl)-2-methoxybenzamide (**21**) in 30% of yield. This relatively low yield was affected by the less nucleophilic of aniline due to bearing nitro group in para position so that it will withdraw electron density through resonance. The compound **21** was then demethylated using BBr_3 and the compound **16** was afforded with 37% of yield.

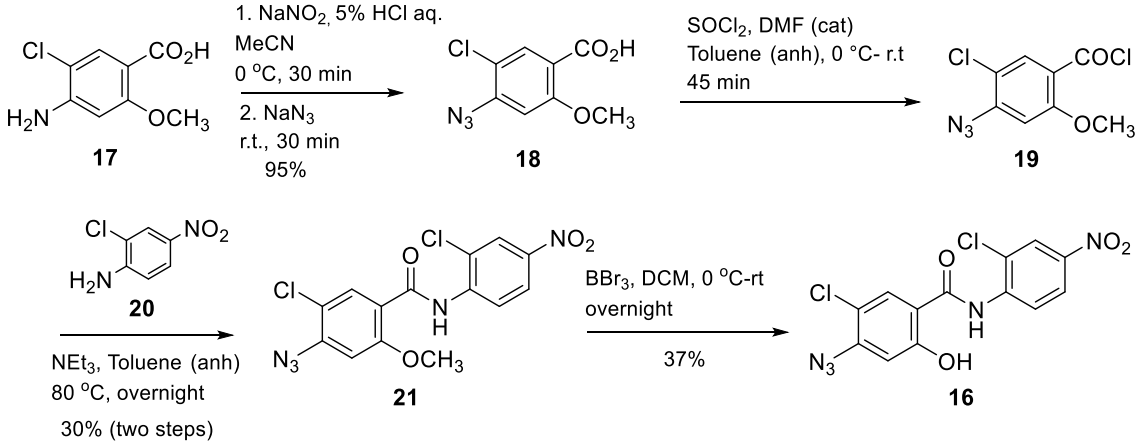

Scheme 4-1. Synthesis of compound **16**

4.3 Evaluation of niclosamide azide as photoaffinity labeling probe

Before conducting the PAL experiment, compound **16** was evaluated for its effect on HIF-1α and CAIX protein expression in HeLa cells. estern blot results revealed that compound **16** suppresses CAIX protein levels without affecting HIF-1α, starting at a concentration of 10 μM in a concentration-dependent manner (Figure 4-2). Compound **16** was also shown to inhibit luciferase enzyme directly, with comparable efficacy to compound **15** (Figure 4-3). In the FA assay, compound **16** has activity to inhibit HIF-

1α/p300 with IC_{50} value of 83.5 nM (Figure 4-4). Since compound **16** shows similar activity to compound **15**, it can be used as a probe for PAL experiment.

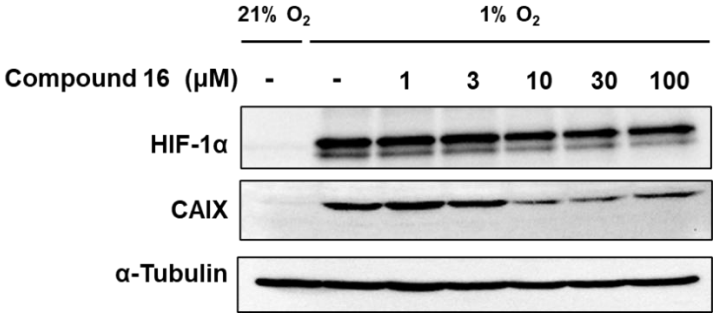

Figure 4-2. Effects of compound **16** on expression levels of HIF-1α and its downstream protein CAIX. HeLa cells were treated with various concentrations of compound **16** for 8 h under hypoxia. Cell lysates were separated by SDS-PAGE and immunoblotting was performed using HIF-1α, CAIX, and α-tubulin antibodies. α-Tubulin was used as an internal control.

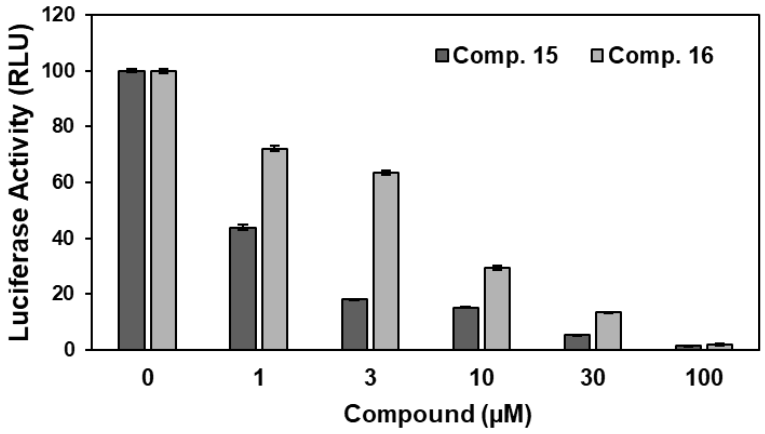

Figure 4-3. Luciferase inhibitory activity of compounds **15** and **16**. Each concentration of compounds and luciferase was incubated for 10 min on ice. After incubation, the luciferase activity was detected using a luciferase assay system (Promega, USA), and luminescence from luciferase was measured using a microplate reader (Infinite F200, Tecan Japan Co., Ltd., Japan).

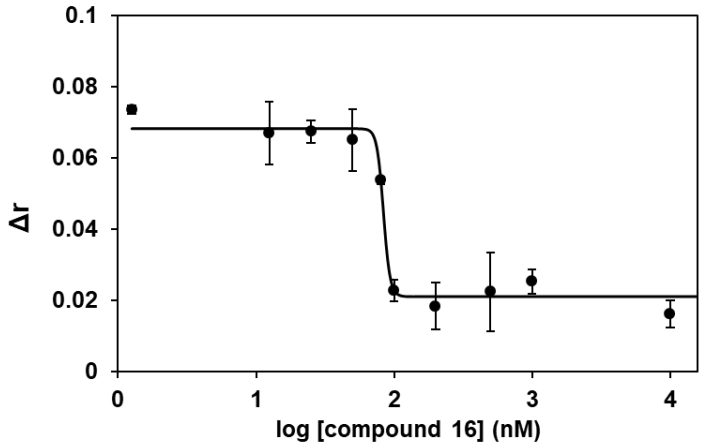

Figure 4-4. Competition assay of compound **16** for p300 CH1 protein. The p300 CH1 protein was incubated with dansyl-labeled HIF-1α α_B and the addition of compound **16**. Anisotropy was measured using SpectraMax iD5 Multi-Mode Microplate Reader (Molecular Devices, USA) with 330 nm of excitation wavelength and 510 nm of emission wavelength. All assays were performed in 200 nM dansyl-labeled HIF-1α α_B peptide, 200 nM recombinant p300 CH1 protein, 20 mM Tris-HCl (pH = 8.0), 60 mM NaCl, 2 mM DTT, 1.5 μM $ZnCl_2$, and 0.5% DMSO in PBS. IC_{50} values competition assay of compound **16** on p300 CH1 and dansyl-labeled HIF-1α α_B PPI was calculated 83.5 ± 1.1 nM. Data are presented as means ± S.D. of three separate experiments. Error bars, S.D.

4.4 Binding site identification of niclosamide in p300 CH1 protein

The PAL experiment was conducted in 2 μg of p300 CH1 protein solution in PBS and compound **16** (0.1 and 1 μM) with or without compound **15** (10 μM) for the competitive PAL experiment (Table 4-1). The mixture was incubated at room temperature for 1 h. For the competitive PAL experiment, compound **15** was preincubated for 1 h in a protein solution before the addition of the probe. The mixture was then irradiated with 365 nm UV light (610 μW/cm^2) for 30 min to form a covalent bond with the target protein. The sample was resolved on SDS-PAGE and subjected to in-gel trypsin digestion to degrade the proteins into peptide fragments. The peptide samples were analyzed using MALDI-TOF MS/MS, followed by a Mascot search to identify the amino acid sequences targeted by compound **16**.

Table 4-1. PAL experiment with or without compound **15** pretreatment.

Entry	[Protein] (µg in 40 µL PBS)	[Compound **16**] (µM)	[Compound **15**] (µM)
Negative Control (C)	2	-	-
P1	2	0.1	-
P2	2	1	-
P3	2	0.1	10
P4	2	1	10

Table 4-2. Summary of peptides identified in Mascot Search

P1	**P2**	**P3**	**P4**
R.KLIQQQLVLLLHAHK.C	R.KLIQQQLVLLLHAHK.C	R.KLIQQQLVLLLHAHK.C	R.KLIQQQLVLLLHAHK.C
K.LIQQQLVLLLHAHK.C	K.LIQQQLVLLLHAHK.C	K.LIQQQLVLLLHAHK.C	K.LIQQQLVLLLHAHK.C
K.LIQQQLVLLLHAHKCQR.R	K.LIQQQLVLLLHAHKCQR.R	K.LIQQQLVLLLHAHKCQR.R	K.LIQQQLVLLLHAHKCQR.R
R.QCNLPHCR.T	R.QCNLPHCR.T	R.QCNLPHCR.T	R.QCNLPHCR.T
K.NVLNHMTHCQSGK.S	K.NVLNHMTHCQSGK.S	K.NVLNHMTHCQSGK.S	K.NVLNHMTHCQSGK.S
K.SCQVAHCASSR.Q	K.SCQVAHCASSR.Q	K.SCQVAHCASSR.Q	K.SCQVAHCASSR.Q
K.SCQVAHCASSRQIISHWK.N	R.QIISHWK.N	R.QIISHWKNCTR.H	R.QIISHWK.N
R.QIISHWK.N	R.QIISHWK.N + Comp. **16**	K.NCTRHDCPVCLPLK.N	R.QIISHWKNCTR.H
R.QIISHWKNCTR.H	R.QIISHWKNCTR.H	R.HDCPVCLPLK.N	K.NCTRHDCPVCLPLK.N
K.NCTRHDCPVCLPLK.N	K.NCTRHDCPVCLPLK.N		R.HDCPVCLPLK.N
R.HDCPVCLPLK.N	R.HDCPVCLPLK.N		

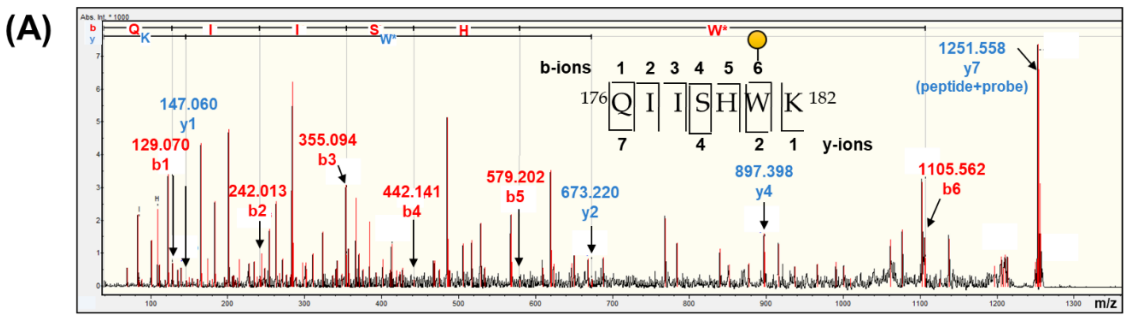

Figure 4-5. Identification of labeled peptide. (A). MS/MS spectra of ^{176}QIISHW*K^{182} peptide, showing binding site of compound **16** in p300 CH1 protein. (B). Summary of the identified labeled peptide. The potential amino acid conjugated with compound **16** is indicated in red, while the labeled peptide is presented in bold. The amino acid labeled

probe is underlined, and the amino acids detected through the Mascot search are highlighted.

The identified peptides were summarized in Table 4-2. A labeled peptide was detected from the PAL treatment using a 1 μM concentration of the PAL probe. Binding competition with 10 μM of compound **15** in the P3 and P4 sample treatment shows the result of no labeled peptide detected. MS/MS analysis detected fragmented peptides, including b1, b2, b3, b4, b5, b6, y1, y2, y4 and y7 ions with the modification probe attached to tryptophan (Trp^{181}) (Figure 4-5A). Despite several possible amino acid conjugations with compound **16**, only one labeled peptide was detected (Figure 4-5B). This finding suggests that the binding of compound **16** to Trp^{181} is selective. Furthermore, the identified binding site is localized within the Zn^{2+}-coordination site of HIF-1α/p300 (Figure 4-6).

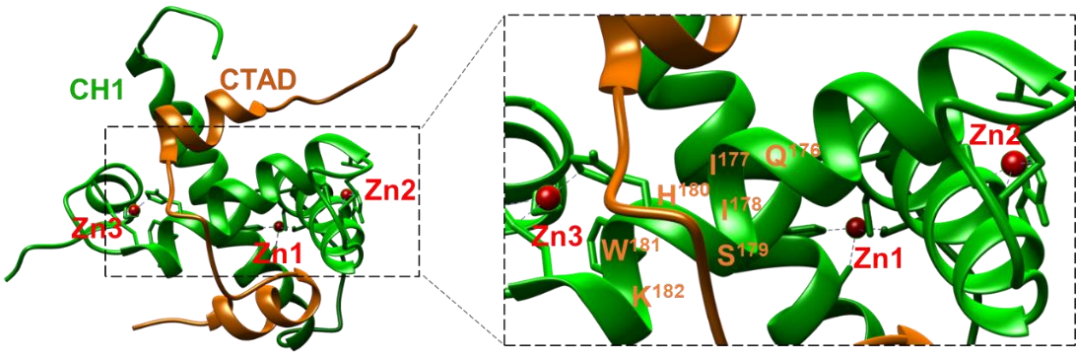

Figure 4-6. Identified binding site located in Zn^{2+}-coordination site of HIF-1α/p300.

4.5 Binding mode identification of niclosamide in p300 CH1 protein

Based on the information observed from the PAL experiment, the binding interaction between compound **16** and p300 CH1 protein was further investigated using Discovery Studio (Figure 4-7). Docking studies revealed that the azide moiety of compound **16** forms key interactions, including a carbon-hydrogen bond and an attractive charge interaction with His^{180}, and is located near Trp181, which supports the binding of compound **16** in the PAL experiment. The probe interacts with several amino acid residues in p300 CH1 domain. Specifically, the nitro group engages in a pi-cation interaction with Asp^{109}, while the benzene ring exhibits pi-alkyl interactions with Lys^{112} and Ile^{116}. Additional van der Waals's interactions were observed with Gln^{176}, Leu^{120}, Ile^{177}, and Trp^{181}. Chloro substituents also play a critical role by forming alkyl-binding interactions with Val^{191} and His^{180}.

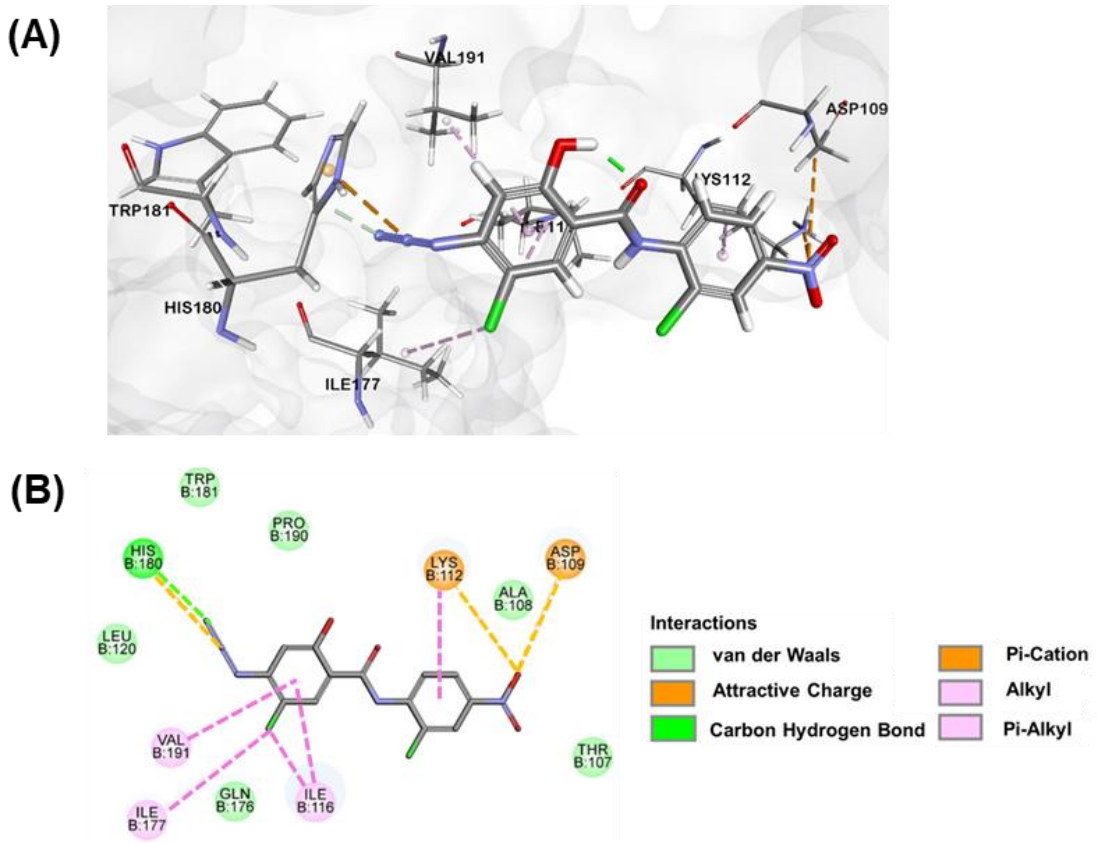

Figure 4-7. Prediction of the binding site for compound **16** to p300. (A) Molecular docking simulation of compound **16** and p300 CH1 protein. (B) Binding interaction between compound **16** and p300.

According to the investigation of compound **16**, the same binding site was used to study the interaction between compound **15** and p300 CH1 protein (Figure 4-8). The molecular docking showed that the nitro group of compound **15** forms a carbon-hydrogen bond with Pro^{110}, while the benzene ring exhibits pi-alkyl interactions with several amino acids such as Pro^{190}, Val^{191}, and Ile^{116}. The chloro substituents also contribute to significant alkyl-binding interactions with Ile^{177}, Leu^{120}, and His^{180}. Compounds **15** and **16** interact with His^{180}, which is important in the Zn^{2+} binding site in p300 CH1 protein.

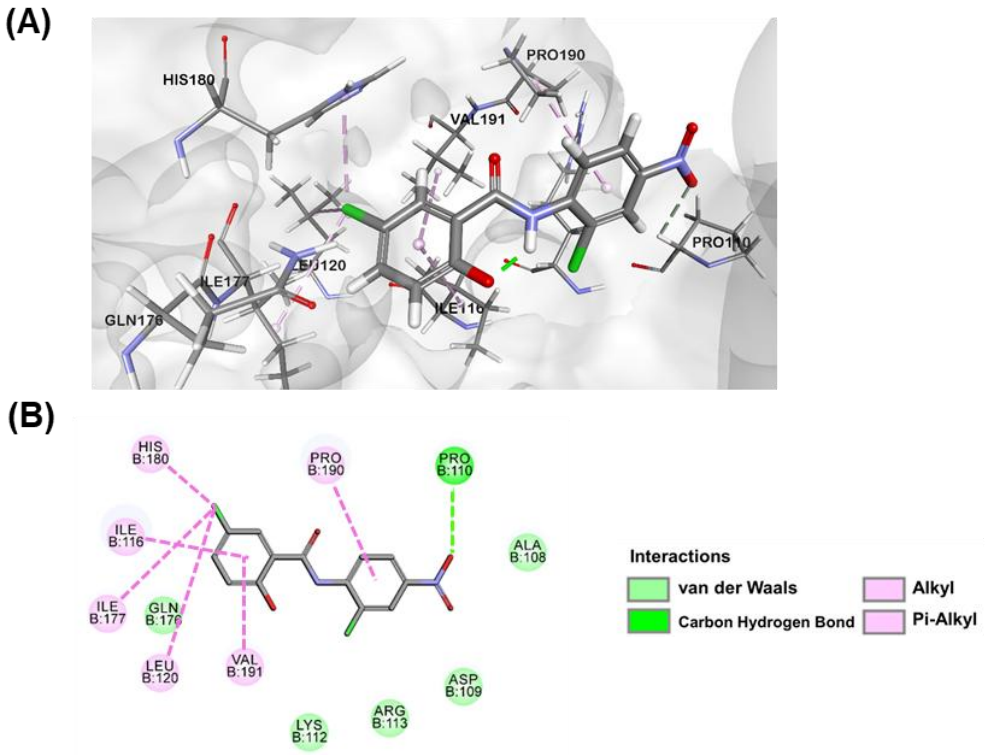

Figure 4-8. Prediction of the binding site for compound **15** to p300. (A) Molecular docking simulation of compound **15** and p300 CH1 protein. (B) Binding interaction between compound **15** and p300.

Having successfully elucidated the binding interaction of compound **15** with the p300 CH1 protein, the FA-based assay for compound **15** derivatives (**15a-r**), which were provided by RIKEN, Japan were examined. The structures, anisotropy changes (Δr) and binding energies of compound **15** derivatives **15a-r** are summarized in Appendix 2. A certain correlation was observed between the binding energies and inhibitory activities of compound **15** and its derivatives **15a-r**. The compounds with high -CDOCKER energy values, such as compounds **15**, **15d**, **15f**, **15h**, and **15k**, corresponded with low anisotropy values, indicating reduced binding affinity. In contrast, compounds with low -CDOCKER energy values, including compounds **15a**, **15b**, **15c**, **15g**, **15n**, and **15r**, displayed higher anisotropy values, suggesting stronger binding interactions. Among them, derivatives **15d** and **15k** were found to possess an ability to disrupt the HIF-1α/p300 PPI similar to compound **15**.

4.6 Summary

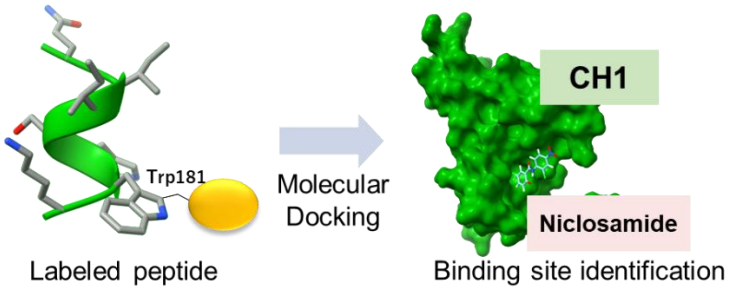

Figure 4-9. Summary of chapter 4

In chapter 4, compound **16** was synthesized as a probe for PAL experiments. Its inhibition of HIF-1α/p300 PPI was confirmed through FA and cell-based assays, demonstrating that it retains activity comparable to compound **15**. The PAL experiment successfully identified the binding site of compound **16** in the p300 CH1 protein, which is located in the Zn^{2+}-coordination site of HIF-1α/p300. Molecular docking experiments revealed that the docking positions and interactions of compounds **15** and **16** with p300 are almost identical, indicating that compound **15** binds to the Zn^{2+} coordination site of p300.

4.7 References

(1) Guo, Z.; Li, B.; Cheng, L. T.; Zhou, S.; McCammon, J. A.; Che, J. Identification of Protein-Ligand Binding Sites by the Level-Set Variational Implicit-Solvent Approach. *J. Chem. Theory Comput.* **2015**, *11*, 753–765.

(2) Cenini, S.; Gallo, E.; Caselli, A.; Ragaini, F.; Fantauzzi, S.; Piangiolino, C. Coordination Chemistry of Organic Azides and Amination Reactions Catalyzed by Transition Metal Complexes. *Coord. Chem. Rev.* **2006**, *250*, 1234–1253.

(3) Singh, A.; Thornton, E. R.; Westheimer, F. H. The Photolysis of Diazoacetylchymotrypsin. *J. Biol. Chem.* **1962**, *237*, 3006–3008.

(4) Chen, Y.; Topp, E. M. Photolytic Labeling and Its Applications in Protein Drug Discovery and Development. *J. Pharm. Sci*. **2019**, *108*, 791–797.

(5) Brandenberg, O. F.; Fasan, R.; Arnold, F. H. Exploiting and Engineering Hemoproteins for Abiological Carbene and Nitrene Transfer Reactions. *Curr. Opin. Biotechnol.* **2017**, *47*, 102–111.

(6) Marcinek, A.; Platz', M. S.; Chan, S. Y.; Floresca, R.; Rajagopalan, K.; Gounski, M.; Watt', D. Unusually Long Lifetimes of the Singlet Nitrenes Derived from 4-Azido-2,3,5,6-Tetrafluorobenzamides; *J. Phys. Chem.* **1994**, *98*, 412-419.

(7) Kyba, E. P.; Abramovitch, R. A. Photolysis of Alkyl Azides. Evidence for a Nonnitrene Mechanism. *J. Am. Chem. Soc.* **1980**, *102*, 735-740.

4.8 Experimental section

Biology

Western Blot

HeLa cells were seeded in a 6-well plate at a density of 2×10^5 cells/well and cultured at 37 ℃ overnight. The cells were treated with different concentrations of each compound or DMSO and cultured for 8 h under hypoxia condition. The medium was removed, and the cells were washed with cold PBS and lysed with RIPA buffer (50 mM Tris-HCl (pH = 8.0), 150 mM sodium chloride, 0.5% (w/v) sodium deoxycholate, 0.1% (w/v) sodium dodecyl sulfate (SDS), 1.0% (w/v) NP-40 substitute, and protease inhibitor cocktail (Sigma-Aldrich, USA)). The obtained cell lysate was centrifuged at 16,000 x *g* for 10 min at 4 ℃. The protein concentration of each sample was determined by BCA assay. The samples were diluted in sample buffer (1 M Tris-HCl (pH = 6.8), 10% (w/w) sodium dodecyl sulfate (SDS), 500 mM DTT, 50%(v/w) glycerol, and 0.5%(w/w) bromophenol blue) and boiled for 5 min at 98 ℃. Proteins in the samples were separated by SDS-PAGE and transferred to a polyvinylidene fluoride (PVDF) membrane (Merck Millipore, USA). The membrane was blocked by 5% skim milk in TTBS buffer (Tris-buffered saline containing 0.1% Tween-20) and incubated with each primary antibody (Antibody: TTBS = 1: 1000) for 12 h at 4 ℃, followed by incubation with each secondary antibody conjugated with horseradish peroxidase (Antibody: TTBS = 1: 5000). Signals were detected with ECL using ImmunoStar LD (FUJIFILM Wako Pure Chemical Corporation, Japan) or Immobilon Forte Western HRP substrates (Merck KGaA, USA). Primary antibodies were listed as follows: anti-HIF-1α (#610959, BD Biosciences, USA), anti-CAIX (#sc-365900, Santa Cruz Biotechnology, Inc., USA), and anti-α-tubulin (#013-25033, FUJIFILM Wako Pure Chemical Corporation, Japan) antibodies. The secondary antibody was used anti-mouse IgG horseradish peroxidase-linked antibody (#W4021, Promega, Madison, WI, USA).

Determination of luciferase activity

Each compound and 10 nM QuantiLum recombinant luciferase (Promega, USA, diluted in stability buffer: 25 mM Tris-HCl (pH = 7.5), 8 mM $MgSO_4$, 0.1 mM EDTA, 10 mg/mL bovine serum albumin (BSA), 10% glycerol, and 0.25% Triton X-100) were incubated in reaction buffer (10 mM Tris-HCl (pH = 7.5), 3 mM $MgCl_2$, 50 mM KCl, 2 mM DTT, and 10 mM adenosine triphosphate (ATP)) for 10 min at on ice. After incubation,

the luciferase activity was detected luciferase assay system (Promega, USA), and luminescence from luciferase was measured using a microplate reader (Infinite F200, Tecan Japan Co., Ltd., Japan).

FA measurement of compound 16

A solution of 200 nM p300 CH1 protein and 125 nM labeled peptide was incubated at 25 °C. After 1 h, compounds with certain concentrations were added. After incubation for 1 h at room temperature, the amount of dissociated fluorescent probe was determined by SpectraMax iD5 Multi-Mode Microplate Reader (Molecular Devices, USA) with 330 nm of excitation wavelength and 510 nm of emission wavelength. The difference anisotropy was calculated as the anisotropy of the compound and subtracted with the buffer.

Photoaffinity labeling and protein purification

Recombinant p300 CH1 protein (2 μg) and each compound (0.1 and 1 μM of compound **16** with or without 10 μM of compound **15**) was placed on ice and exposed to 365 nm UV light for 30 min. The samples were diluted in PBS containing 1.5 μM $ZnCl_2$ and boiled for 5 min at 98 °C. The photoaffinity labeled p300 CH1 protein was purified by SDS-PAGE using 22.5% polyacrylamide gel. The proteins in the gel were visualized with coomassie brilliant blue (CBB) G-250.

In-gel trypsin digestion

Protein band stained by CBB was excised from polyacrylamide gel and diced into small pieces (approximately 1 mm^3). The gel was destained by vortexing for 10 min with destaining buffer (30% of acetonitrile (MeCN) in 100 mM aqueous NH_4HCO_3 solution), followed by removing the supernatant. The destaining step was repeated several times until the gel become transparent. Subsequently, the gel was vortexed with MeCN for 10 min and dehydrated for 15 min using a centrifugal evaporator (CVE-2000, EYELA). The proteins in the gel were reduced using reduction buffer (100 mM DTT in 100 mM aqueous NH_4HCO_3 solution) at 56 °C for 45 min, and exposed cysteine residues were protected with acetamide group by incubation with alkylation buffer (250 mM 2-iodoacetamide in 100 mM aqueous NH_4HCO_3 solution) for 45 min in the dark. The resulting gel pieces were washed with 100 mM aqueous NH_4HCO_3 solution and 50% MeCN in 100 mM aqueous NH_4HCO_3 solution and dehydrated by addition of MeCN. The dehydrated gels were incubated with trypsin solution (100 ng/μL trypsin in 50 mM aqueous NH_4HCO_3 for 16 h

at 37 °C. Extraction solution (50% MeCN solution containing 1% trifluoroacetic acid (TFA)) was used to stop the trypsin digestion reaction and the peptides in gel were extracted by vortexing the gel with the extraction solution for 20 min. This step was repeated at least three times to collect all extraction solutions, followed by evaporation of the peptide solution to dryness. The obtained residue was dissolved in aqueous TFA solution (final conc. 0.1%) and the peptide solution was desalted using a Ziptip C18 tip (Nikkyo Technos Co., Ltd.). The desalted sample was directly subjected to MALDI TOF MS analysis.

Mascot search

The raw MS data were searched against the p300 CH1 protein database using the Mascot search algorithm. The search parameters were set as follows: peptide mass tolerance, 1.2 ppm; MS ion mass tolerance, 1.2 ppm; enzyme set as trypsin and allowance of up to two missed cleavages; variable modifications included oxidation on methionine, carbamidomethylation of cysteine residues and all the possible modifications of probe.

Molecular Docking experiments

Molecular docking was performed to predict the binding poses of compound **15** derivative on the p300 CH1 protein. All the calculations were performed on an Intel CPU@2.90 GHz with 32 GB RAM compiled under the Windows 11 Pro operating system. Discovery Studio was provided by the Institute of Science Tokyo. The crystal structure of p300 CH1 protein (PDB ID: 1L3E) was obtained from a protein data bank for docking simulation. The crystal structure contains two chains, i.e., chain A is CTAD of HIF-1α and chain B is CH1 domain of p300 and 3 Zn2+, which this cation maintains the protein structure. Chain A and Zn^{2+} residue were deleted from the structure and the protein was prepared by removing all water molecules using the protein preparation tool. The binding sites were generated using a pharmacophore-ligand binding site. The binding site was chosen based on photoaffinity labeling results. The ligand was prepared and the docking was started using CDOCK, a grid-based molecular docking method. Docking energy was then compared between the derivatives to study the relationship of the structure and activity.

Chemistry

General Information

NMR spectra were recorded on a Bruker biospin AVANCE II (400 MHz for 1H, 100 MHz for ^{13}C) or Bruker biospin AVANCE III (500 MHz for ^{1}H, 125 MHz for ^{13}C) instrument in the indicated solvent. Chemical shifts are reported in parts per million (ppm) relative to $CDCl_3$ (7.26 ppm for ^{1}H NMR, 77.16 ppm for ^{13}C NMR) or DMSO-d_6 (2.50 ppm for ^{1}H NMR, 39.52 ppm for ^{13}C NMR). Multiplicities are reported using the following abbreviations: s, singlet; d, doublet; dd, doublet of doublets; t, triplet; q, quartet; m, multiplet; brs, broad; *J*, coupling constants in Hertz. High-resolution mass spectra (HRMS) were recorded on a Bruker electrospray ionization (ESI)–time of flight (TOF)–mass spectrometer (micrOTOF II). Analytical thin-layer chromatography (TLC) was performed on a glass plate of silica gel 60 GF254 (Merck). All chemicals and reagents for biological experiments were obtained from commercial sources and used without further purification. The purity of all assayed compounds was determined by a reverse-phase HPLC system (JASCO Corporation, Japan) equipped with a C18 column (Finepak SIL C18S (4.6 x 75 mm), JASCO Corporation, Japan). All synthesized compounds were detected using a UV detector at 215 nm with 0.1% formic acid in H_2O: 0.1% formic acid in MeCN from 0-100% of solvent B for 20 min; flow rate 1.0 mL/min). All organic synthesis experiments encountered no unexpected or unusually high safety hazards.

Synthesis of 4-azido-5-chloro-2-methoxybenzoic acid (18)

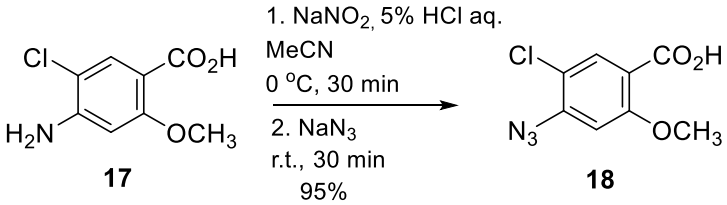

To a solution of 4-amino-5-chloro-2-methoxybenzoic acid (100 mg, 0.496 mmol, 1.0 equiv.) and 5% HCl aq. (2 mL) in 20 mL of MeCN, an aqueous solution of $NaNO_2$ (2 mL; 41.3 mg, 0.599 mmol, 1.2 equiv.) was added dropwise at 0 ºC. After stirring for 30 min at 0 ºC, an aqueous solution of NaN_3 (2 mL; 48.8 mg, 0.750 mmol, 1.5 equiv.) was added dropwise at 0 ºC, and the reaction mixture was warmed to room temperature and stirred for 30 min. The reaction mixture was extracted with ethyl acetate (EtOAc) three times. The combined organic layers were washed with water and brine, dried over $MgSO_4$,

filtered, and concentrated under reduced pressure. The obtained residue was purified by silica gel column chromatography (*n*-hexane/EtOAc) = 50 : 50 to 25 : 75) to afford compound **18** (108 mg, 0.474 mmol, 95% yield) as a yellow solid. Mp: 160-161 °C. ^{1}H NMR (400 MHz, $CDCl_3$) δ 10.29 (br, 1H), 8.17 (s, 1H), 6.77 (s, 1H), 4.10 (s, 3H); ^{13}C NMR (125 MHz, $CDCl_3$) δ 163.5, 157.5, 143.3, 135.8, 118.9, 115.3, 103.2, 57.5. HRMS (ESI, positive) calcd for $C_8H_6ClN_3O_3Na^+$ $[M + Na]^+$ 249.9990, found 249.9991.

Synthesis of 4-azido-5-chloro-N-(2-chloro-4-nitrophenyl)-2-methoxybenzamide (21)

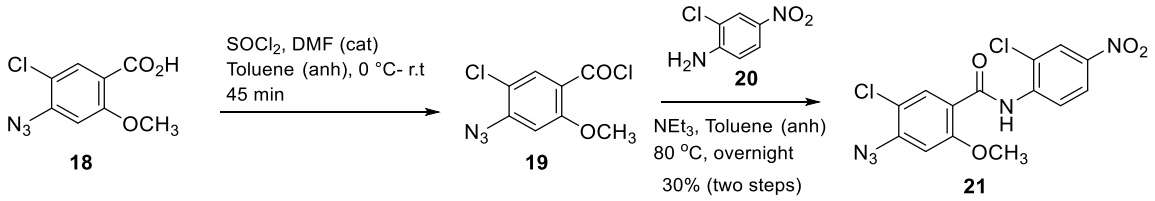

To a solution of compound **18** (97.0 mg, 0.426 mmol, 1.0 equiv.) in 5 mL of dry dichloromethane (DCM), $SOCl_2$ (309 μL, 4.27 mmol, 10.0 equiv.) and a drop of DMF was added at 0 °C. After stirring at room temperature for 45 min, the reaction mixture was concentrated under reduced pressure to afford crude acid chloride **19** as a brown solid. To a suspension of crude acid chloride **19** in 5 mL of DCM, a solution of 2-chloro-4-nitroaniline (**20**) (88.0 mg, 0.511 mmol, 1.2 equiv.) and triethylamine (Et_3N; 71.0 μL, 0.511 mmol, 1.2 equiv.) in 5 mL of DCM was added at 0 °C. After stirring for 18 h at room temperature, the reaction mixture was concentrated under reduced pressure, and the obtained residue was dissolved in DCM. The organic layer was washed with 10% NaOH and 10% HCl, dried over $MgSO_4$ filtered and concentrated under reduced pressure. The obtained residue was purified by PTLC (*n*-hexane/EtOAc = 70 : 30, R_f value = 0.5) to afford compound **21** (48.0 mg, 0.127 mmol, 2 steps 30% yield) as a pale yellow solid. ^{1}H NMR (400 MHz, $CDCl_3$) δ 10.75 (br, 1H), 8.93 (d, *J* = 7.4 Hz, 1H), 8.35 (d, *J* = 2.1 Hz, 1H), 8.31 (s, 1H), 8.20-8.21 (dd, *J* = 7.4 and 1.9 Hz, 1H), 6.79 (s, 1H), 4.16 (s, 3H); ^{13}C NMR (125 MHz, $CDCl_3$) δ 161.7, 156.7, 142.9, 142.3, 141.3, 134.8, 124.8, 123.7, 122.5, 120.7, 118.6, 118.4, 103.1, 57.1. HRMS (ESI, negative) calcd for $C_{14}H_9Cl_2N_5O_4^-$ $[M - H]^-$ 379.9959, found 379.9952.

Synthesis of compound 16

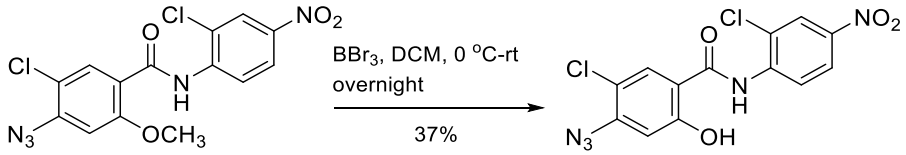

21 **16**

To a solution of compound **21** (18.0 mg, 0.047 mmol, 1.0 equiv.) in 5 mL of anhydrous DCM, BBr_3 (18.0 μL, 0.188 mmol, 4.0 equiv) was added at 0 °C. After stirring at room temperature overnight, the reaction mixture was poured into ice water and the obtained precipitation was dissolved in 1 M NaOH aqueous solution. The aqueous layer was washed with DCM and 6 N HCl was added with stirring at 0 °C to form a precipitate. The precipitate was extracted in $CHCl_3$ and the obtained organic layer was filtered and concentrated under reduced pressure. The obtained residue was purified by silica gel column chromatography (*n*-hexane/EtOAc = 50 : 50 to 25 : 75) to afford compound **16** (6.4 mg, 0.017 mmol, 37% yield) as a yellow solid. ^{1}H NMR (400 MHz, DMSO-d_6) δ 12.35 (br, 1H), 8.83 (d, J = 9.2 Hz, 1H), 8.40 (d, J = 2.2 Hz, 1H), 8.26 (dd, J = 9.1 and 2.2 Hz, 1H), 7.95 (s, 1H), 6.84 (s, 1H); ^{13}C NMR (125 MHz, DMSO-d_6) δ 162.6, 156.8, 142.9, 142.3, 141.7, 132.7, 125.3, 124.4, 122.8, 121.1, 116.4, 114.8, 108.7. HRMS (ESI, negative) calcd for $C_{13}H_7Cl_2N_5O_4^-$ $[M - H]^-$ 365.9796, found 365.9814.

HPLC analysis of compound 16

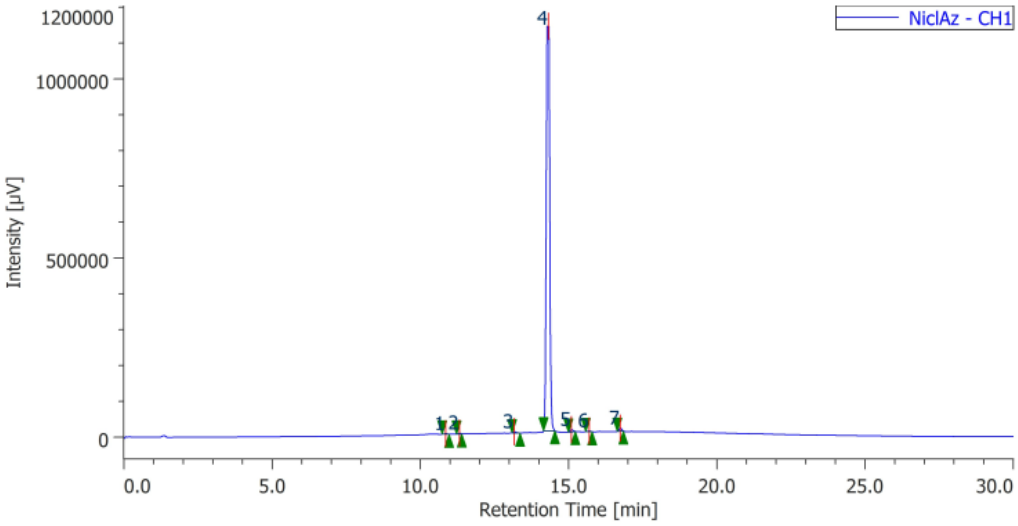

Peak	Area (%)	Retention time (min)
1	0.131	10.850
2	0.118	11.317
3	0.225	13.158
4	**98.319**	**14.317**
5	0.470	15.092
6	0.151	15.692
7	0.587	16.742

NMR spectra

Compound 18

^{1}H NMR ($CDCl_3$, 400 MHz)

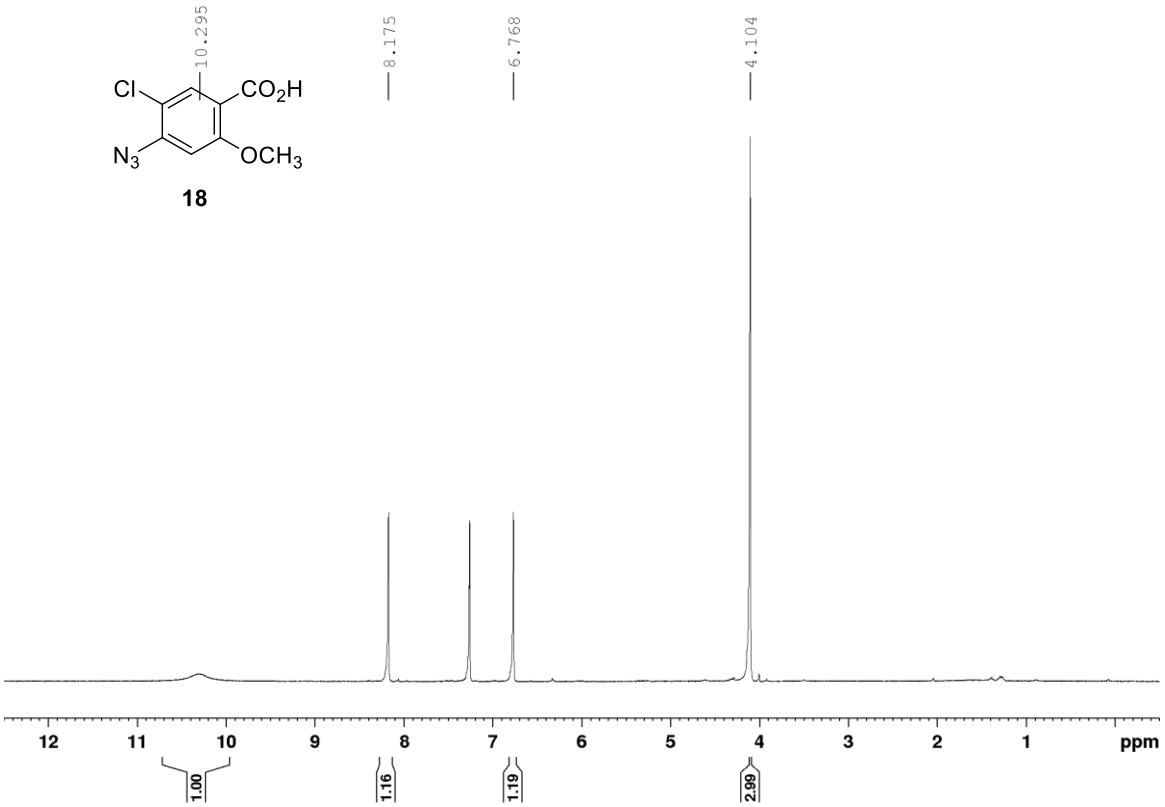

^{13}C NMR ($CDCl_3$, 125 MHz)

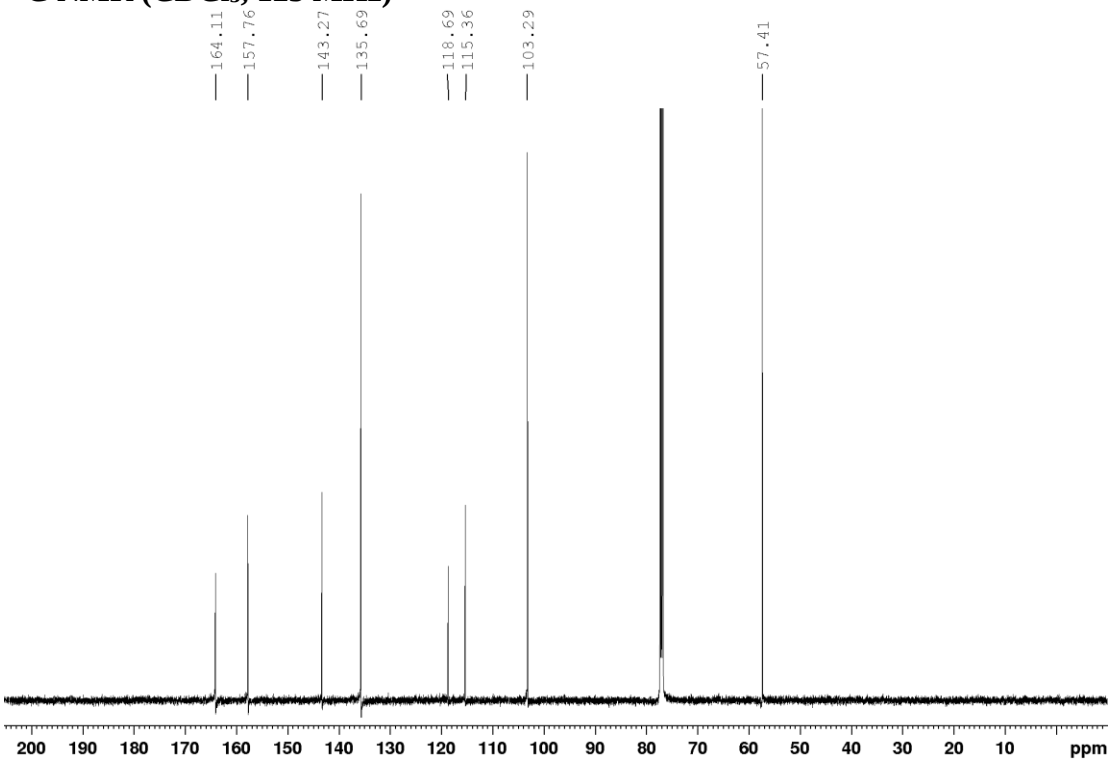

Compound 21

^{1}H NMR ($CDCl_3$, 500 MHz)

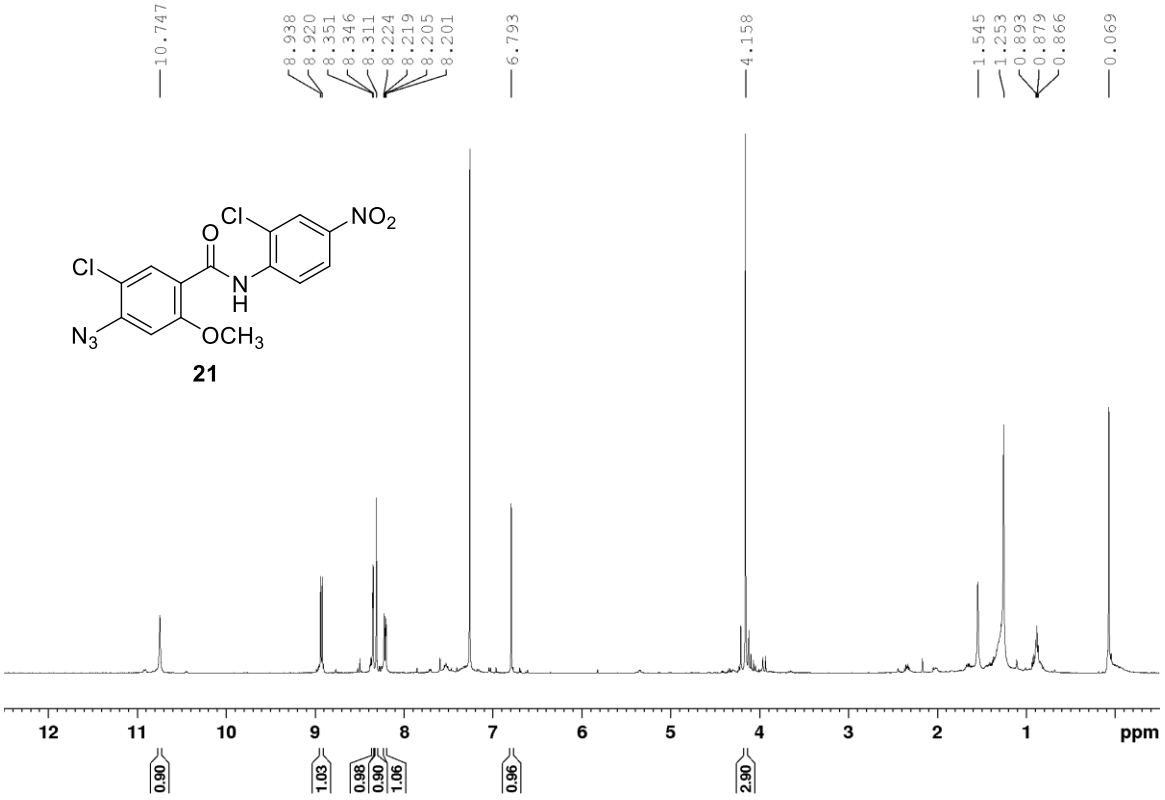

^{13}C NMR ($CDCl_3$, 125 MHz)

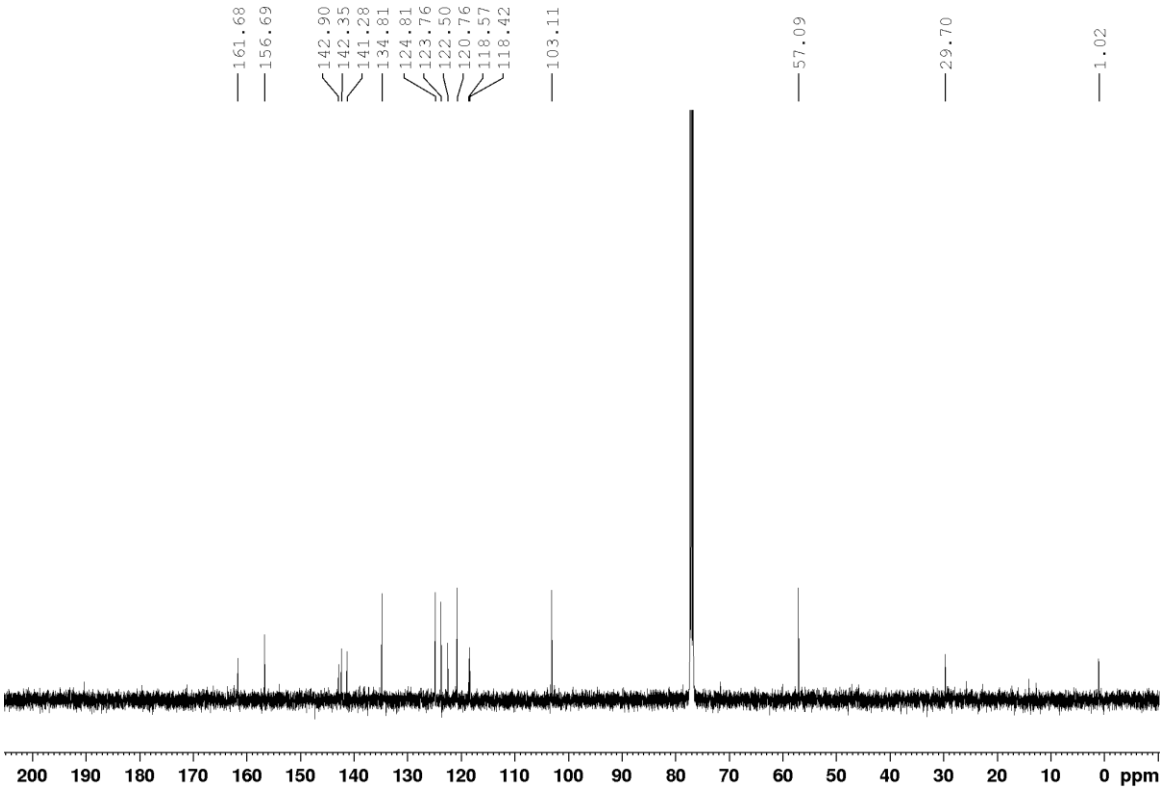

Compound 16

^{1}H-NMR (DMSO-*d*$_6$, 400 MHz)

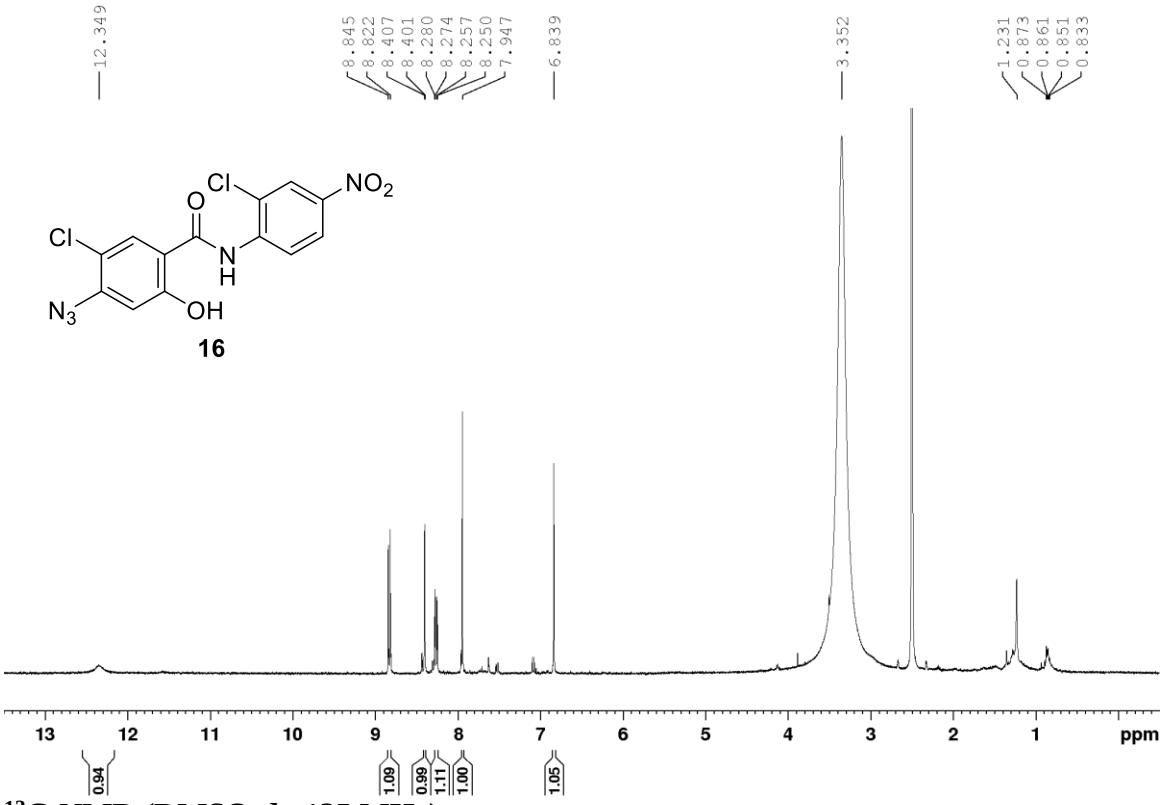

^{13}C-NMR (DMSO-*d*$_6$, 125 MHz)

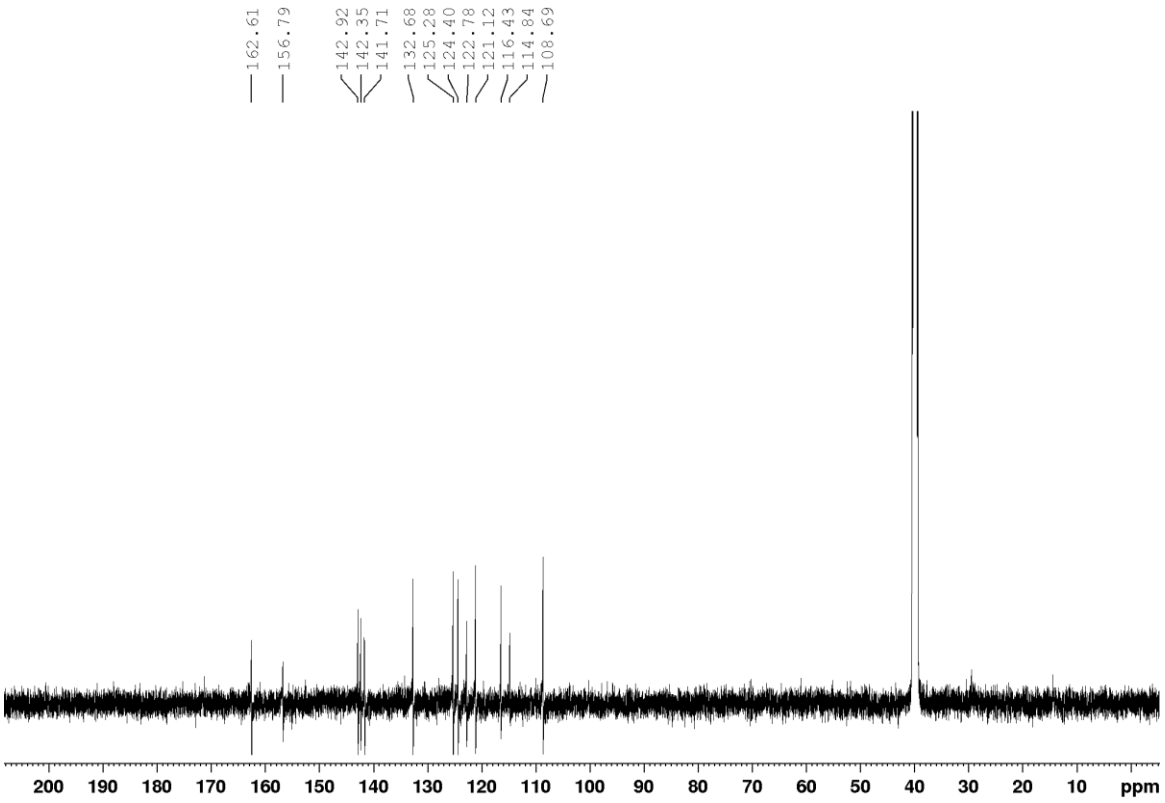

(A)

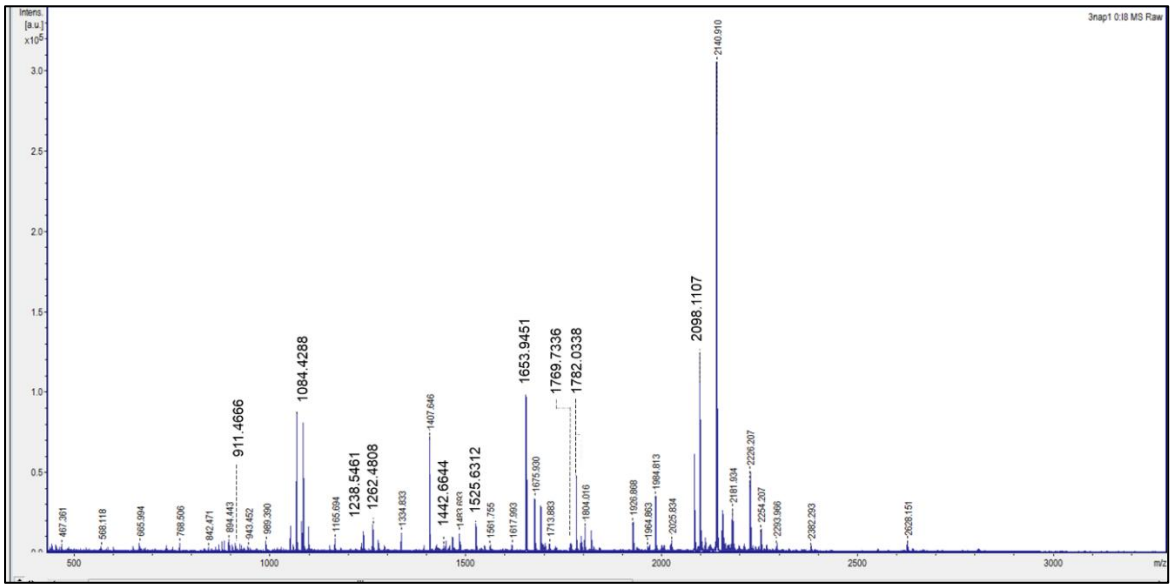

Protein sequence coverage: 70%

Matched peptides shown in ***bold red***.

```
   1 MGSGAHTADP EKRKLIQQQL VLLLHAHKCQ RREQANGEVR QCNLPHCRTM
  51 KNVLNHMTHC QSGKSCQVAH CASSRQIISH WKNCTRHDCP VCLPLKNAGD
 101 K
```

Start - End	Observed	Mr(expt)	Mr(calc)	ppm	M	Peptide
14 - 28	1782.0338	1781.0265	1781.1039	-43.5	1	R.KLIQQQLVLLLHAHK.C
15 - 28	1653.9451	1652.9378	1653.0090	-43.0	0	K.LIQQQLVLLLHAHK.C
15 - 31	2098.1107	2097.1034	2097.1993	-45.7	1	K.LIQQQLVLLLHAHKCQR.R
41 - 48	1084.4288	1083.4215	1083.4702	-45.0	0	R.QCNLPHCR.T
52 - 64	1525.6312	1524.6239	1524.6926	-45.0	0	K.NVLNHMTHCQSGK.S
65 - 75	1262.4808	1261.4735	1261.5292	-44.1	0	K.SCQVAHCASSR.Q
76 - 82	911.4666	910.4593	910.5025	-47.4	0	R.QIISHWK.N
76 - 86	1442.6644	1441.6571	1441.7248	-47.0	1	R.QIISHWKNCTR.H
83 - 96	1769.7336	1768.7263	1768.8171	-51.3	1	K.NCTRHDCPVCLPLK.N
87 - 96	1238.5461	1237.5388	1237.5948	-45.2	0	R.HDCPVCLPLK.N

(B)

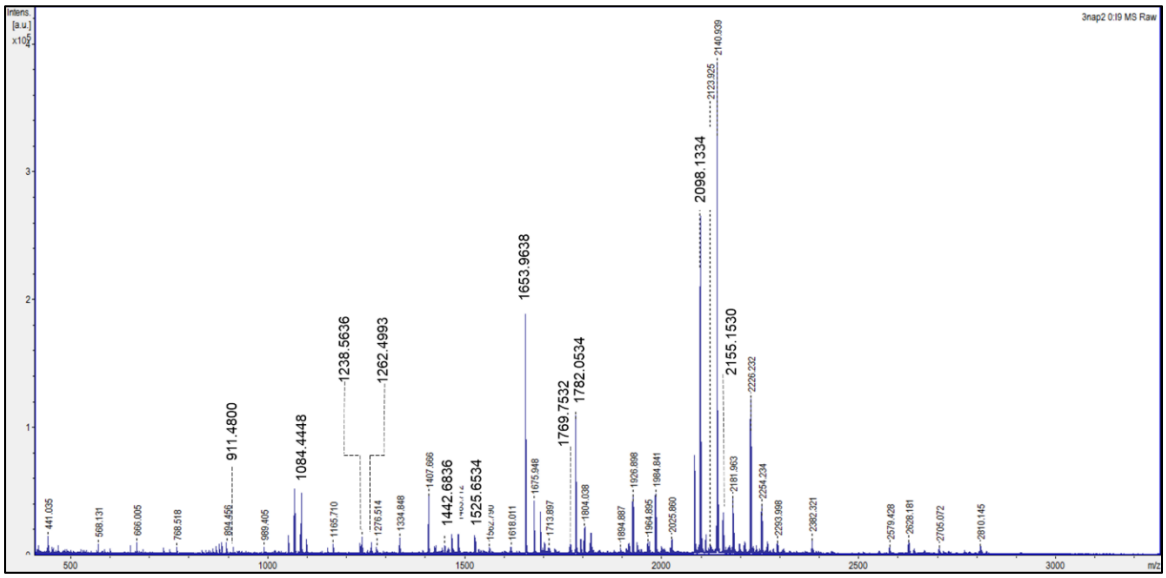

Protein sequence coverage: 70%

Matched peptides shown in ***bold red***.

```
   1 MGSGAHTADP EKRKLIQQQL VLLLHAHKCQ RREQANGEVR QCNLPHCRTM
  51 KNVLNHMTHC QSGKSCQVAH CASSRQIISH WKNCTRHDCP VCLPLKNAGD
 101 K
```

Start - End	Observed	Mr(expt)	Mr(calc)	ppm	M	Peptide
14 - 28	1782.0534	1781.0461	1781.1039	-32.5	1	R.KLIQQQLVLLLHAHK.C
15 - 28	1653.9638	1652.9565	1653.0090	-31.8	0	K.LIQQQLVLLLHAHK.C
15 - 31	2098.1334	2097.1261	2097.1993	-34.9	1	K.LIQQQLVLLLHAHKCQR.R
41 - 48	1084.4448	1083.4376	1083.4702	-30.1	0	R.QCNLPHCR.T
52 - 64	1525.6534	1524.6461	1524.6926	-30.5	0	K.NVLNHMTHCQSGK.S
65 - 75	1262.4993	1261.4921	1261.5292	-29.4	0	K.SCQVAHCASSR.Q
65 - 82	2155.1530	2154.1458	2154.0211	57.9	1	K.SCQVAHCASSRQIISHWK.N
76 - 82	911.4800	910.4727	910.5025	-32.7	0	R.QIISHWK.N
76 - 86	1442.6836	1441.6763	1441.7248	-33.7	1	R.QIISHWKNCTR.H
83 - 96	1769.7532	1768.7460	1768.8171	-40.2	1	K.NCTRHDCPVCLPLK.N
87 - 96	1238.5636	1237.5563	1237.5948	-31.1	0	R.HDCPVCLPLK.N

(C)

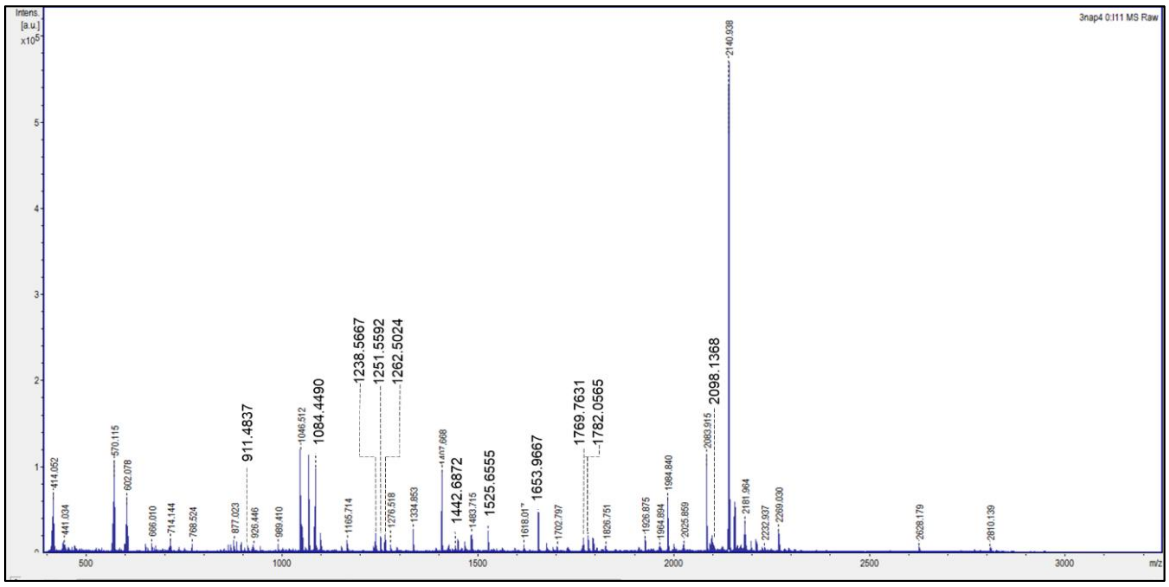

Protein sequence coverage: 70%

Matched peptides shown in ***bold red***.

```
  1 MGSGAHTADP EKRKLIQQQL VLLLHAHKCQ RREQANGEVR QCNLPHCRTM
 51 KNVLNHMTHC QSGKSCQVAH CASSRQIISH WKNCTRHDCP VCLPLKNAGD
101 K
```

Start - End	Observed	Mr(expt)	Mr(calc)	ppm	M	Peptide
14 - 28	1782.0565	1781.0492	1781.1039	-30.7	1	R.KLIQQQLVLLLHAHK.C
15 - 28	1653.9667	1652.9595	1653.0090	-30.0	0	K.LIQQQLVLLLHAHK.C
15 - 31	2098.1368	2097.1295	2097.1993	-33.3	1	K.LIQQQLVLLLHAHKCQR.R
41 - 48	1084.4490	1083.4417	1083.4702	-26.3	0	R.QCNLPHCR.T
52 - 64	1525.6555	1524.6483	1524.6926	-29.1	0	K.NVLNHMTHCQSGK.S
65 - 75	1262.5024	1261.4952	1261.5292	-27.0	0	K.SCQVAHCASSR.Q
76 - 82	911.4837	910.4765	910.5025	-28.6	0	R.QIISHWK.N
76 - 82	1251.5592	1250.5519	1250.4917	48.2	0	R.QIISHWK.N + compound 16
76 - 86	1442.6872	1441.6799	1441.7248	-31.2	1	R.QIISHWKNCTR.H
83 - 96	1769.7631	1768.7558	1768.8171	-34.6	1	K.NCTRHDCPVCLPLK.N
87 - 96	1238.5667	1237.5595	1237.5948	-28.5	0	R.HDCPVCLPLK.N

(D)

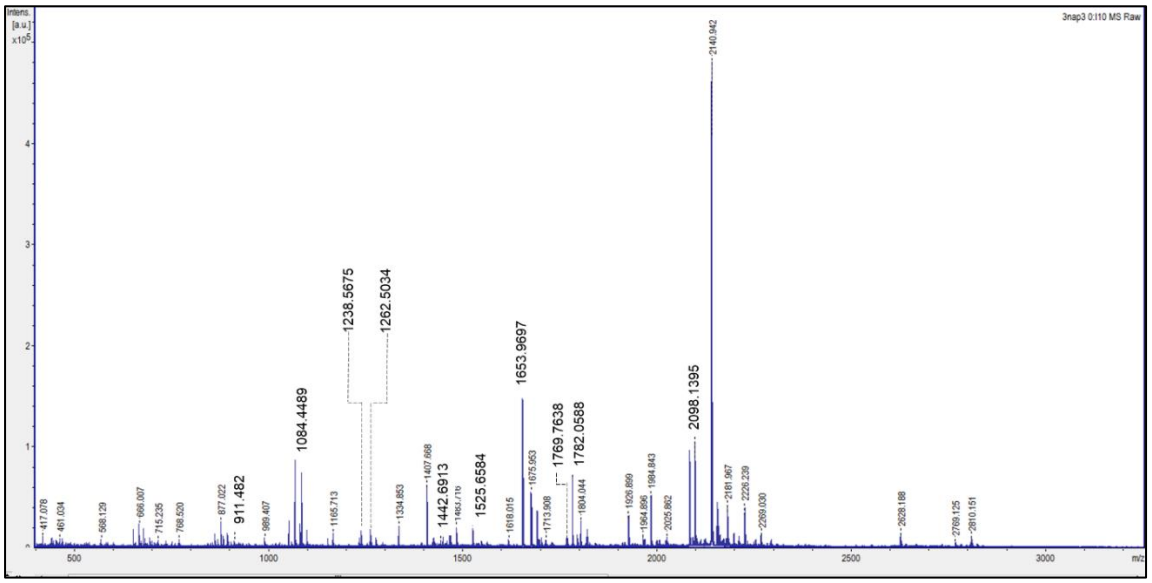

Protein sequence coverage: 70%

Matched peptides shown in ***bold red***.

```
   1 MGSGAHTADP EKRKLIQQQL VLLLHAHKCQ RREQANGEVR QCNLPHCRTM
  51 KNVLNHMTHC QSGKSCQVAH CASSRQIISH WKNCTRHDCP VCLPLKNAGD
 101 K
```

Start – End	Observed	Mr(expt)	Mr(calc)	ppm	M	Peptide
14 – 28	1782.0588	1781.0515	1781.1039	-29.4	1	R.KLIQQQLVLLLHAHK.C
15 – 28	1653.9697	1652.9624	1653.0090	-28.2	0	K.LIQQQLVLLLHAHK.C
15 – 31	2098.1395	2097.1322	2097.1993	-32.0	1	K.LIQQQLVLLLHAHKCQR.R
41 – 48	1084.4489	1083.4416	1083.4702	-26.4	0	R.QCNLPHCR.T
52 – 64	1525.6584	1524.6511	1524.6926	-27.2	0	K.NVLNHMTHCQSGK.S
65 – 75	1262.5034	1261.4961	1261.5292	-26.2	0	K.SCQVAHCASSR.Q
76 – 86	1442.6913	1441.6840	1441.7248	-28.3	1	R.QIISHWKNCTR.H
83 – 96	1769.7638	1768.7565	1768.8171	-34.3	1	K.NCTRHDCPVCLPLK.N
87 – 96	1238.5675	1237.5602	1237.5948	-27.9	0	R.HDCPVCLPLK.N

(E)

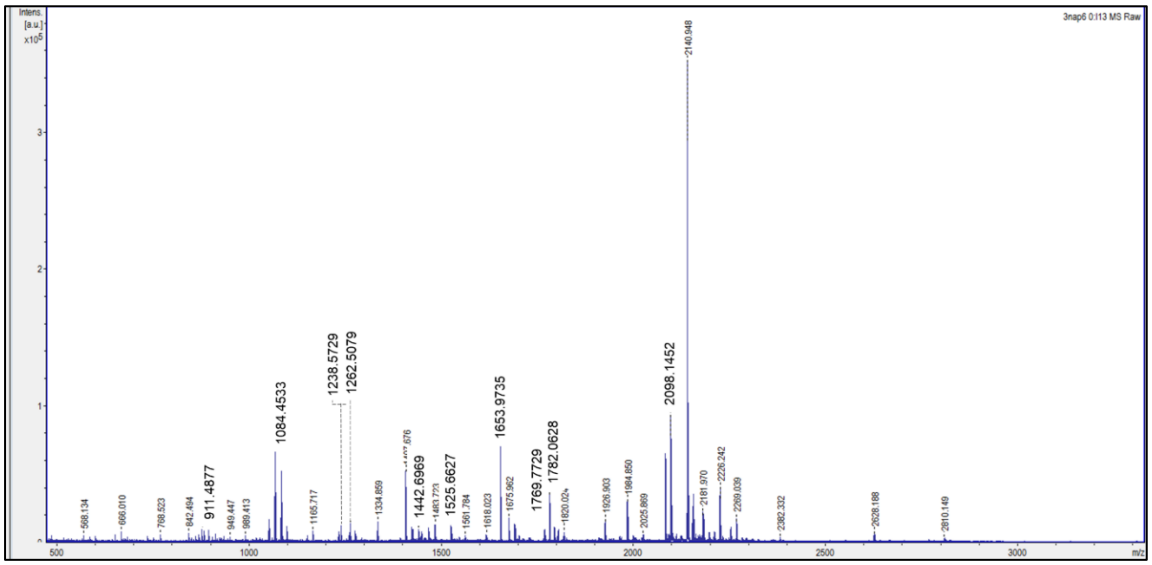

Protein sequence coverage: 70%

Matched peptides shown in ***bold red***.

```
   1 MGSGAHTADP EKRKLIQQQL VLLLHAHKCQ RREQANGEVR QCNLPHCRTM
  51 KNVLNHMTHC QSGKSCQVAH CASSRQIISH WKNCTRHDCP VCLPLKNAGD
 101 K
```

Start – End	Observed	Mr(expt)	Mr(calc)	ppm	M	Peptide
14 – 28	1782.0628	1781.0556	1781.1039	-27.2	1	R.KLIQQQLVLLLHAHK.C
15 – 28	1653.9735	1652.9662	1653.0090	-25.9	0	K.LIQQQLVLLLHAHK.C
15 – 31	2098.1451	2097.1379	2097.1993	-29.3	1	K.LIQQQLVLLLHAHKCQR.R
41 – 48	1084.4533	1083.4460	1083.4702	-22.3	0	R.QCNLPHCR.T
52 – 64	1525.6627	1524.6555	1524.6926	-24.3	0	K.NVLNHMTHCQSGK.S
65 – 75	1262.5079	1261.5007	1261.5292	-22.6	0	K.SCQVAHCASSR.Q
76 – 82	911.4877	910.4805	910.5025	-24.2	0	R.QIISHWK.N
76 – 86	1442.6969	1441.6896	1441.7248	-24.5	1	R.QIISHWKNCTR.H
83 – 96	1769.7729	1768.7657	1768.8171	-29.1	1	K.NCTRHDCPVCLPLK.N
87 – 96	1238.5729	1237.5656	1237.5948	-23.6	0	R.HDCPVCLPLK.N

Figure S4-1. Identification of labeled peptide in p300 CH1 by photoaffinity labeling with compound 16. Samples of (A) p300 CH1 protein only (control); p300 CH1 protein incubated with (B) 0.1 μM and (C) 1 μM of compound **16** were irradiated for 30 min. Competition assay was also performed using p300 CH1 pre-incubated with 10 μM of compound **15** then incubated with (D) 0.1 μM and (E) 1 μM of compound **16**. The samples were resolved on SDS-PAGE and staining with CBB stain. After destaining, the protein gel band was cut and digested using in-gel trypsin digestion. After desalting, the peptide sample was subjected to MALDI-TOF MS/MS analysis, followed by a Mascot search to identify the proteins targeted by the probe.

Chapter 5

Investigation of the Effect of Niclosamide in Other p300/Transcription Factor Protein-Protein Interaction

5.1 Introduction

The modular structure of CBP/p300 consists of eight distinct domains: the nuclear receptor interaction (NRID), CH1 (TAZ1), KIX, bromo, CH2 (PHD), the enzymatic lysine acetyltransferase (HAT), CH3 (which also contains the ZZ and TAZ2 domain), and the nuclear co-activator-binding (NCBD) domains (Figure 5-1A).[1–3] The transcriptional coactivator protein CBP and its paralog p300 each contain two homologous TAZ (transcriptional adaptor zinc-binding) domains, TAZ1 and TAZ2, which are important sites of protein−protein interaction. TAZ1 and TAZ2 each contain three highly homologous zinc-binding sites with the consensus sequence His1-X_3-Cys2-X_{4-12}-Cys3-X_{2-4}-Cys4 (where X is any amino acid and the subscript denotes the number of residues between the zinc ligands).[4] The primary function of the TAZ domains appears to be in protein recognition. Currently, more than 30 different transcription factors have been reported to associate with CBP/p300 via its TAZ domains. Although the TAZ1 and TAZ2 domains share sequence homology, they bind different subsets of transcription factors.[5]

The p300 CH1 domain comprises four α-helices and three Zn^{2+}-coordination sites formed by HCCC sequence motifs and the Zn^{2+} ion of the third Zn^{2+}-coordination site in the p300 CH1 is essential for its structure and function.[6] (Figure 5-1B). The three longer helices (designated α1, α2, and α3) pack together to create a roughly triangular structure. The three Zn^{2+} sites lie at the vertices of this triangle, and the coordinating histidine and cysteine residues that compose the HCCC motif are found near the ends of the helices and in the intervening turns. The short C-terminal helix, α4, completes the third Zn^{2+}-coordination site and packs against α1 in a parallel. The fold of the CH1 domain is stabilized in part by Zn^{2+} binding. It is reported that the addition of ethylenediaminetetraacetic (EDTA) disrupts the HIF-1/p300 complex.[6] HIF-1α/CTAD folds onto a scaffold provided by the CH1-Zn^{2+} domain, and the two proteins may form a single structural domain.[7]

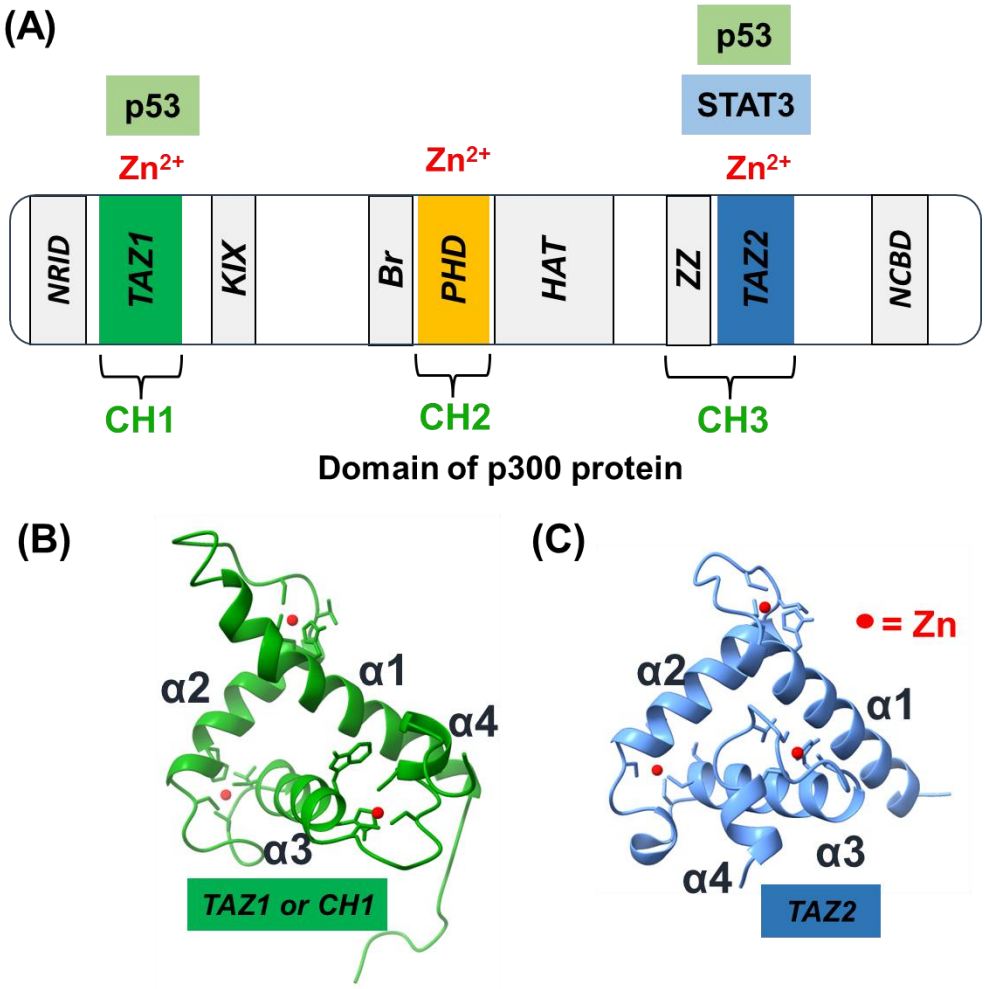

Figure 5-1. (A) PPI of zinc finger domain in p300 protein and transcription factors. (B) Structure of CH1 or TAZ1 domains of p300 protein (PDB: 1L3E). (C) Structure of TAZ2 domains of p300 protein (PDB: 1F81).

Identification of the binding site of compound **15** in p300 CH1 showed that compound **15** binds to the same residue as Zn^{2+}-binding (see chapter 4.4). Although there is no conclusive evidence, such as crystal structures or binding studies, that compound **15** directly inhibits zinc chelation, there are indirect evidence from reports such as the inhibition of zinc-dependent enzymes matrix metalloproteinases (MMPs).[8]

In p300/CBP, the Zn^{2+}-binding domains CH1 and CH3 are identical (Figures 5-1 B and 5-1 C) and contain many cysteine and histidine residues.[6] The p53 tumor-suppressor protein binds both CH1 and CH3[9,10] while signal transducer and activator of transcription-3 (STAT3) was reported to bind with CH3 domain of p300 (Figure 5-1 A).[11] Based on the observation that compound **15** interacts with the Zn^{2+}-binding

site of the p300 CH1 protein to inhibit the HIF1 signaling pathway, the author further extended its effects on other p300-related transcription factors, such as p53 and STAT3.

5.2 Effect of niclosamide on p300/p53 interaction

The p53 is activated in response to various stress signals, initiating a diverse set of cellular responses depending on the specific cell type, tissue, and stress conditions. p300 functions as a cofactor for p53 cofactors, modulating its activity by regulating proteins involved in its activation or repression, affecting promoter specificity. For example, p300-mediated acetylation of p53 enhances the activation of the BAX gene promoter, contributing to p53's apoptotic function (Figure 5-2).[12]

As a ubiquitous transcriptional co-activator, p300/CBP activity is tightly regulated by a range of associated proteins. Acetylation of p53 by p300/CBP and the p300/CBP-associated factor (PCAF) occurs in response to DNA-damaging agents, such as UV and ionizing radiation, and is associated with the induction of sequence-specific DNA binding and transactivation by p53. During the DNA-damage response, p300 interacts with its cofactor, junction-mediating and regulatory protein (JMY), resulting in increased p53 acetylation and subsequently enhancing p53-dependent transcription and apoptosis.[13] The third p300 cofactor, SKP2, was identified and shown to affect p53 activity by preventing the interaction between p300 and p53, thereby preventing acetylation of p53 and suppressing p53 transactivation and apoptosis.[14]

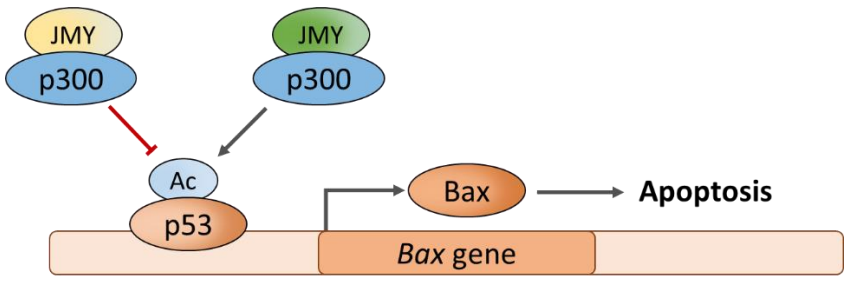

Figure 5-2. Activation of the Bax gene promoter enhanced by p300-mediated acetylation of p53

To assess whether compound **15** affects p53, the mRNA expression levels of p53 and its downstream gene, BAX, were measured using real-time PCR (RT-PCR).

As shown in Figure 5-3, compound **15** significantly suppressed BAX gene expression without affecting the p53 gene levels.

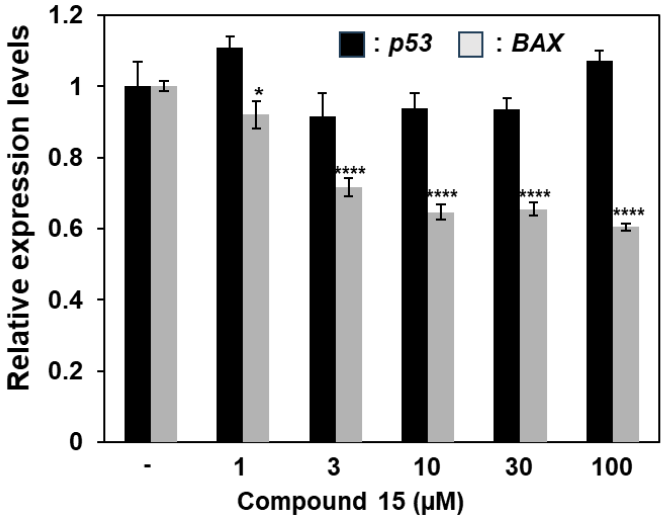

Figure 5-3. Effects of compound **15** on mRNA expression levels of p53 and its downstream gene BAX. HeLa cells were treated with various concentrations of compound **15** for 8 h. Total RNA was isolated from each cell, and mRNA was converted to cDNA. Gene expression levels were detected using real-time PCR. Each condition of compound untreatment was defined as 1.00. Data are presented as means ± the standard deviation (SD) of three separate experiments. Error bars, SD. Significance was determined as $*P < 0.05$, $****P < 0.0001$ compared with sample treated without compound.

5.3 Effect of niclosamide on p300/STAT3 interaction

An evaluation of the effect of compound **15** on STAT3 was also conducted. STAT3 is a member of the Janus kinase (JAK)-STAT signaling pathway, which coordinates central cellular mechanisms including differentiation, development, proliferation, immune function, or apoptosis.[15] Mechanistically, JAK-STAT3 signaling is activated by diverse growth factors, peptide hormones and all interleukin (IL)-6-type cytokines including IL-6, IL-11, IL-27, IL-31, leukemia inhibitory factor (LIF), oncostatin M (OSM), ciliary neurotrophic factor (CNTF) neuropoietin (NP), cardiotrophin-1 (CT-1) and cardiotrophin-like cytokine (CLC).[16,17] Once these factors bind to their corresponding receptors, Janus kinases (JAKs) are activated.[18,19] JAKs phosphorylate the cytoplasmic tail of the cognate receptor and STAT3 via its SH2 domain binds to phosphorylated tyrosine residues. The phosphorylated STAT3 forms homodimers and translocate into nucleus and, thus, can exchange signals

between the cytoplasm and nucleus. Upon translocation into the nucleus, pSTAT3 forms a complex with some coactivators, including p300/CBP, and binds to the promotor region of target genes to activate their transcription (Figure 5-4).[20]

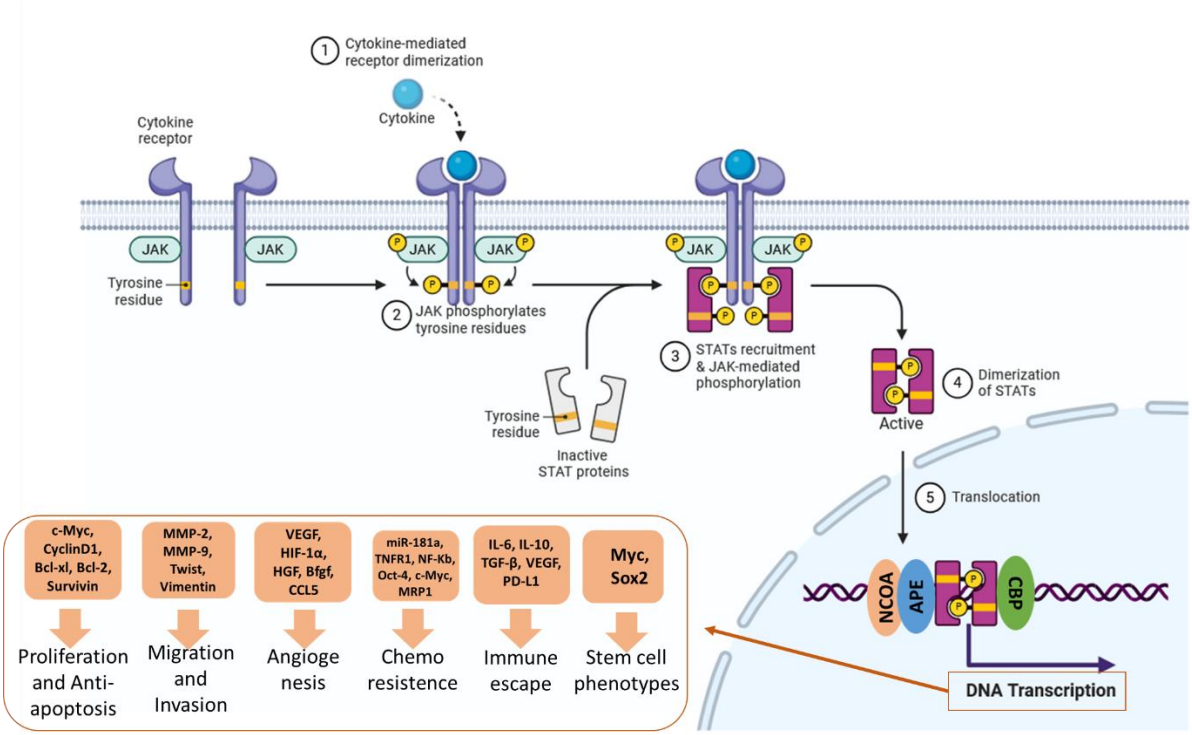

Figure 5-4. Cytokine signaling through the JAK/STAT pathway. This figure was created with BioRender.com.

The mRNA expression levels of STAT3 and its downstream gene, c-MYC, were measured using RT-PCR. Figure 5-5 showed that compound **15** significantly suppressed c-MYC gene expression without affecting STAT3 gene levels. This result further supports the finding that compound **15** acts as an inhibitor of p300-transcription factor PPIs.

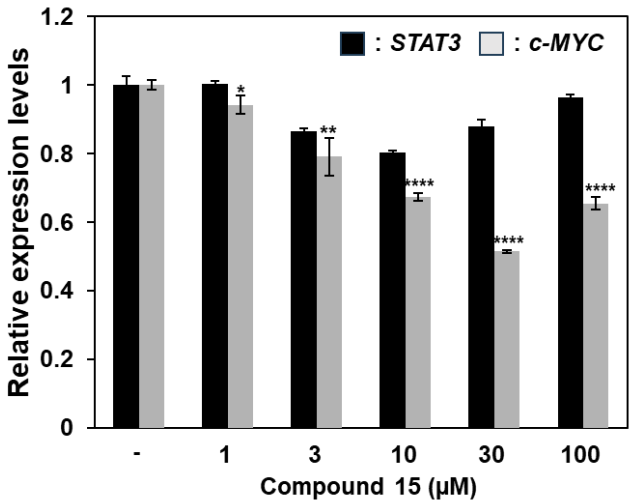

Figure 5-5. Effects of compound **15** on mRNA expression levels of STAT3 and its downstream gene c-MYC. HeLa cells were treated with various concentrations of compound **15** for 8 h. Total RNA was isolated from each cell, and mRNA was converted to cDNA. Gene expression levels were detected using real-time PCR. Each condition of compound untreatment was defined as 1.00. Data are presented as means ± the standard deviation (SD) of three separate experiments. Error bars, SD. Significance was determined as $*P < 0.05$, $**P < 0.01$, $****P < 0.0001$ compared with sample treated without compound.

5.4 Summary

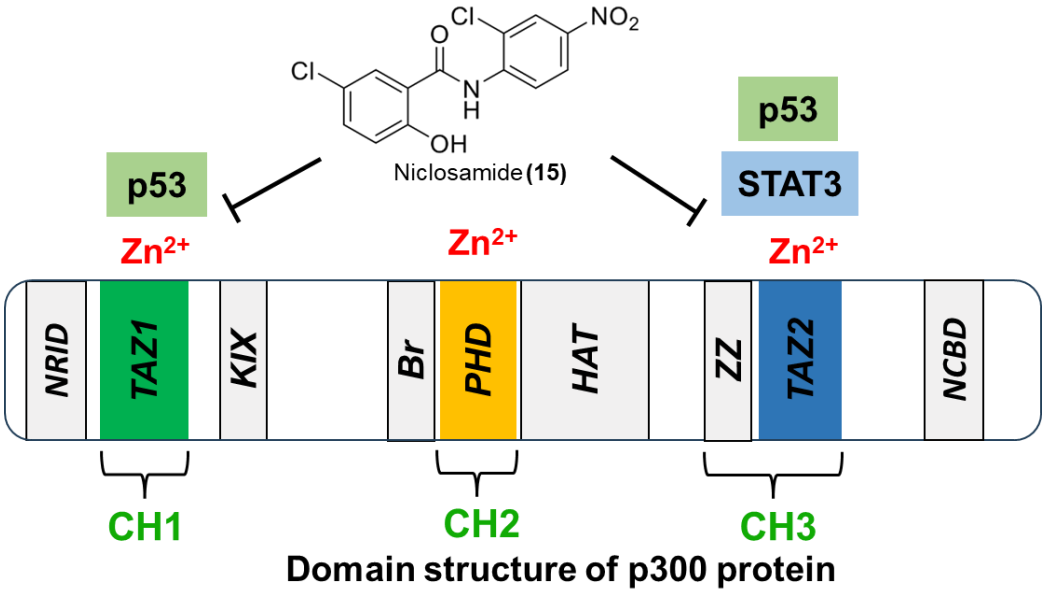

Figure 5-4. Summary of chapter 5

As reported in chapter 4, compound **15** was found to bind to the same residue as Zn^{2+}-binding in p300 CH1. In this chapter, the author investigated the effect of compound **15** on other p300/transcription factor PPIs that are related to the Zn^{2+} binding site in p300 CH1. Compound **15** significantly suppressed BAX gene expression without affecting the p53 gene levels. Moreover, compound **15** also significantly suppressed c-MYC gene expression without affecting STAT3 gene levels. These results further confirm that compound **15** acts as an inhibitor of p300-transcription factor PPIs.

5.5 References

(1) Dancy, B. M.; Cole, P. A. Protein Lysine Acetylation by p300/CBP. *Chem. Rev.* **2015**, *115*, 2419−2452.

(2) Park, S.; Stanfield, R. L.; Martinez-Yamout, M. A.; Dyson, H. J.; Wilson, I. A.; Wright, P. E. Role of the CBP Catalytic Core in Intramolecular SUMOylation and Control of Histone H3 Acetylation. *Proc. Natl. Acad. Sci. U S A* **2017**, *114* (27), E5335–E5342.

(3) Teufel, D. P.; Freund, S. M.; Bycroft, M.; Fersht, A. R. Four Domains of p300 Each Bind Tightly to a Sequence Spanning Both Transactivation Subdomains of p53, *Proc. Natl. Acad. Sci. U S A* **2007**, *104* (17), 7009 –7014.

(4) Ponting, C. P.; Blake, D. J.; Davies, K. E.; Kendrick-Jones, J.; Winder, S. J. New Putative Zinc Fingers in Dystrophin and Other Proteins. *Trends Biochem. Sci.* **1996**, *21*, 11–13.

(5) De Guzman, R. N.; Wojciak, J. M.; Martinez-Yamout, M. A.; Dyson, H. J.; Wright, P. E. CBP/p300 TAZ1 Domain Forms a Structured Scaffold for Ligand Binding. *Biochem.* **2005**, *44* (2), 490–497.

(6) Freedman, S. J.; Sun, Z.-Y. J.; Poy, F.; Kung, A. L.; Livingston, D. M.; Wagner, G.; Eck, M. J. Structural Basis for Recruitment of CBP/p300 by Hypoxia-Inducible Factor-1. *Proc. Natl. Acad. Sci. U S A* **2002**, *99* (8), 5367-5372.

(7) Dial, R.; Sun, Z. Y. J.; Freedman, S. J. Three Conformational States of the p300 CH1 Domain Define Its Functional Properties. *Biochem.* **2003**, *42* (33), 9937-9945.

(8) El-fatatry, B. M.; El-Haggar, S. M.; Ibrahim, O. M.; Shalaby, K. H. Niclosamide from an Anthelmintic Drug to a Promising Adjuvant Therapy for Diabetic Kidney Disease: Randomized Clinical Trial. *Diabetol. Metab. Syndr.* **2023**, *15* (1), 1-9.

(9) Grossman, S. R. p300/CBP/p53 Interaction and Regulation of the p53 Response. *Eur. J. Biochem*. **2001**, *268* (10), 2773-2778.

(10) Grossman, S. R.; Perez, M.; Kung, A. L.; Joseph, M.; Mansur, C.; Xiao, Z.-X.; Kumar, S.; Howley, P. M.; Livingston, D. M. p300/MDM2 Complexes Participate in MDM2-Mediated p53 Degradation. *Mol. Cell.* **1998**, *2*, 405-415.

(11) Wojciak, J. M.; Martinez-Yamout, M. A.; Dyson, H. J.; Wright, P. E. Structural basis for recruitment of CBP/p300 coactivators by STAT1 and STAT2 transactivation domains. *EMBO J.* **2009**, *28*, 948-958.
(12) Murray-Zmijewski, F.; Slee, E. A.; Lu, X. A complex barcode underlies the heterogeneous response of p53 to stress. *Nat. Rev. Mol. Cell. Biol.* **2008**, *9*, 702-712.
(13) Shikama, N.; Lee, C.-W.; France, S.; Delavaine, L.; Lyon, J. A Novel Cofactor for P300 That Regulates the P53 Response. *Mol. Cell.* **1999**, *4* (3), 365-76.
(14) Kitagawa, M.; Lee, S. H.; McCormick, F. Skp2 Suppresses p53-Dependent Apoptosis by Inhibiting p300. *Mol. Cell*. **2008**, *29* (2), 217-231.
(15) Cacalano, N. A. Regulation of Natural Killer Cell Function by STAT3. *Front. Immunol.* **2016**, *7*, 128.
(16) Xu, J.; Lin, H.; Wu, G.; Zhu, M.; Li, M. IL-6/STAT3 Is a Promising Therapeutic Target for Hepatocellular Carcinoma. *Front. Oncol.* **2021**, *11*, 760971.
(17) Johnson, D. E.; O'Keefe, R. A.; Grandis, J. R. Targeting the IL-6/JAK/STAT3 Signalling Axis in Cancer. *Nat. Rev. Clin. Oncol.* **2018**, *15* (4), 234-248.
(18) Ma, J. H.; Qin, L.; Li, X. Role of STAT3 Signaling Pathway in Breast Cancer. *Cell. Commun. Signal*. **2020**, *18* (1), 33.
(19) Garbers, C.; Aparicio-Siegmund, S.; Rose-John, S. The IL-6/Gp130/STAT3 Signaling Axis: Recent Advances towards Specific Inhibition. *Curr. Opin. Immunol.* **2015**, *34*, 75-82.
(20) Qin, J. J.; Yan, L.; Zhang, J.; Zhang, W. D. STAT3 as a Potential Therapeutic Target in Triple Negative Breast Cancer: A Systematic Review. *J. Exp. Clin. Cancer Res.* **2019**, *38*, 195.

5.6 Experimental section

Quantitative PCR

HeLa cells were seeded in a 6-well plate at a density of 2×10^5 cells/well and cultured at 37 ℃ overnight. Cells were treated with different concentrations of each compound or DMSO and cultured with indicated conditions. Subsequently, the medium was removed, and the cells were washed with cold PBS. The total RNAs were extracted using TRIzol (Thermo Fisher Scientific, Inc., USA). The reverse-transcription reaction using the High-Capacity cDNA Reverse Transcription Kit (Thermo Fisher Scientific, Inc., MA, USA) was conducted according to the instructions. The obtained cDNA library was used for real-time PCR. Real-time PCR was carried out with THUNDERBIRD SYBR qPCR Mix (TOYOBO Co. LTD., Japan) using a real-time PCR system (Thermal Cycler Dice Real Time System III, Takara bio inc., Japan). The gene expression levels were analyzed by ΔΔCt method. The sequences of the primers used were shown as follows; Cellular tumour antigen p53 (p53): 5′-CCTCAGCATCTTATCCGAGTGG-3′ (forward) and 5′-TGGATGGTGGTACAGTCAGAGC-3′ (reverse); Apoptosis regulator BAX (BAX): 5′-TCAGGATGCGTCCACCAAGAAG-3′ (forward) and 5′-TGTGTCCACGGCGGCAATCATC-3′ (reverse); Signal transducer and activator of transcription 3 (STAT3): 5′-CTTTGAGACCGAGGTGTATCACC-3′ (forward) and 5′-GGTCAGCATGTTGTACCACAGG-3′ (reverse); Myc proto-oncogene protein (c-MYC): 5′- CCTGGTGCTCCATGAGGAGAC-3′ (forward) and 5′-CAGACTCTGACCTTTTGCCAGG-3′ (reverse); β2-microglobulin (B2M): 5′-TACATGTCTCGATCCCACTT-3′ (forward) and 5′-TACACTGAATTCACCCCCAC-3′ (reverse).

Chapter 6

Conclusion

This thesis focuses on the discovery of a novel inhibitor targeting the interaction between HIF-1α and p300, a critical pathway involved in cellular responses to hypoxia. Despite extensive research in this area, no HIF-1α/p300 inhibitors have been approved for clinical use to date. This study aims to address this gap by contributing to the development of HIF-1α/p300 inhibitors and investigating the drug's binding site, which is essential for understanding its mechanism of action. The following is summary of each chapter.

In chapter 1, “Introduction”, the importance of PPIs in cellular processes and their potential as therapeutic targets is described. The chapter highlights the significance of targeting the HIF-1α/p300 interaction, a critical pathway involved in the cellular response to hypoxia, and discusses strategies for drug development aimed at disrupting this interaction. Additionally, the development and application of screening assay systems, such as FA assays, are introduced as essential tools for detecting PPIs and identifying potential inhibitors. The role of a compound library in facilitating the discovery of novel drugs targeting PPIs is also emphasized.

In chapter 2, “Construction of Fluorescence Anisotropy Screening Assay System for the Discovery of HIF-1α/p300 PPI Inhibitor”, the methods and techniques used in the study are outlined. The introduction provides an overview of the study's objectives and significance. The construction of a vector for overexpression of human p300 CH1 protein is described, followed by protein expression and purification from *E. coli*. The synthesis of dansyl-labeled peptides using Fmoc solid-phase peptide synthesis is detailed, along with the synthesis of OHM 1, a potential HIF-1α/p300 interaction inhibitor. The chapter also discusses the evaluation of the binding affinity of the synthesized peptides for the p300 CH1 protein. It concludes with the validation of the screening assay system used for detecting inhibitors.

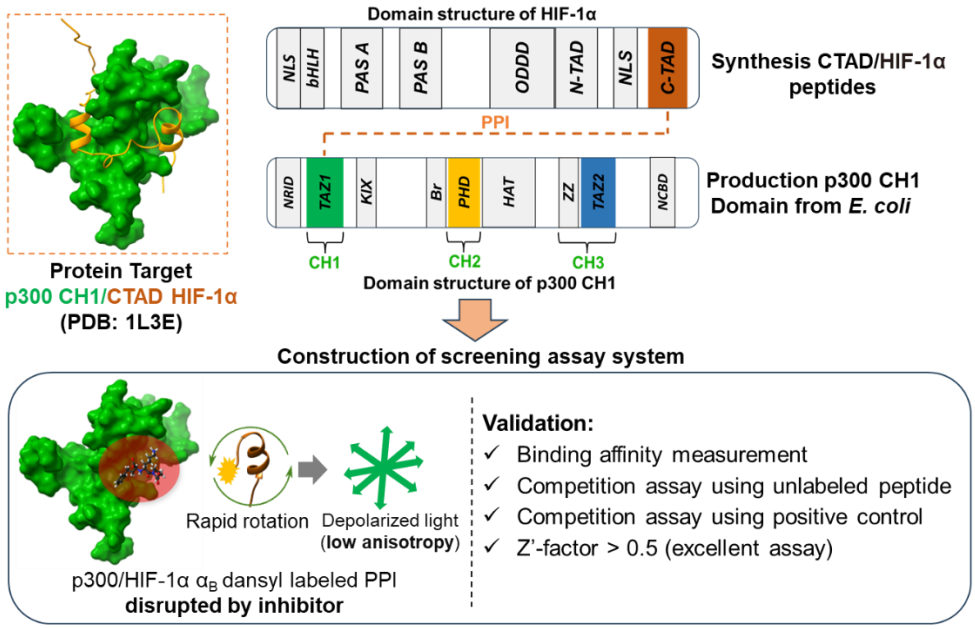

Figure 6-1. Summary of chapter 2

In chapter 3, "Screening of Compound Library using Constructed Assay System and Validation of Lead Compounds as HIF-1α/p300 PPI Inhibitors", the screening and evaluation of potential HIF-1α/p300 interaction inhibitors are described. The introduction provides an overview of the objectives and importance of the study. The in-house and NPDepo compound libraries are introduced as the source of candidate compounds. The screening process for HIF-1α/p300 PPI inhibitors from the library is explained, followed by a detailed description of the reporter gene assay conducted in HeLa cells to assess the activity of candidate inhibitors. The chapter also examines the effects of the candidate inhibitor on the protein expression levels of HIF-1α and its downstream targets in HeLa cells. Finally, the impact of niclosamide on the gene expression of HIF-1α and its downstream targets is analyzed, providing further insights into its potential as a HIF-1α/p300 PPI inhibitor.

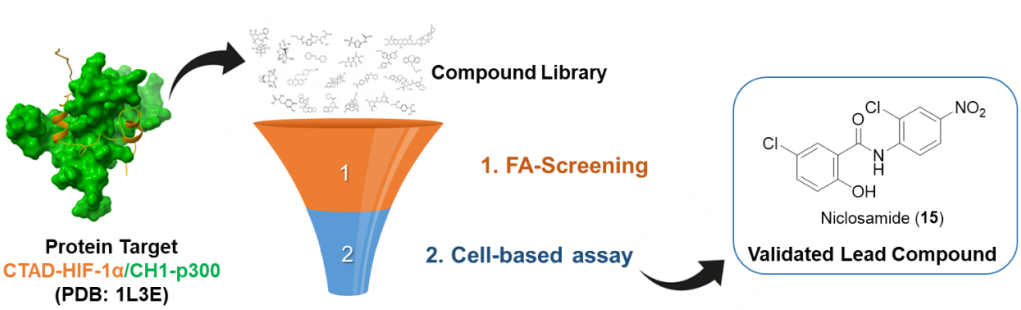

Figure 6-2. Summary of chapter 3

In chapter 4, “Identification of the Binding Site of Niclosamide using Photoaffinity Labeling”, the design, synthesis, and evaluation of niclosamide azide as a photoaffinity labeling probe are discussed. The introduction provides an overview of the significance of photoaffinity labeling in identifying drug-protein interactions. The chapter details the design and synthesis process of niclosamide azide, followed by an evaluation of its effectiveness as a photoaffinity labeling probe. The study then focuses on identifying the binding site of niclosamide in the p300 CH1 protein, which is a key aspect of understanding its mechanism of action. Finally, the binding mode of niclosamide in the p300 CH1 protein is investigated, providing insights into how it interacts with the target and potentially inhibits the HIF-1α/p300 interaction.

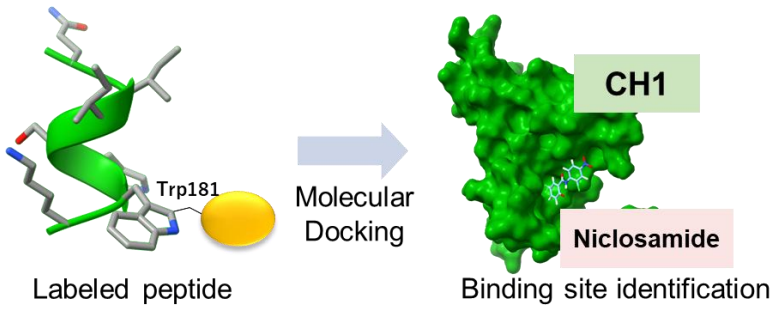

Figure 6-3. Summary of chapter 4

In chapter 5, the investigation of the effects of niclosamide on other p300/transcription factor PPIs is presented. The introduction provides a background on the importance of p300 in various cellular processes and its interactions with different transcription factors. The chapter explores the effect of niclosamide on the p300/p53 interaction, discussing how niclosamide might influence this critical tumor-suppressor pathway. Additionally, the impact of niclosamide on the p300/STAT3 interaction is examined, highlighting its potential role in modulating STAT3-driven signaling, which is often implicated in cancer and inflammation. This chapter contributes to understanding the broader effects of niclosamide on p300-mediated transcriptional regulation.

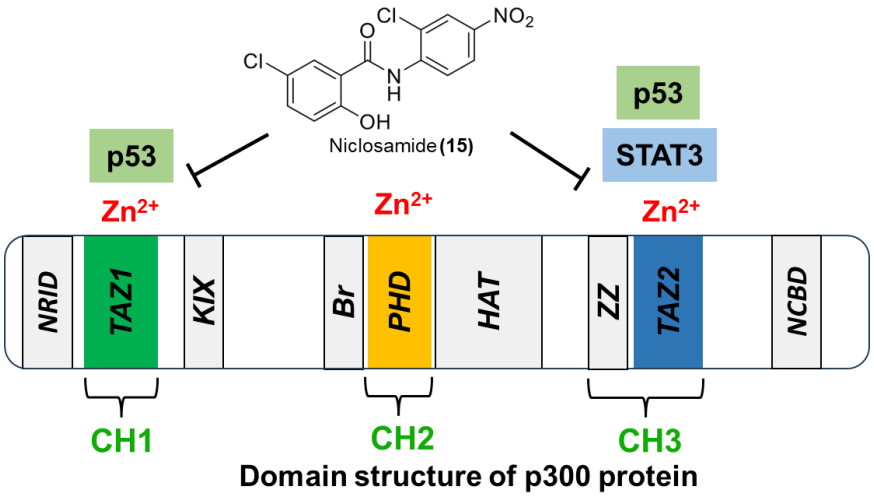

Figure 6-4. Summary of chapter 5

Appendices

A. Profile of NPDepo compound library

Compound	Well	Name	Structure	Formula	Origin	Bioactivity
S1	A02	(+)-Bicuculline	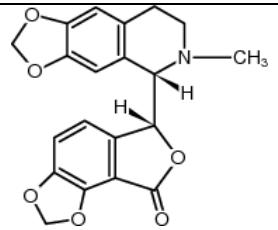	$C_{20}H_{17}NO_6$	*Adlumia fungosa* *Capnoides sempervirens* *Corydalis govaniana* *Dicentra cucullaria*	$GABA_A$ antagonist **Therapeutic:** Antidepressant Antiepileptic **Target:** $GABA_a$ receptor channels SK channels
S2	A03	Acetohexamide	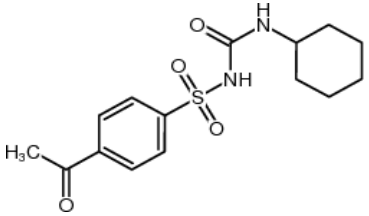	$C_{15}H_{20}N_2O_4S$	Chemically synthesized	Increasing insulin release from the beta cells in the pancreas **Therapeutic:** Antidiabetes (diabetes mellitus type 2) Hypoglycemic agent **Target:** ATP-sensitive inward rectifier potassium channel 11
S3	A04	Betamethasone	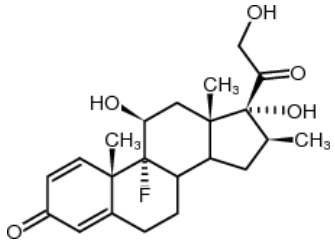	$C_{22}FH_{29}O_5$	Chemically synthesized	Function as a potent glucocorticoid steroid **Therapeutic:** Antiinflammatory Immunosuppressive **Target:** Glucocorticoid receptor

Compound	Well	Name	Structure	Formula	Origin	Bioactivity
S4	A05	Ibuprofen	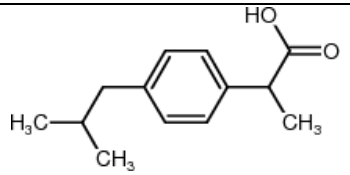	$C_{13}H_{18}O_2$	Chemically synthesized	Inhibition of the COX-dependent formation of PGH2 **Therapeutic:** Nonsteroidal antiinflammatory **Target:** COX-1; COX-2
S5	A06	Imipramine	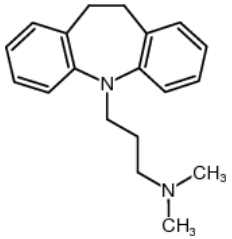	$C_{19}H_{24}N_2$	Chemically synthesized	Inhibition of the neuronal reuptake of neurotransmitters, noradrenaline and serotonin **Therapeutic:** Antidepressant **Target:** Sodium-dependent noradrenaline transporter (NET) Sodium-dependent serotonin transporter (5HTT)
S6	A07	Indomethacin	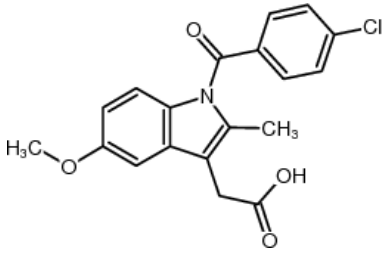	$C_{19}ClH_{16}NO_4$	Chemically synthesized	Inhibition of the COX-dependent formation of prostaglandin precursors **Therapeutic:** Antiinflammatory Antipyretic **Target:** COX-1 COX-2 Phospholipase A2 (PLA2)

Compound	Well	Name	Structure	Formula	Origin	Bioactivity
S7	A08	Reserpine	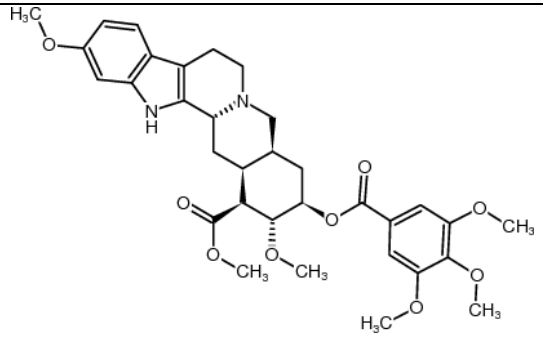	$C_{33}H_{40}N_2O_9$	*Rauvolfia serpentina*	Inhibition of vesicular uptake of neurotransmitters, catecholamine and serotonin **Therapeutic:** Antihypertensive Antipsychotic **Target:** Vesicular monoamine transporter (VMAT)
S8	A09	Naloxone	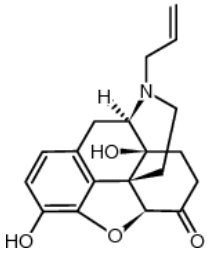	$C_{19}H_{21}NO_4$	Chemically synthesized	Suppression of the opiate overdose effects **Therapeutic:** Antinarcotic **Target:** Opioid receptors Cyclic AMP-responsive element-binding protein 1
S9	A10	Novobiocin	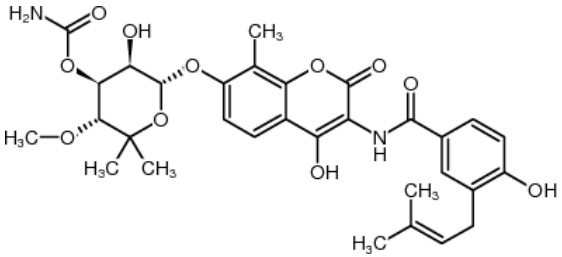	$C_{31}H_{36}N_2O_{11}$	*Streptomyces niveus*	Inhibition of DNA replication in bacteria **Therapeutic:** Antibacterial **Target:** GyrB ParE

Compound	Well	Name	Structure	Formula	Origin	Bioactivity
S10	A11	Rifampicin	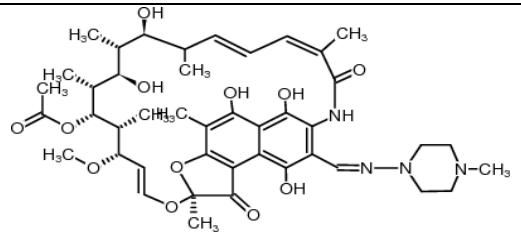	$C_{43}H_{58}N_4O_{12}$	Chemically synthesized	Inhibits RNA synthesis by blocking transcription in bacteria **Therapeutic:** Antibacterial **Target:** RNA polymerase Serum albumin
S11	B02	Naramycin	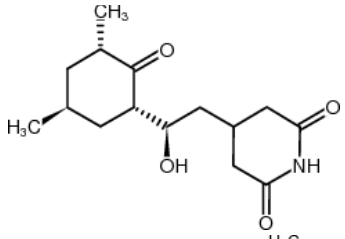	$C_{15}H_{23}NO_4$	*Streptomyces griseus*	Inhibition of eukariotic protein synthesis **Therapeutic:** Anticancer Antifungal **Target:** 60S ribosomes
S12	B03	Monensin	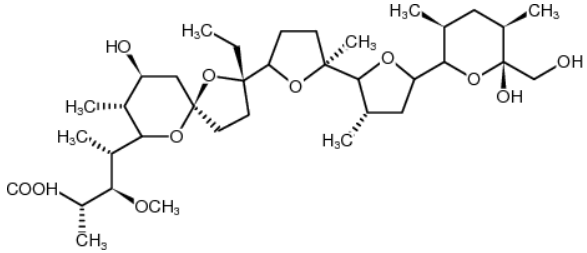	$C_{36}H_{62}O_{11}$	*Streptomyces cinnamonensis*	Ionophore **Therapeutic:** Antibacterial; Anticoccidial; Antifungal Antimalarial **Target:** Monovalent cation
S13	B04	Streptozocin	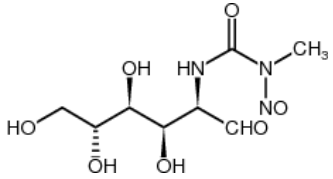	$C_8H_{15}N_3O_7$	*Streptomyces achromogenes*	Causing DNA damage **Therapeutic:** Antibiotics; Anticancer **Target:** DNA Solute carrier family 2, facilitated glucose transporter member 2

Compound	Well	Name	Structure	Formula	Origin	Bioactivity
S14	B05	Spiramycin	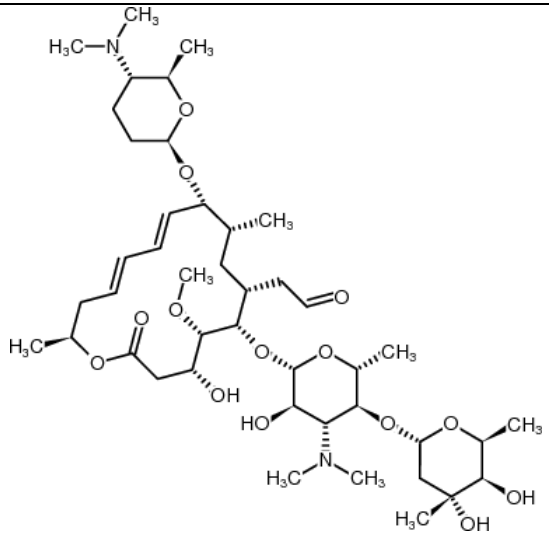	$C_{43}H_{74}N_2O_{14}$	*Streptomyces ambofaciens*	Inhibition of bacterial protein synthesis **Therapeutic:** Antibacterial **Target:** bacterial 50S ribosomal subunits
S15	B06	4,4'-Dithiodimorpholine	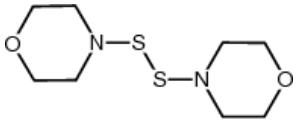	$C_8H_{16}N_2O_2S_2$	Chemically synthesized	Inhibition of cell viability and induction for apotosis. **Therapeutic:** Anticancer Antiviral **Target:** HPV E6 protein
S16	B07	Alendronate	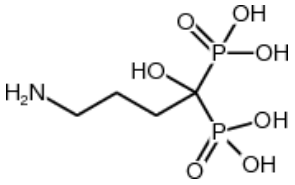	$C_4H_{13}NO_7P_2$	Chemically synthesized	Inhibition of the prenylation of small GTP-binding proteins in osteoclasts and disruption of their cytoskeleton. **Therapeutic:** Malignant Paget's disease bone Postmenopausal osteoporosis **Target:** Farnesyl pyrophosphate synthase (FPPS)

Compound	Well	Name	Structure	Formula	Origin	Bioactivity
S17	B08	alpha-Glucosylrutin	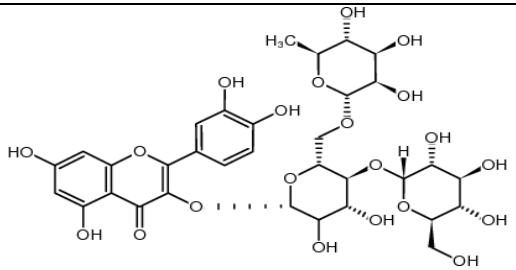	$C_{33}H_{40}O_{21}$	Chemically synthesized	Chelating trace metals and scavenging free radicals **Therapeutic** Antioxidant **Target** Trace metals (Fe/Cu), free radical
S18	B09	Etoposide	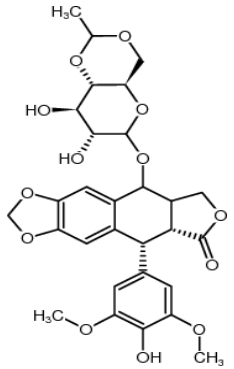	$C_{29}H_{32}O_{13}$	Chemically synthesized	Antineoplastic Induction of DNA damage **Therapeutic:** Anticancer **Target:** Topoisomerase II (TOP-2)
S19	B10	G-418	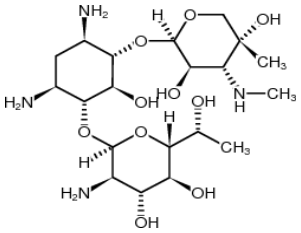	$C_{20}H_{40}N_4O_{10}$	*Micromonospora echinospora*	Inhibition of protein synthesis **Therapeutic:** Antibacterial Antiprotozoal Coccidiostats **Target:** 80S ribosomes

Compound	Well	Name	Structure	Formula	Origin	Bioactivity
S20	B11	Gliclazide	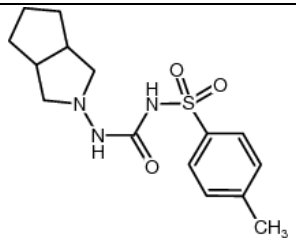	$C_{15}H_{21}N_3O_3S$	Chemically synthesized	Insulin secretion **Therapeutic:** Antidiabetic **Target:** Sulfonylurea receptors (SUR-1)
S21	C02	Paeoniflorin	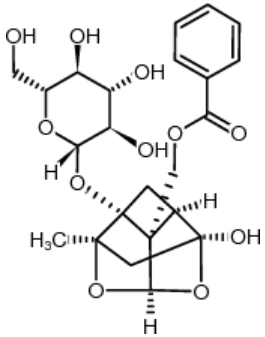	$C_{23}H_{28}O_{11}$	*Paeonia lactiflora*	Inhibition of inflammatory responses Inhibition of oxidative stress and Ca^{2+} overload **Therapeutic:** Analgesic Antiallergic Antidepressant Antihyperglycemia Antiinflammatory **Target:** Intercellular adhesion molecule-1 (ICAM-1)
S22	C03	Picrotoxin	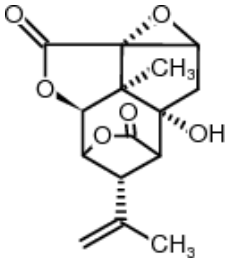	$C_{15}H_{16}O_6$	*Anamirta cocculus*	A noncompetitive antagonist at GABA receptors **Therapeutic:** CNS stimulant **Target:** GABA-A receptors

Compound	Well	Name	Structure	Formula	Origin	Bioactivity
S23	C04	Podophyllotoxin	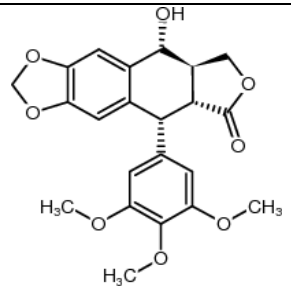	$C_{22}H_{22}O_8$	*Podophyllum peltatum*	Antineoplastic Inhibition of tubulin polymerization **Therapeutic:** Anticancer **Target:** Tubulin Topoisomerase II
S24	C05	Suramin	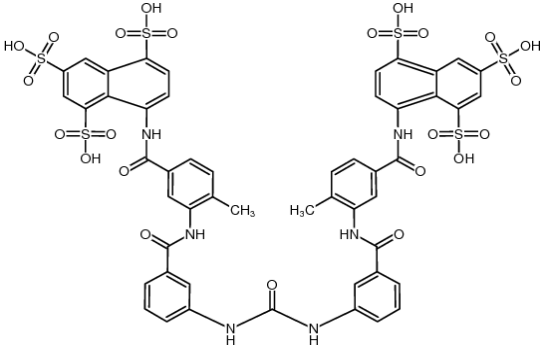	$C_{51}H_{40}N_6O_{23}S_6$	Chemically synthesized	Inhibition of catalytic activity of topoisomerase II **Therapeutic:** Anticancer Antifiliarial Antitrypanosomal **Target:** Topoisomerase II
S25	C06	Dextromycin	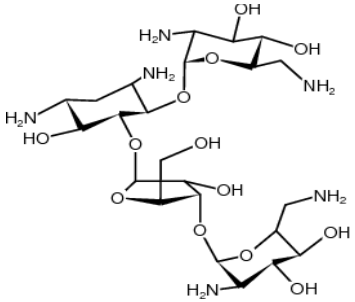	$C_{23}H_{46}N_6O_{13}$	*Streptomyces fradiae*	Inhibition of prokaryotic protein synthesis **Therapeutic:** Antibacterial **Target:** 30S ribosomal protein S12

Compound	Well	Name	Structure	Formula	Origin	Bioactivity
S26	C07	Anisomycin	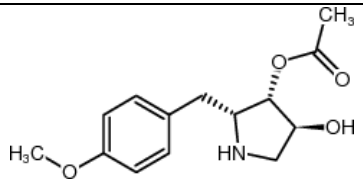	$C_{14}H_{19}NO_4$	*Streptomyces* sp.	Inhibition of protein synthesis **Therapeutic:** Antifungal **Target:** 60S ribosomal subunit
S27	C08	Praziquantel	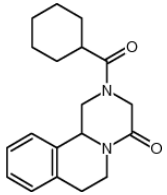	$C_{19}H_{24}N_2O_2$	Chemically synthesized	Increases the permeability of the membranes towards calcium ions Therapeutic Anthelmintic Antihydatidosis Broad spectrum Target Schistosome Calcium (Ca^{2+}) Channel
S28	C09	Ouabain	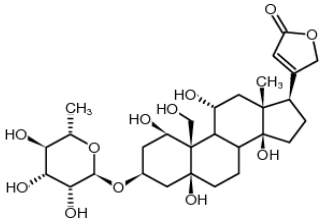	$C_{29}H_{44}O_{12}$	*Acokanthera oubaio* *Strophanthus gratus*	An increase in intracellular sodium and calcium concentrations **Therapeutic:** Cardiotonic **Target:** Sodium/potassium-transporting ATPase
S29	C10	Limonin	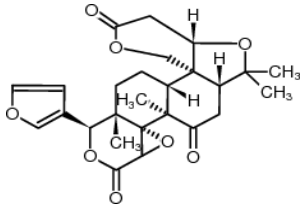	$C_{26}H_{30}O_8$	*Citrus*	Inhibition of HIV-1replication **Therapeutic:** Anticancer Antiviral **Target:** Unknown

Compound	Well	Name	Structure	Formula	Origin	Bioactivity
S30	C11	Aristolochic acid	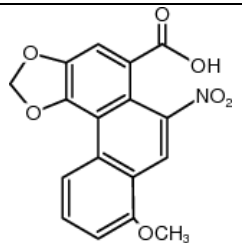	$C_{17}H_{11}NO_7$	*Aristolochia* sp.	Formation of DNA adduct Inhibition of phospholipase A2 **Therapeutic:** Antiinflammatory; Carcinogenic; Mutagenic; Nephrotoxic **Target:** DNA (purine base); Phospholipase A2
S31	D02	Aspirin	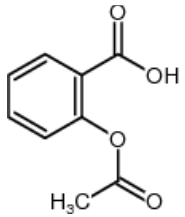	$C_9H_8O_4$	Chemically synthesized	Inhibition of the production of prostaglandins and thromboxanes **Therapeutic:** Analgesic and antipyretic; Antiinflammatory; Antiplatelet **Target:** Cyclooxygenase
S32	D03	Camptothecin	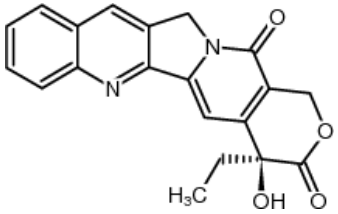	$C_{20}H_{16}N_2O_4$	*Camptotheca acuminata*	antineoplastic Inhibition of DNA synthesis **Therapeutic:** Anticancer **Target:** Topoisomerase I
S33	D04	N-(6-aminohexyl)-1-naphthalene sulfonamide	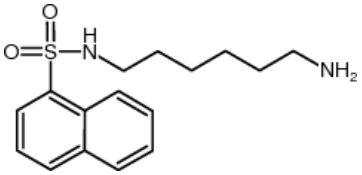	$C_{16}H_{22}N_2O_2S$	Chemically synthesized	Calmodulin antagonist that binds to calmodulin and inhibits Ca^{2+}-calmodulin-regulated activities, including phosphodiesterase activation and myosin light chain kinase **Therapeutic:** Vasodilator **Target:** Calmodulin

Compound	Well	Name	Structure	Formula	Origin	Bioactivity
12	D05	Cantharidin	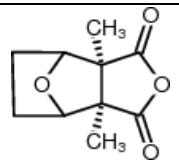	$C_{10}H_{12}O_4$	*Epicauta* *Lytta vesicatoria*	Inhibition of protein phosphatase 2A **Therapeutic:** Anticancer **Target:** Protein phosphatase 2A (PP2A)
S34	D06	Bestatin	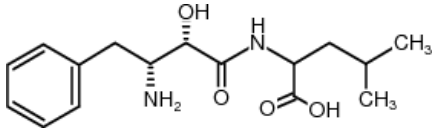	$C_{16}H_{24}N_2O_4$	*Streptomyces olivoreticuli*	Inhibition of aminopeptidase B **Therapeutic:** Anticancer **Target:** Aminopeptidase B
S35	D07	Nocodazole	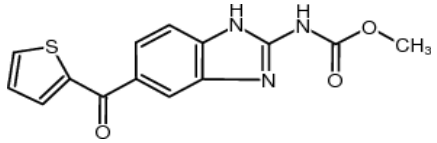	$C_{14}H_{11}N_3O_3S$	Chemically synthesized	Antineoplastic Inhibition of microtubule polymerization **Therapeutic:** Anticancer **Target:** Tubulin
S36	D08	Streptomycin	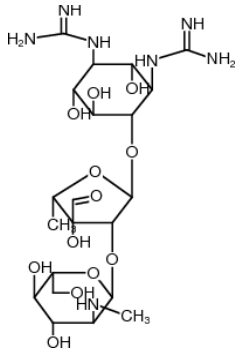	$C_{21}H_{39}N_7O_{12}$	*Streptomyces griseus*	Inhibition of bacterial protein synthesis **Therapeutic:** Antibacterial Antituberculosis **Target:** 30S ribosomal protein S12

Compound	Well	Name	Structure	Formula	Origin	Bioactivity
S37	D09	Tetracycline	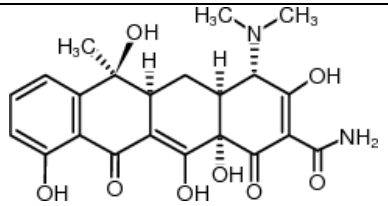	$C_{22}H_{24}N_2O_8$	*Streptomyces* sp.	Inhibition of bacterial protein synthesis **Therapeutic:** Antibacterial **Target:** 30S ribosomal subunit
S38	D10	Benfluorex hydrochloride	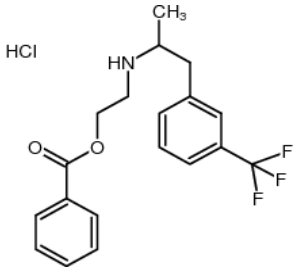	$C_{19}H_{20}F_3NO_2.ClH$	Chemically synthesized	Activate the nuclear receptor transcription factor HNF4a **Therapeutic:** Anorectic Antihyperglycemic Hypolipidemic **Target:** HNF4a
S39	D11	Colistin A	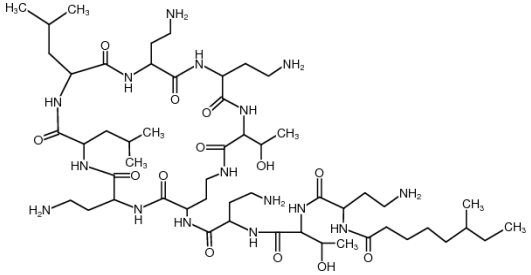	$C_{53}H_{100}N_{16}O_{13}$	*Paenibacillus polymyxa* var. *colistinus*	Disruption of the outer cell membrane of Gram-negative bacilli **Therapeutic:** Antibacterial **Target:** Bacterial outer cell membrane
S40	E02	(+/-)-Vesamicol hydrochloride	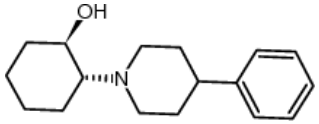	$C_{17}H_{25}NO$	Chemically synthesized	Inhibition of acetylcholine transport **Therapeutic:** Molecular beacon for a cholinergic marker **Target:** Vesicular acetylcholine transporter (VAChT)

Compound	Well	Name	Structure	Formula	Origin	Bioactivity
S41	E03	Apomorphine hydrochloride hemihydrate	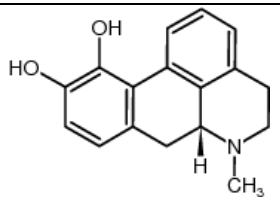	$C_{17}H_{17}NO_2$	Chemically synthesized	Nonselective dopamne agonist **Therapeutic:** Antiparkinsonian **Target:** Dopamine receptor
S42	E04	Atenolol	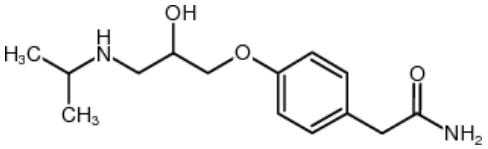	$C_{14}H_{22}N_2O_3$	Chemically synthesized	Antihypertensive drug **Therapeutic:** Arrhythmia Hypertension **Target:** β1 adrenoreceptor
S43	E05	Benomyl	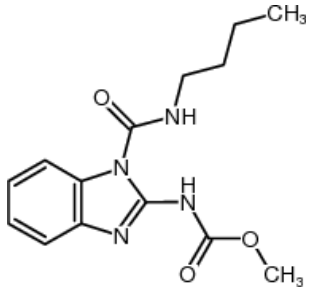	$C_{14}H_{18}N_4O_3$	Chemically synthesized	Inhibition of microtubule polymerization **Therapeutic:** Antifungal **Target:** β-Tubulin
S44	E06	Colchicine	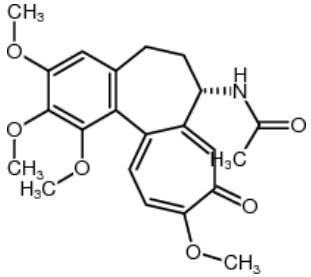	$C_{22}H_{25}NO_6$	*Colchicum autumnale*	Inhibition of microtubule polymerization **Therapeutic:** Anticancer **Target:** Tubulin beta-1 chain

Compound	Well	Name	Structure	Formula	Origin	Bioactivity
S45	E07	Folic acid	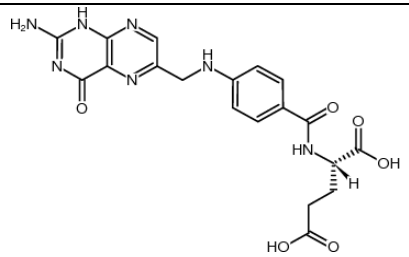	$C_{19}H_{19}N_7O_6$	N/A	Essential nutrient for metabolic maintenance and nucleotide biosynthesis **Therapeutic:** Vitamin **Target:** Folate receptors (FRα, FRβ, FRγ)
S46	E08	Ginkgolide A	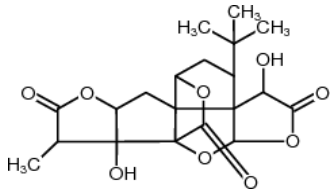	$C_{20}H_{24}O_9$	*Ginkgo biloba*	Antagonist of Glycin and $GABA_a$ receptors PAF membrane platelet receptor **Therapeutic:** Antiinflammatory **Target:** Glycin and $GABA_a$ receptors
S47	E09	Fulvicin	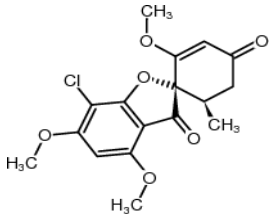	$C_{17}ClH_{17}O_6$	*Penicillium griseofulvum*	Inhibition of mitosis **Therapeutic:** Antifungal **Target:** Tubulin Keratin
S48	E10	L-Mimosine	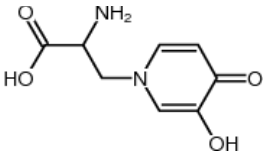	$C_8H_{10}N_2O_4$	*Leucaena leucocephala* *Mimosa pudica*	Inhibition of DNA replication and cell cycle arrest at G1 **Therapeutic:** DNA synthesis inhibitor **Target:** Iron/zinc chelation Serine methyltransferase Deoxyhypusyl hydroxylase

Compound	Well	Name	Structure	Formula	Origin	Bioactivity
S49	E11	D-(+)-Melibiose, Monohydrate	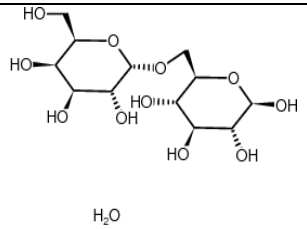	$C_{12}H_{22}O_{11}.H_2O$	N/A	Unknown
S50	F02	Nialamide	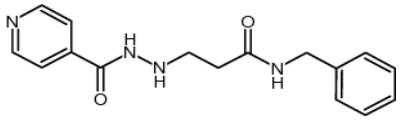	$C_{16}H_{18}N_4O_2$	Chemically synthesized	Increasing the concentrations of various neurotransmitters, such as serotonin, epinephrine and dopamine **Therapeutic:** Antidepressant **Target:** Monoamine oxidase
S51	F03	Sulfaquinoxaline sodium salt	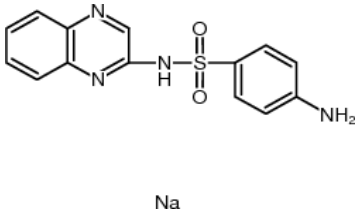	$C_{14}H_{12}N_4O_2S.Na.H$	Chemically synthesized	Reversible inhibitor of the dithiothreitol-dependent reduction of both vitamin K epoxide and vitamin K quinone **Therapeutic:** Anticoccidial **Target:** Vitamin K epoxide Quinone reductase
S52	F04	(-)-Berberine chloride	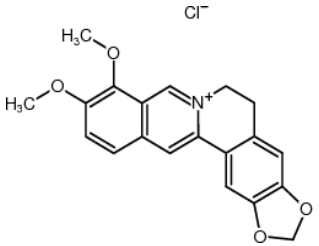	$C_{20}H_{18}NO_4.ClH$	*Berberis* sp.	Wide range of pharmacological activities. **Therapeutic:** Antibacterial; Anticancer; Antidiabetes; Antifungal; Antiinflammation;Antiviral **Target:** RNA transcription Kinase inhibition

Compound	Well	Name	Structure	Formula	Origin	Bioactivity
13	F05	Perphenazine	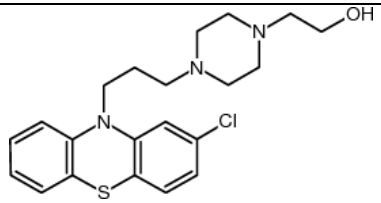	$C_{21}ClH_{26}N_3OS$	Chemically synthesized	Dopamine antagonist **Therapeutic:** Antipsycotic **Target:** Dopamine D2 receptor
S53	F06	Oxybutynin chloride	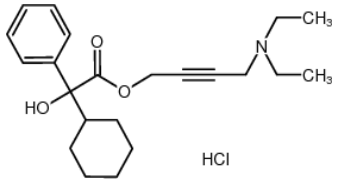	$C_{22}H_{31}NO_3.ClH$	Chemically synthesized	Anticholinergic activity **Therapeutic:** Antispasmodic **Target:** Muscarinic acetylcholine receptor
S54	F07	Trimebutine	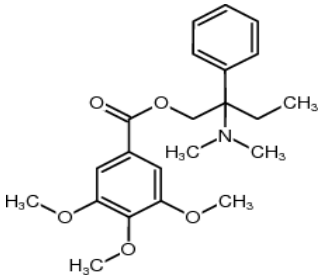	$C_{22}H_{29}NO_5$	Chemically synthesized	Gastrointestinal peptides releasing (motilin) Modulation of peptides (vasoactive intestinal peptide, gastrin , glucagon) Opiate agonist (peripheral) μ, κ, δ **Therapeutic:** Antimuscarinic **Target:** Opiate receptors

Compound	Well	Name	Structure	Formula	Origin	Bioactivity
S55	F08	Acebutolol hydrochloride	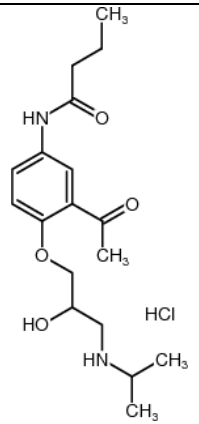	$C_{18}H_{28}N_2O_4.ClH$	Chemically synthesized	β-adrenoreceptor antagonist Mild intrinsic sympathomimetic activity **Therapeutic:** Antiangina Antiarrhythmic (class II) Antihypertensive **Target:** Selective β1-adrenergic receptors
S56	F09	Acetazolamide	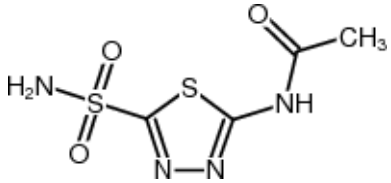	$C_4H_6N_4O_3S_2$	Chemically synthesized	Inhibition of carbonic anhydrase **Therapeutic:** Antiglaucoma Diuretics **Target:** Carbonic anhydrase
S57	F10	Biochanin a	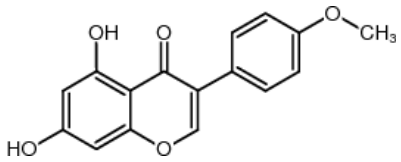	$C_{16}H_{12}O_5$	*Trifolium pratens*	No general activity **Therapeutic:** Anticancer **Target:** No specific molecular target (several molecular targets such as aromatase were reported)

Compound	Well	Name	Structure	Formula	Origin	Bioactivity
S58	F11	Brucine	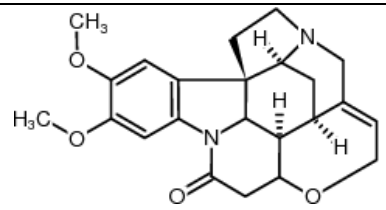	$C_{23}H_{26}N_2O_4$	*Strychnos nux-vomica*	Glycine receptors brocker Inducion of apoptosis Inhibition of COX-2 gene expression Paralyzes inhibitory neurons **Therapeutic:** Anticancer **Target:** NF-κB
S59	G02	Bumetanide	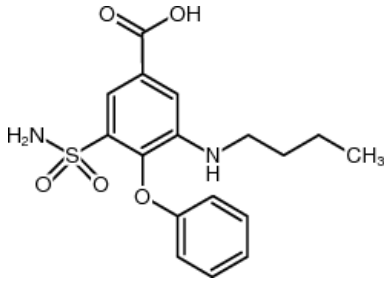	$C_{17}H_{20}N_2O_5S$	Chemically synthesized	Sodium potassium chloride symporter Inhibitors **Therapeutic:** Diuretic (loop diuretic) Heart failure **Target:** NKCC1 cation-chloride co-transporter
S60	G03	Digitoxin	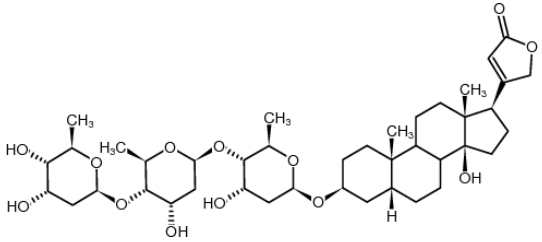	$C_{41}H_{64}O_{13}$	*Digitalis purpurea*	Na^+/K^+ ATPase membrane pump inhibition **Therapeutic:** Antiarrhythmic Cardiotonic **Target:** Na^+/K^+-ATPase

Compound	Well	Name	Structure	Formula	Origin	Bioactivity
14	G04	Flunarizine hydrochloride	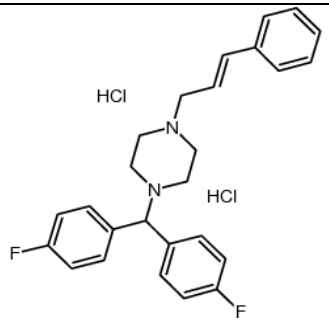	$C_{26}H_{26}F_2N_2.{}_2ClH$	Chemically synthesized	Blocking Ca^{2+} entry Blocking histamine H1 **Therapeutic:** Anticonvulsant **Target:** Voltage-dependent T-type calcium channel subunit α-1G,1H, 1I. Histamine H1 receptor Calmodulin
S61	G05	Gemfibrozil	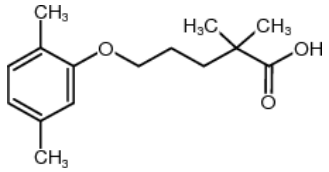	$C_{15}H_{22}O_3$	Chemically synthesized	PPAR activation (up-regulation of tripeptidyl-peptidase) **Therapeutic:** Hyperlipidemia (lipid-lowering drug) **Target:** Peroxisome proliferator-activated receptor α (PPARα)
S62	G06	Sulfamerazine	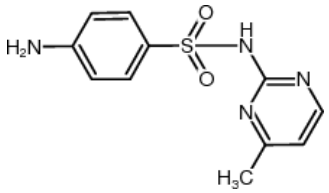	$C_{11}H_{12}N_4O_2S$	Chemically synthesized	Inhibition of folic acid synthesis in bacteria **Therapeutic:** Antibacterial **Target:** Dihydropteroate synthase (DHPS)
S63	G07	Xylometazoline hydrochloride	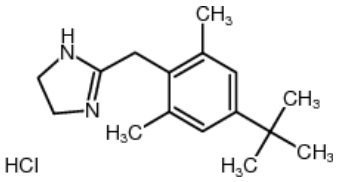	$C_{16}H_{24}N_2.ClH$	Chemically synthesized	α-adrenoceptor agonist Vasoconstriction **Therapeutic:** Nasal catarrh **Target:** α-adrenergic receptor

Compound	Well	Name	Structure	Formula	Origin	Bioactivity
S64	G08	Hycanthone	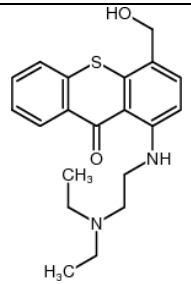	$C_{20}H_{24}N_2O_2S$	Chemically synthesized	Inhibition of DNA repair **Therapeutic:** Anticancer Antischistosomiasis **Target:** Apurinic endonuclease-1 (APE1)
S65	G09	Atractyloside potassium salt	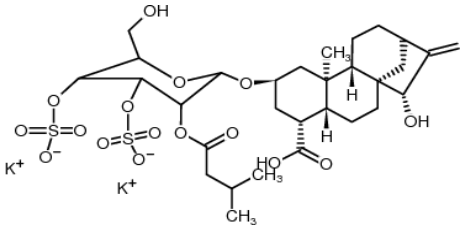	$C_{30}H_{46}O_{16}S_2{\cdot}_2K$	*Atractylis gummifera*	Inhibition of oxidative phosphorylation **Therapeutic:** Herbal poisoning **Target:** Adenine nucleotide translocase
S66	G10	Clozapine	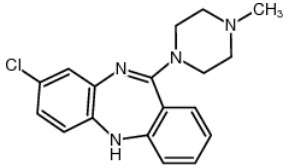	$C_{18}ClH_{19}N_4$	Chemically synthesized	Dopaminergic activity coupled with a broad spectrum of cholinergic, adrenergic, and sertonerigic activity **Therapeutic:** Antipsychotic **Target:** Neurotransmitter receptors
S67	G11	Tolnaftate	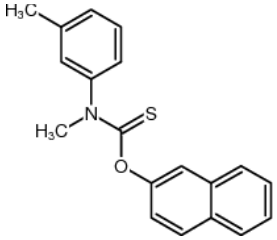	$C_{19}H_{17}NOS$	Chemically synthesized	Inhibition of microsomal squalene epoxidase in ergosterol biosynthesis Selectively active against dermatophytes **Therapeutic:** Antifungal **Target:** Squalene epoxidase

Compound	Well	Name	Structure	Formula	Origin	Bioactivity
S68	H02	Amiodarone hydrochloride	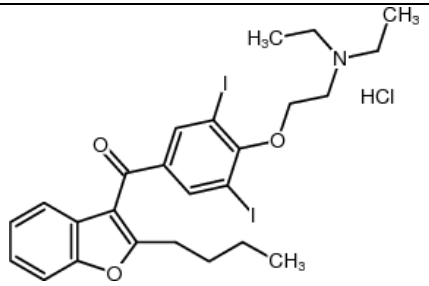	$C_{25}H_{29}I_2NO_3.ClH$	Chemically synthesized	The class III antiarrhythmic action partly through blockade of multi channels **Therapeutic:** Antiarrhythmic (class III) Vasodilator **Target:** Multi channels (K^+, Na^+, Ca^{2+}) PTX-sensitive G protein
S69	H03	Procyclidine hydrochloride	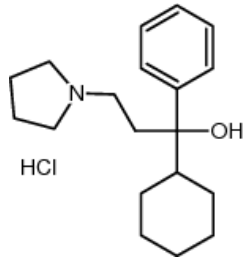	$C_{19}H_{29}NO.ClH$	Chemically synthesized	An anticholinergic effect (muscarinic antagonist) **Therapeutic:** Anticholinergic Antiparkinsonian **Target:** Muscarinic acetylcholine receptor M_1, M_2, and M_4
S70	H04	Warfarin	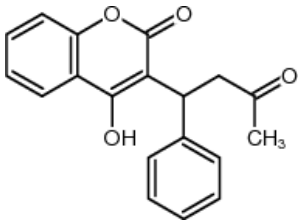	$C_{19}H_{16}O_4$	N/A	Inhibition of vitamin K epoxide reductase **Therapeutic:** Anticoagulant Pesticide **Target:** Vitamin K epoxide reductase
15	H05	Niclosamide	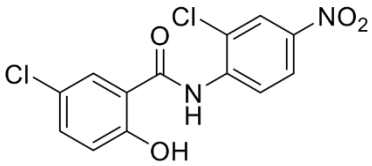	$C_{13}Cl_2H_8N_2O_4$	Chemically synthesized	Inhibition of mitochondrial oxidative phosphorylation of parasitic helminths Inhibition of Wnt/β-catenin signaling **Therapeutic:** Anthelmintic;Antiparasitic **Target:** Unknown

Compound	Well	Name	Structure	Formula	Origin	Bioactivity
S71	H06	Bicyclomycin	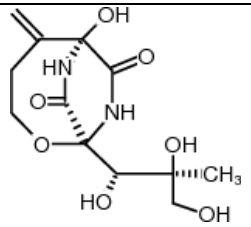	$C_{12}H_{18}N_2O_7$	*Streptomyces* sp.	Inhibition of Rho **Therapeutic:** Antibiotics **Target:** Rho
S72	H07	Siccanin	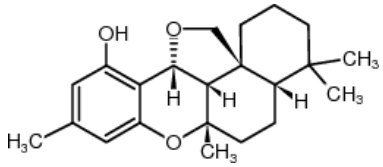	$C_{22}H_{30}O_3$	*Helminthosporium siccans*	Inhibition of succinate dehydrogenase **Therapeutic:** Antifungal **Target:** Succinate dehydrogenase
S73	H08	Polyoxin D	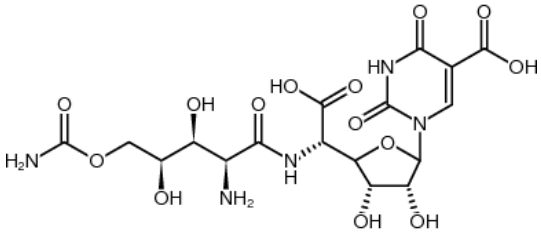	$C_{17}H_{23}N_5O_{14}$	*Streptomyces cacaoi* var. *asoensi*	Inhibition of fungal cell wall biosynthesis **Therapeutic:** Antifungal **Target:** Chitin synthase
S74	H09	Reveromycin A	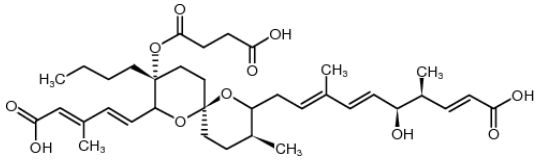	$C_{36}H_{52}O_{11}$	*Streptomyces reveromyceticus*	epidermal growth factor inhibitor (*Eukaryota*) Inhibition of eukaryotic protein synthesis (*Eukaryota*) protein synthesis inhitibion (*Eukaryota*) **Therapeutic:** Anticancer Antifungal Osteoporosis **Target:** Ile-tRNA synthase (IleRS)

Compound	Well	Name	Structure	Formula	Origin	Bioactivity
S75	H10	(+)-Staurosporine	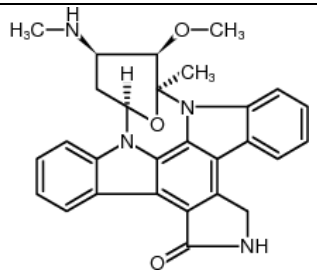	$C_{28}H_{26}N_4O_3$	*Actinomycete* N96C-47 *Lentzea albida*	Broad kinase inhibition **Therapeutic:** Anticancer Antifungal **Target:** Protein kinases
S76	H11	RK-682	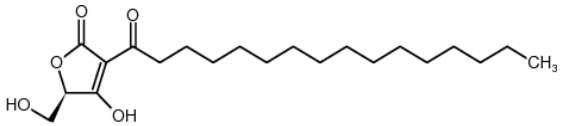	$C_{21}H_{36}O_5$	*Streptomyces* sp. *88-682* *Streptomyces* sp. AL-462	Inhibition of PTPase **Therapeutic:** Anticancer **Target:** Protein tyrosine phosphatase (PTPase) Heparanase Phospholipase A2 HIV protease

B. The structures, anisotropy changes (Δr) and binding energies of niclosamide and niclosamide derivatives

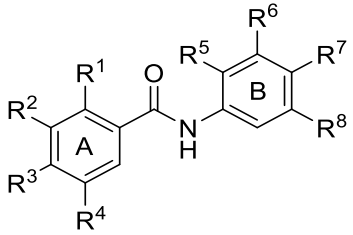

Compound	Structure								Δr[1)]	-CDOCKER energy (kcal/mol)[2)]
	R¹	**R²**	**R³**	**R⁴**	**R⁵**	**R⁶**	**R⁷**	**R⁸**		
Niclosamide (**15**)	OH	H	H	Cl	Cl	H	NO_2	H	0.009± 0.006	19.775
15-a	Cl	H	H	NO_2	H	H	Cl	H	0.054± 0.003	4.465
15-b	Cl	H	H	Cl	OEt	H	H	H	0.080± 0.003	10.423
15-c	OH	H	H	Cl	H	H	$NHCOC(CH_3)_2$	H	0.052± 0.003	5.864
15-d	H	Cl	OEt	Cl	OH	H	H	H	0.008± 0.004	16.995
15-e	OMe	H	H	Cl	H	Cl	H	Cl	0.054± 0.006	11.941
15-f	OMe	H	H	Cl	H	H	OH	H	0.018± 0.005	17.922
15-g	H	Cl	OEt	Cl	CO_2H	H	Cl	H	0.071± 0.003	0.904
15-h	Cl	H	Cl	H	H	H	OMe	H	0.017± 0.002	13.400
15-i	OMe	H	H	Cl	H	H	$CONH_2$	H	0.028± 0.006	9.882
15-j	OMe	H	H	Cl	H	H	H	H	0.023± 0.002	9.891
15-k	OMe	H	H	Cl	H	H	CO_2H	H	0.008± 0.002	14.848
15-l	OMe	H	H	Cl	H	H	F	H	0.026± 0.004	10.524
15-m	OMe	H	H	Cl	H	H	Br	H	0.048± 0.004	11.045
15-n	OMe	H	H	Cl	H	H	Me	H	0.047± 0.020	9.577
15-o	H	Cl	OMe	Cl	CO_2H	H	H	H	0.013± 0.010	11.807

Compound	Structure								Δr[1)]	-CDOCKER energy (kcal/mol)[2)]
	R^1	R^2	R^3	R^4	R^5	R^6	R^7	R^8		
15-p	OMe	H	H	Cl	H	H	CH_3CO	H	0.044± 0.005	12.190
15-q	OMe	H	H	Cl	H	H	Et	H	0.055± 0.006	12.162
15-r	OMe	H	H	Cl	H	H	CH_3OCO	H	0.053± 0.006	9.243

[1)] Measured using FA assay at 10 μM.

[2)] The binding energy was calculated using CDOCKER, a molecular docking algorithm in Discovery Studio Modeling 2022 that uses a CHARMM-based force field to simulate the binding of small molecules to proteins.

Acknowledgements

Alhamdulillah, I would like to thank Almighty Allah, who always gives me His divine help and guidance to finish this study. For You I serve, and to You I will return.

In carrying out research and completing this thesis, I received a lot of help and encouragement from various parties, so I would like to thank:

1. Professor Hiroyuki Nakamura as my academic supervisor, who has provide excellent supervision, invaluable support, patience, motivation, and sincere care throughout my studies at Science Tokyo. Thank you for giving me the opportunity to study here. I am deeply grateful for this experience.
2. Assoc. Prof. Satoshi Okada as my sub-academic supervisor, for the valuable advises and support in my research and social life during my studies.
3. Assist. Prof. Kazuki Miura as my research supervisor, for always provides continuous support, constructive feedback, and valuable comments. I owe him an incredible amount of gratitude for his exceptional guidance and patience in supervising me.
4. Assist. Prof. Taiki Morita as the former staff in our lab, for supporting me with many research experiences, especially in organic synthesis.
5. Dr. Hiroyuki Hirano (RIKEN, Japan) and Dr. Hiroyuki Osada (RIKEN and BIKAKEN, Japan) as collaborators in this research, for providing the compound library.
6. Doctoral thesis review committee: Prof. Katsunori Tanaka, Prof. Nobuhiro Nishiyama, Prof. Mako Kamiya, and Prof. Takeharu Tsuge for their constructive comments and suggestions for completion of my thesis.
7. Indonesia Endowment Fund for Education Agency (LPDP) of the Ministry of Finance of the Republic of Indonesia for providing scholarship during my doctoral study.
8. Directorate General of Higher Education, Ministry of Education and Culture of the Republic of Indonesia, and the Department of Chemistry, Faculty of Mathematics and Science Universitas Islam Indonesia (UII) for permitting me to study abroad.
9. My fellow Doctoral student: Kai Nishimura, Shao Yujie, and Yuan Yuchen, for their friendly atmosphere and scientific discussions.

10. The former Doctoral student: Dr. Masato Tsuda, Dr. Kohei Umedera, Dr. Rohmad Yudi Utomo, and Dr. Yasunobu Asawa, for their valuable experience and help in my research.
11. All Nakamura-Okada laboratory members: Mr. Kakeru Miyamoto, Mr. Nao Yamamoto, Ms. Akari Nakanishi, Mr. Chen Keyi, Mr. Zhang Leiting, Mr. Iwagaki Tatsuki, Mr. Oki Gakuto, Mr. Masahiro Kawaura, Ms. Chika Sato, Mr. Shun Arioka, Ms. Yuri Nojiri, Mr. Kenichi Izawa for their kindness and inspiring work.
12. The former lab members: Ms. Qarri Ainaya, Ms. Yijin Wen, Mr. Tomoyuki Araki, Ms. Yuka Takashima, Ms. Yuka Muto, Ms. Non Ito, Mr. Shota Saiki, Mr. Tomoya Doi, Mr. Yuya Miura, Mr. Hikaru Niimi, Mr. Kentaro Makino, Mr. Shunya Kitahara, Mr. Lishan Liu, Ms. Nguyen Emylie, and Ms. Xu Taoran.

This dissertation is dedicated to my beloved family, my husband Huda Muhamad Badri and my children, Muhammad Hafidz Al Badri and Shakayla Salsabila Hafidzah, for their endless love, support, and prayer throughout my ups and downs.